

# **Immunomagnetic separation of bacteria by iron oxide nanoparticles**

**Maarten Bloemen**

Examination committee:

Prof. dr. M. Smet, chair

Prof. dr. T. Verbiest, supervisor

dr. N. Geukens, co-supervisor

Prof. dr. A. Gils, co-supervisor

Prof. dr. G. Koeckelberghs

Prof. dr. S. De Feyter

Prof. dr. F. Ollevier

Prof. dr. M. Ameloot

(UHasselt)

Dissertation presented in partial  
fulfillment of the requirements for  
the degree of Doctor  
in Science

May 2015

© 2015 KU Leuven – Faculty of Science

Uitgegeven in eigen beheer, Maarten Bloemen , Celestijnenlaan 200D box 2425, B-3001 Heverlee (Belgium)

Alle rechten voorbehouden. Niets uit deze uitgave mag worden vermenigvuldigd en/of openbaar gemaakt worden door middel van druk, fotokopie, microfilm, elektronisch of op welke andere wijze ook zonder voorafgaande schriftelijke toestemming van de uitgever.

All rights reserved. No part of the publication may be reproduced in any form by print, photoprint, microfilm, electronic or any other means without written permission from the publisher.

*The story of science is often told as a series of eureka moments.  
But the truth is that influence, passion and sheer blind chance  
have played equally significant parts.*

Michael Mosley



# Preface

The booklet in front of you is the result of my great PhD adventure. It was a combination of many bold ideas, successes (and as many failures), perseverance, persistence, enthusiasm and the occasional disappointment when a chemical reaction was not cooperating. Even though there is only one name on the cover, this PhD was a combined effort by many people, who contributed scientifically, practically or mentally. I would like to seize this opportunity to thank everyone who helped, influenced or supported me.

First and foremost, I want to thank Prof. Thierry Verbiest for being a terrific promotor and supervisor. I fully enjoyed the early morning coffee moments, brainstorming sessions and scientific discussions (even though you were mostly right in the end). Your enthusiasm and never-ending optimism created a great working environment. Thank you for giving me the freedom to pursue my own ideas and the possibility to see the world by visiting conferences abroad. I honestly cannot imagine a better promotor!

I was given the unique opportunity to conduct multidisciplinary research, combining chemistry with pharmacology and biology. It goes without saying that my limited knowledge in these new fields had to be compensated. Therefore I would like to thank my co-supervisors Prof. Ann Gils and dr. Nick Geukens for their support, mentoring, insights and for providing me with (ridiculously) large amounts of antibodies whenever I needed them. The synergy between our research has proven to be very valuable. I would also like to express my gratitude for funding the first year of my PhD.

While performing experiments away from the safe haven of chemistry, I received (read: I needed) a lot of practical assistance and guidance. On the pharmacology side, Miet Peeters and Thomas Van Stappen helped me out regularly. Thank you for teaching me the basics of ELISAs and protein purification, and answering all my questions (over and over again). On the biology side, Carla Denis and dr. Louise Vanysacker introduced me into the world of bacteria. Special thanks

to Carla for doing all preparations, guidance and performing the DNA-related measurements!

Collaborations with other research groups allowed me to use their scientific equipment and discuss the results with experts in their respective fields. Special thanks to the groups of Prof. Luc De Meester, Prof. Guy Koeckelberghs, Prof. Koen Binnemans, Prof. Tatjana Parac-Vogt, Prof. Carmen Bartic, Prof. Bart Goderis, Prof. Wim Annaert and Prof. Jeroen Lammertyn. More specific, I am grateful for all assistance by dr. Pieter Willot, Frederic "Fred" Monnaie, David Dupont, Sophie Carron, Vincent Goovaerts, Matthias Ceulemans, David Debruyne, dr. Marlies Van De Wouwer, Arun Kumar Tharkeshwar and dr. Karel Knez. Not to forget, my exemplary master student Ben, for all the hard (and perhaps repetitive) work in the lab.

I also would like to express my gratitude to the jury members: Prof. Mario Smet (KU Leuven), Prof. Guy Koeckelberghs (KU Leuven), Prof. Steven de Feyter (KU Leuven), Prof. Frans Ollevier (KU Leuven) and Prof. Marcel Ameloot (UHasselt). Thank you for reading my dissertation and providing me with comments and remarks, that greatly improved the manuscript.

Scientific research is dependent on funding, so I want to thank the Agency for Innovation by Science and Technology (IWT) Flanders for awarding me a grant that funded my PhD.

Thanks to all of my LCBD colleagues for the fun and laughter, lab trips, cake-time (for every possible reason) and coffee breaks. Special thanks to PJ for being my fellow lab responsible and making our lab a safer and cleaner place, and to Rik for turning my ideas into working hardware and the swift repairs. Of course I cannot forget my office buddies: Ward, the other Maarten, Stefaan and Stefan; for making our office the best (and most productive) in the building. We clearly had a shared preference for a certain music genre (at least on Friday).

Luckily there is more to life than just working and studying. Throughout my time in Leuven I had the pleasure of sharing countless evenings with my friends Bram, Bellie (the other Maarten) en Kevin. The 2-for-1 pizza and game nights were legendary!

I also would like to thank the Rebus-clan for the sportive evenings, BBQs and bar visits. And of course all my friends from Geel and surroundings, for the weekend entertainment and great New Year's eve parties.

To my parents, thank you for supporting, stimulating and encouraging me throughout my studies and for always showing great interest in my work. Driving back and forth to Leuven on numerous occasions was a tedious task but it was worth it in the end. Special mention to my zusje and broertje, for all

the joking around, dinners and mental support.

And last but definitely not least, my girlfriend Sara, thank you for supporting me, sharing my happiness and frustration, and providing me with lots of hugs and love. My tendency to get up as early as possible, "nerdy" talking, total lack of patience (seriously, none whatsoever) and exaggerated never-ending happiness were sometimes hard to bear, but you never complained. You are awesome!

Thank you all!!!!

Maarten



# Abstract

The development of multifunctional nanomaterials has proven to be beneficial for many applications. Nanoparticles in particular have been intensively investigated, which resulted in large advances in particle synthesis and control of their properties. From a biomedical point of view, iron oxide nanoparticles are especially valuable thanks to their biocompatibility and low toxicity. Their magnetic properties are already applied in medical imaging, hyperthermia for cancer therapy and advanced drug delivery techniques.

In this dissertation we present the development of multifunctional iron oxide nanoparticles that can be used for the magnetic isolation of bacteria from an aqueous solution, as a pre-concentration technique.

The synthesis and characterization of the core nanoparticle is described in the first part of this work. An enhanced method of surface functionalization was developed, that enabled us to efficiently coat the particles with multiple different ligands. We applied a covalent surface modification method to improve the robustness and long-term stability and storage of the material. The influence of the different ligands on the colloidal stability was investigated, providing a solid base for further development.

In order to provide sufficient colloidal stability to the nanoparticles, a new ligand was designed and synthesized. By modifying a poly(ethylene glycol) chain with two different functional groups, a new heterobifunctional ligand was produced. Thanks to the presence of the water soluble backbone, the functionalized nanoparticles showed excellent stability in various complex environments. Moreover, we covalently coupled antibodies to these particles and confirmed that their activity was retained, which is crucial for their applicability. The synthesis protocol to form these bioconjugated nanoparticles is described in the second part of this work.

*Legionella pneumophila* bacteria were chosen as the model target for magnetic isolation experiments. These bacteria are known to cause various diseases,

including severe types of pneumonia. Consequently their detection is mandatory by law in all public water systems. We investigated by flow cytometry measurements, whether or not the bioconjugated nanoparticles are capable of isolating these bacteria from an aqueous solution. The results indicated that the developed nanoparticles can very efficiently isolate these targeted organisms. Furthermore, we were able to capture *L. pneumophila* from a mixture of bacteria, which underlines the potential and robustness of the proposed methodology.

The results showed that the new heterobifunctional ligand can efficiently stabilize nanoparticles and allows for subsequent modification with antibodies. We developed a nanoparticle platform for highly efficient magnetic isolation of bacteria in complex environments. By choosing the correct antibodies, a wide range of proteins or organisms can be targeted. This makes the methodology highly valuable for monitoring water quality or for magnetic purifications in complex media.

# Beknopte samenvatting

De ontwikkeling van multifunctionele nanomaterialen is voordelig gebleken voor vele toepassingen. Nanopartikels in het bijzonder zijn intensief onderzocht, wat geleid heeft tot grote vooruitgang in de productie van partikels en controle over hun eigenschappen. Vanuit een biomedisch standpunt zijn ijzeroxide nanopartikels bijzonder waardevol dankzij hun biocompatibiliteit en lage toxiciteit. Hun magnetische eigenschappen worden al benut in medische beeldvorming, hyperthermie voor kankertherapie en geavanceerde afgifte van geneesmiddelen.

In dit proefschrift presenteren we de ontwikkeling van een multifunctioneel ijzeroxide nanopartikel dat kan gebruikt worden voor de magnetische scheiding van bacteriën uit een waterige oplossing, als een preconcentratie techniek.

De aanmaak en karakterisatie van de nanopartikels is beschreven in het eerste deel van dit werk. We ontwikkelden een verbeterde oppervlaktefunctionalisatie methode die het mogelijk maakte om de partikels efficiënt te coaten met verschillende liganden. Dankzij het gebruik van een covalente oppervlaktemodificatie werd de robuustheid en stabiliteit op lange termijn van het materiaal verbeterd. De invloed van de verschillende liganden op de colloïdale stabiliteit werd onderzocht, wat een solide basis vormde voor verdere ontwikkelingen.

Om de nanopartikels voldoende colloïdale stabiliteit te bieden, werd een nieuwe ligand ontworpen en aangemaakt. Door het modifieren van een poly(ethyleenglycol)-keten met twee verschillende functionele groepen werd een nieuwe heterobifunctionele ligand gevormd. Dankzij de aanwezigheid van de wateroplosbare keten werd de stabiliteit van de gefunctionaliseerde nanopartikels in complexe omgevingen sterk verbeterd. Daarenboven koppelden we antilichamen via een covalente binding aan de partikels en werd hun activiteit gecontroleerd, wat cruciaal is voor hun verdere toepasbaarheid. Het protocol voor de aanmaak van deze bioconjugeerde nanopartikels wordt beschreven in het tweede deel van dit werk.

*Legionella pneumophila* bacteriën werden als modelorganismen gekozen voor de magnetische isolatie experimenten. Deze bacteriën zijn gekende veroorzakers van verschillende ziektes, inclusief gevaarlijke vormen van longonsteking. Bijgevolg is hun detectie wettelijk verplicht in alle publieke watersystemen. We onderzochten met behulp van flowcytometrie of de biogeconjugeerde nanopartikels al dan niet in staat zijn om deze bacteriën aan te trekken uit een waterige oplossing. De resultaten gaven aan dat de ontwikkelde nanopartikels zeer efficiënt deze organismen kunnen isoleren. Daarenboven werd *Legionella pneumophila* ook geïsoleerd uit een mengsel van bacteriën, wat het potentieel van de ontwikkelde methodologie onderlijnt.

De resultaten toonden aan dat de nieuwe heterobifunctionele ligand nanopartikels efficiënt kan stabiliseren en dat een verdere modificatie met antilichamen mogelijk is. We ontwikkelden een nanopartikelpatform voor een zeer efficiënte scheiding van bacteriën uit een complexe omgeving. Door het zorgvuldig selecteren van antilichamen, kan een breed spectrum aan proteïnes of micro-organismen als doelwit gekozen worden. Dit maakt de methodologie zeer waardevol voor de controle van de waterkwaliteit of voor magnetische opzuiveringen uit complexe media.

# Abbreviations

Ab	antibodies
Ag	antigen
CDI	N,N'-carbonyl diimidazole
CFU	colony forming units
CMC	1-cyclohexyl-3-(2-morpholinoethyl) carbodiimide
CTAB	cetyltrimethyl ammonium bromide
DCC	dicyclohexyl carbodiimide
DIC	diisopropyl carbodiimide
DMAP	4-dimethylaminopyridine
DMPAP	2,2-dimethoxy-2-phenyl-acetophenone
EDC	1-ethyl-3-(3-dimethylaminopropyl)- carbodiimide hydrochloride
ELISA	enzyme-linked immunosorbent assay
FCM	flow cytometry
FTIR	Fourier transform infrared
GFP	green fluorescent protein
Ig	immunoglobulins
IgG	immunoglobulin G
<i>L. pneumophila</i>	<i>Legionella pneumophila</i>
MES	2-(N-morpholino)-ethanesulfonic acid
MRI	magnetic resonance imaging
NHS	N-hydroxy succinimide
nm	nanometer
NP	nanoparticles
PAI-1	plasminogen activator inhibitor-1
PEG	polyethylene glycol
PFA	paraformaldehyde
PVA	polyvinyl alcohol
qPCR	quantitative polymerase chain reaction

RFP	red fluorescent protein
SN	supernatant
SPR	surface plasmon resonance
TAFI	Thrombin Activatable Fibrinolysis inhibitor
TEM	transmission electron microscopy
TEOS	tetraethyl orthosilicate
TFA	trifluoroacetic acid
TRIS	2-amino-2-hydroxymethyl-propane-1,3-diol
VSM	vibrating sample magnetometry
XRD	X-ray powder diffraction

# Contents

<b>Abstract</b>	<b>v</b>
<b>Abbreviations</b>	<b>x</b>
<b>Contents</b>	<b>xi</b>
<b>1 General introduction to bioconjugated nanoparticles</b>	<b>1</b>
1.1 Magnetic nanoparticles . . . . .	2
1.1.1 General introduction to magnetism . . . . .	3
1.1.2 Superparamagnetism . . . . .	4
1.2 Synthesis of iron oxide nanoparticles . . . . .	5
1.3 Surface functionalization . . . . .	9
1.4 Colloidal stability . . . . .	13
1.5 Protein coronas . . . . .	15
1.6 Antibodies . . . . .	18
1.7 Coupling chemistry . . . . .	20
1.8 <i>Legionella pneumophila</i> . . . . .	24
1.9 Objectives and outline . . . . .	27
<b>2 Functionalization of oleic acid-coated iron oxide nanoparticles</b>	<b>31</b>

2.1	Introduction . . . . .	32
2.2	Materials and methods . . . . .	33
2.3	Results & Discussion . . . . .	35
	Characterization of the core nanoparticle . . . . .	35
	Colloidal stability . . . . .	40
2.4	Conclusions . . . . .	43
2.5	Supporting information . . . . .	44
<b>3</b>	<b>Heterobifunctional PEG ligands for bioconjugation reactions</b>	<b>49</b>
3.1	Introduction . . . . .	50
3.2	Materials and methods . . . . .	51
3.3	Results & Discussion . . . . .	53
	Ligand Design . . . . .	53
	Bioconjugation . . . . .	55
	Activity assessment . . . . .	57
3.4	Conclusions . . . . .	58
3.5	Supporting information . . . . .	59
<b>4</b>	<b>Two-step directional surface modification via protected siloxanes</b>	<b>63</b>
4.1	Introduction . . . . .	64
4.2	Materials and methods . . . . .	65
4.3	Results & Discussion . . . . .	69
	Methodology . . . . .	69
	Nanoparticle multilayers . . . . .	72
4.4	Conclusions . . . . .	73
4.5	Supporting information . . . . .	73

**5 Design of nanoparticles for efficient magnetic isolation of aquatic pathogens 85**

5.1 Introduction . . . . . 86

5.2 Materials and methods . . . . . 87

5.3 Results & Discussion . . . . . 91

    Synthesis and characterization of the bioconjugates . . . . . 91

    Magnetic isolation results . . . . . 92

5.4 Conclusions . . . . . 96

5.5 Supporting information . . . . . 97

**6 Conclusions and outlook 101**

6.1 Conclusions . . . . . 101

6.2 Outlook . . . . . 103

**A Selected experimental techniques 107**

A.1 Enzyme-linked immunosorbent assay (ELISA) . . . . . 107

A.2 Flow cytometry (FCM) . . . . . 109

A.3 Quantitative polymerase chain reaction (qPCR) . . . . . 110

**Health, safety and environment 134**

**List of publications 137**



# Chapter 1

## General introduction to bioconjugated nanoparticles

The continuous quest in materials development has gained momentum in the past decades thanks to the introduction of nanomaterials. This new field of research lies on the boundary between the scale of atomic or quantum phenomena and bulk materials. As a result of significant investments during the past decade and a broad commercial applicability, the field of nanotechnology has matured to the point of showing significant potential to improve efficiencies and accelerate progress in biomedical, manufacturing, space and energy applications.<sup>1</sup>

To be categorised as a nanomaterial, at least one dimension of the material should be in the 1-100 nanometer (nm) range, while its shape can be planar, rod-like or spherical. At this scale, the properties of the material often differ from its bulk characteristics. Multiple properties are known to change with the size of the object, such as the melting point, conductivity, magnetism and optical properties.<sup>2,3</sup> Figure 1.1 compares the size of nanomaterials (yellow region) with common other objects.

The first uses of nanotechnology were surprisingly not in recent ages, but date back to the 4th century and the Roman Empire. At that point, nanoparticles (NP) were (unknowingly) added to materials to alter their appearance under different lighting conditions.<sup>4</sup> During the past decades a whole new range of nanomaterials have been developed, going from carbon nanotubes, nanorods and nanoparticles with different morphologies, fullerenes and graphene to complex DNA-scaffolds.<sup>5-8</sup> Moreover, multiple techniques have been invented that enable researchers to modify a material on the nanoscale, such as atomic

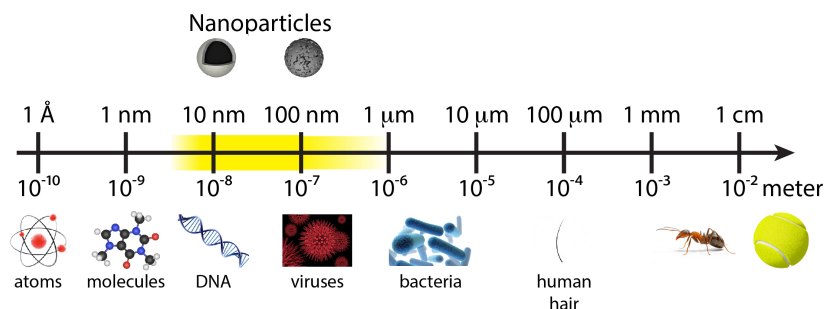


Figure 1.1: One dimension of a nanomaterial should be in the 1-100 nm range. As a comparison, other typical sizes of everyday objects and organisms are shown.

layer deposition, contact printing, photolithography or etching.<sup>9–11</sup>

In this dissertation, the focus lies on the development of a multifunctional nanoparticle, based on a superparamagnetic iron oxide (magnetite) core, with custom-designed ligands and proteins for specific magnetic separation of targeted bacteria or proteins. This type of nanomaterial is considered to be a prime candidate for future applications in biomedical imaging or drug delivery. A model nanoparticle-based system for the magnetic separation and quantification of aqueous pathogens was designed and tested thoroughly for its efficiency and reproducibility. The system described here will provide a generic platform, that combines multiple highly valued properties like magnetism, colloidal stability in complex environments and target specificity.

The following sections will first give a broad overview of different important properties of superparamagnetic NP as well as possible synthetic routes and functionalization approaches. Secondly, the biomedical and biological aspects of the research will be situated to provide sufficient background for the reader. To finish the introduction, the research goals and scope of this dissertation will be described.

## 1.1 Magnetic nanoparticles

A large variety of NP with magnetic properties have been described in scientific literature, but they all have atoms with a large magnetic moment incorporated in their crystal structure. Magnetic NP with different compositions and phases have been produced, such as iron oxides ( $\text{Fe}_3\text{O}_4$ ,  $\gamma\text{-Fe}_2\text{O}_3$ ), spinel-type ferromagnets ( $\text{MnFe}_2\text{O}_4$ ,  $\text{MgFe}_2\text{O}_4$ ), pure metals (Fe, Co) and alloys (FePt).<sup>12–15</sup> Even though

all of these NP have interesting characteristics, including large saturation magnetization, coercivity or biocompatibility, only iron oxides will be discussed in this dissertation. Particularly  $\text{Fe}_3\text{O}_4$  (magnetite) is a promising candidate for biomedical and biological research applications. This type of NP can be produced at a very large scale with a well-defined size and shape, has excellent magnetic properties and shows only minor toxicity.<sup>15–17</sup>

### 1.1.1 General introduction to magnetism

The phenomenon of magnetism is electronic in nature, since it is related to the orbital motion of electric charges. The applied magnetic field strength (see equation 1.1) is represented by  $H$ , while the magnetic moment (per volume) is noted as  $M$ , also known as the magnetization. The parameter that links the applied field and the induced moment, is the volume magnetic susceptibility ( $\chi$ ), which is a measure for how effectively a field induces a magnetic dipole in a material per unit volume.<sup>18</sup>

$$M = \chi H \quad (1.1)$$

The sign and size of the susceptibility ( $\chi$ ) can be used to differentiate between different forms of magnetism. In a diamagnetic material,  $\chi$  is negative and small, as can be seen in Figure 1.2, where the magnetic moments try to oppose the applied magnetic field. All substances show diamagnetic behaviour, but since this effect is very small, any other magnetic response will oppose it. Typical examples are bismuth, water or lead. In a paramagnetic material (see Figure 1.2),  $\chi$  is positive but small, meaning that the magnetic moments align to the external field, but the response is low. These moments are caused by unpaired electrons in the substance. Examples are liquid oxygen, copper sulphate or iron chloride. For a ferromagnetic substance, that have a permanent net magnetic moment,  $\chi$  is positive and large, resulting in a strong attraction towards an external field. Typical substances are iron, nickel and cobalt.<sup>18</sup>

Iron oxide nanoparticles can have different morphologies, such as hematite ( $\alpha\text{-Fe}_2\text{O}_3$ ), maghemite ( $\gamma\text{-Fe}_2\text{O}_3$ ) or magnetite ( $\text{Fe}_3\text{O}_4$ ). The latter differs from most other iron oxides since it has different oxidation states of the same atom in its crystal structure, called a spinel. For magnetite in particular, the full formula should be  $\text{Fe}_1^{2+}\text{Fe}_2^{3+}\text{O}_4$ .<sup>18,19</sup> Moreover, the  $\text{Fe}^{3+}$  atoms are located in the tetrahedral and octahedral lattice sites, while  $\text{Fe}^{2+}$  is only in the octahedral sites, which is called an inverse spinel. This unusual arrangement causes the magnetic moments of  $\text{Fe}^{3+}$  to cancel each other out (tetrahedral and octahedral sites have opposite spins), leaving only the moment of  $\text{Fe}^{2+}$  contributing to

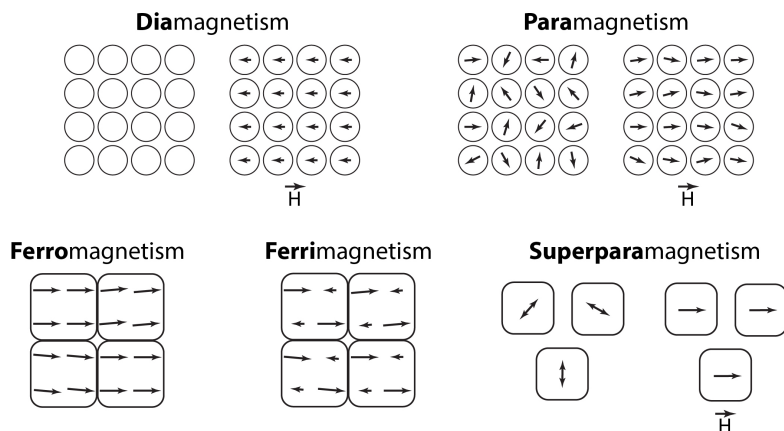


Figure 1.2: Schematic illustration of magnetic materials and their responses to an external field. Atomic spins are shown in circles, while magnetic domains are shown in rectangles. Ferri- is a special case of ferromagnetism, where some spins have an opposite direction, partially cancelling the net magnetic moment. Superparamagnetic materials have only one domain and sufficient thermal energy to flip the magnetic moment.

the overall magnetic moment. As shown in Figure 1.2, this is an example of a ferrimagnetic material.

## 1.1.2 Superparamagnetism

When the dimensions of a particle become sufficiently small, the energy needed to sustain multiple magnetic domains becomes higher than the energy to sustain just one domain. This results in a single magnetic domain in the particle where all spins behave as one superposed magnetic moment (see Figure 1.2).

*Superparamagnetism* is caused by magnetic anisotropy in a material, which can be seen as a preferred direction of electron spin alignment (crystallographic) and hence preferred direction of magnetization. If sufficient energy is supplied, the direction of magnetization can reverse along this axis. This effect is typical for small nanoparticles, that have only one magnetic domain. The time required to reverse the spins, the Néel relaxation time ( $\tau$ ), depends on the anisotropy constant ( $K$ ), the particle volume ( $V$ ), the Boltzmann constant ( $k$ ) and the temperature ( $T$ ) (see Equation 1.2). When temperature increases, the activation energy between the two reversed directions becomes smaller, and hence the

reversal will occur faster. At lower temperatures, on the contrary, the energy hurdle becomes too high to overcome. At a certain point this freezes the magnetic moments in a certain direction, giving the material a ferromagnetic appearance. This temperature is called the blocking temperature.<sup>19–22</sup>

$$\tau \sim \exp \frac{KV}{kT}$$

(1.2)

## 1.2 Synthesis of iron oxide nanoparticles

Multiple synthetic protocols and approaches have been published for the synthesis of magnetite (Fe<sub>3</sub>O<sub>4</sub>) nanoparticles. These include co-precipitation, polyol and hydrothermal reactions, micro-emulsions, laser ablation, thermal decomposition, flow-injection and electrospray syntheses. The properties of the most common methods are compared in Table 1.1.<sup>15,23–26</sup>

Table 1.1: Comparison of the most common methods for the synthesis of magnetite nanoparticles. Thermal decomposition was preferred because of the large scale and high quality nanoparticles it produces.

Method	co-precipitation	microemulsion	hydrothermal	thermal decomposition
Conditions	air	air	high pressure	air/inert gas
T (°C)	20-95	20-50	180-220	180-350
Solvent	water	water in oil	water-alcohols	long hydrocarbons
Distribution	broad	medium	narrow	<b>very narrow</b>
Size	2-100	1-50	10-800	3-50
Shape control	not good	good	very good	<b>very good</b>
Scale (gram)	large (0.1-2)	small (0.1-0.3)	small (0.1-0.5)	<b>large (1-40)</b>

The following section will discuss the basic theory of nanoparticle growth and the reaction mechanism of the thermal decomposition method in more detail, since it is capable of producing high quality monodisperse spherical nanoparticles at a large scale and is the only method used in this dissertation.

### Nucleation and growth

During the very first stages of any crystallization process, nucleation occurs. Although the theoretical understanding of the phenomenon is well developed, the experimental data are hard to obtain because these very small nuclei, consisting of just few atoms, are formed only in the beginning and immediately grow or disappear again. These nuclei can be introduced externally or be formed in situ in solution. The first process, where nucleation is induced by foreign

seeds is called heterogeneous nucleation. The latter process, where a single liquid phase forms the nuclei spontaneously, is called homogeneous nucleation. This homogeneous nucleation has a profound influence on the obtained size distribution of the NP. When the formation of nuclei is happening randomly in time, all particles have a different growth history ( $\sim$  age). This will result in uncontrolled growth and a broad size distribution. However, when all nucleation occurs at once, the particles will have similar ages and will grow simultaneously. Such rapid nucleation generally results in a monodisperse set of NP. Even though a heterogeneous nucleation can achieve similar results, the preparation of highly uniform small seeds is difficult and hence not very popular.<sup>27,28</sup>

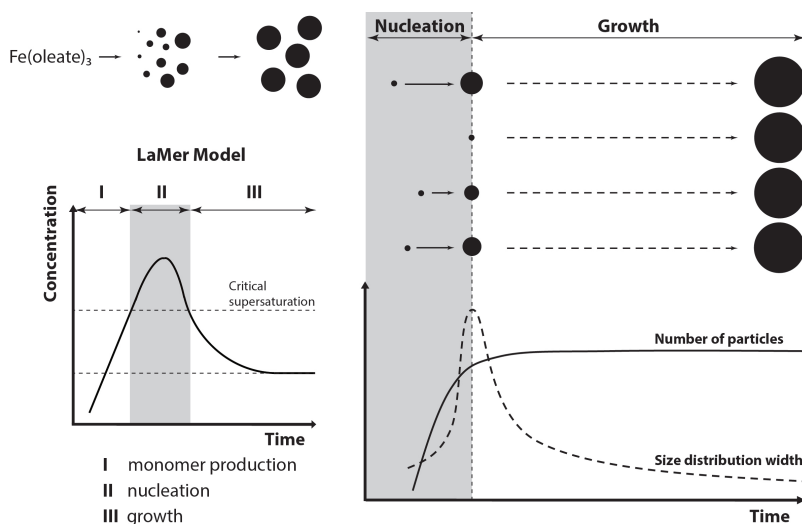


Figure 1.3: The LaMer model is often used to explain the principle of supersaturation and nucleation. When the concentration of monomers reaches the critical supersaturation limit, nucleation will start. During the nucleation stage, the nuclei for further NP growth are formed. After the supersaturation has lowered, the growth regime starts (shown at the right), during which the particle size is focused, resulting in a monodisperse set of NP. The size distribution width shows the transformation of a polydisperse intermediate product to a monodisperse end product.<sup>29</sup>

During homogeneous nucleation (the in situ formation of nuclei) a large energy barrier has to be overcome, which is achieved by the critical supersaturation level of starting products, also called monomers (see Figure 1.3, *LaMer model*).<sup>15,27,29,30</sup> An advantage of this process is that when nucleation and initial growth have started, the supersaturation level quickly lowers, which terminates the nucleation automatically. This largely reduces the time frame in

which nucleation occurs and is therefore known as burst nucleation. Although this system approaches the ideal case of a single nucleation event, it is not a guarantee for a narrow size distribution. During the burst nucleation, the growth of the particles already starts, due to the supersaturation. At the end of the nucleation stage, a series of NP with different growth histories is present in solution (see Figure 1.3). Nevertheless the process of nucleation is crucial to consume the starting products and eliminate unwanted nucleation at later stages in the reaction. As long as the duration of the process is much shorter than the growth process, the NP will have a similar age and a narrow size distribution can be achieved during the next step of the nanoparticle formation.

The reaction on the surface of the growing NP, turning dissolved monomers into solid mass, is reversible. A dissolved monomer precipitates onto the surface of a particle, thereby turning into a solid. This process, called diffusion controlled growth, occurs when the concentration of dissolved monomers is much larger than the solubility of the particle itself. When this concentration lowers, the mass transport direction can reverse, dissolving the particle. At the point where no monomers are present in solution anymore, small particles will be consumed by large particles. This phenomenon is known as *Oswald ripening* and is very important in nanoparticle synthesis. It is caused by the difference in chemical potential between small and large NP, with smaller NP having a higher chemical potential (being more unstable). When the monomer concentration becomes low, the reversed mass transport reaction dissolves small nanoparticle thereby releasing monomers, while the more stable large nanoparticles keep growing by these released monomers.<sup>27</sup>

## Thermal decomposition

A large variety of NP can be produced by the thermal decomposition of organometallic precursors in high boiling organic solvents, with the addition of surfactants. Thanks to the successful synthesis of semiconductor NP by this method, similar methods for the production of magnetic NP were developed. Possible organometallic precursors are based on metal complexes of acetylacetonate (acac), N-nitrosophenylhydroxylamine (cup), carbonyls, oleic acid, other fatty acids or oleylamine. Besides the choice of the precursor, the solvent, extra surfactants, the reaction temperature, the reaction time and the ageing period have a profound influence on the size and shape of the obtained NP.<sup>15,28,30,31</sup> Jana *et al.* reported as one of the first that the synthesis of metal oxide NP was possible by thermal decomposition of metal fatty acid complexes. They proved that the concepts, derived from semiconductor NP syntheses, were valid for metal oxides.<sup>31,32</sup> Six months later later, Park *et al.* published a protocol for a very large scale synthesis of magnetite nanoparticles.<sup>12</sup> They

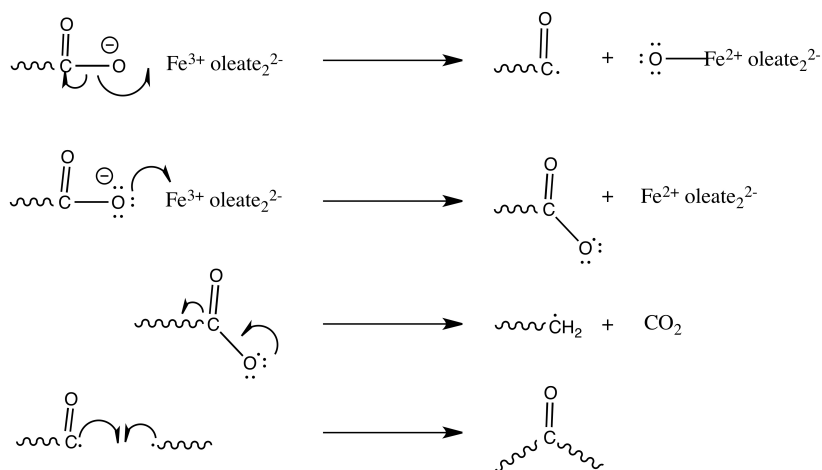


Figure 1.4: The decomposition of iron-oleate at high temperature happens via a radical process. Carbondioxide gas is released from the oleate molecules in one of these reaction steps. (Figure adapted from Perez *et al.*)<sup>34</sup>

used iron-oleate as the organometallic precursor, which was decomposed in 1-octadecene (as solvent) and oleic acid (as surfactant) at 320°C. Later on, the decomposition of iron pentacarbonyl was described, which is known as one of the best syntheses for monodisperse iron NP.<sup>33</sup> A second step is necessary however to oxidize the NP further to magnetite. Nevertheless the latter method is used less often due to the toxicity of the organometallic precursor. In this dissertation, the thermal decomposition of iron-oleate, as described by Park *et al.* was used to produce the magnetic NP.<sup>12</sup>

The so-called ultra-large synthesis of iron oxide NP is based on the decomposition of  $\text{Fe}^{3+}(\text{oleate})_3$ . The exact reaction mechanism is not known yet.<sup>35</sup> Since the magnetite particles have  $\text{Fe}^{3+}$  and  $\text{Fe}^{2+}$  in their crystal lattice, a reduction reaction has to occur. Perez *et al.* have published the most complete description so far.<sup>34</sup> They found out that the heating of the oleate precursor results in the formation of radicals (see Figure 1.4). These reactions provide the oxygen for the oxide formation as well as the reduction of  $\text{Fe}^{3+}$  to  $\text{Fe}^{2+}$ . The radical byproducts can combine to form ketones, that were detected at different stages in the reaction.<sup>34</sup> Several different opinions about the influence of temperature can be found in literature. Perez *et al.* stated that the first decomposition step of the oleate precursor already starts at 200°C.<sup>34</sup> Kwon *et al.* on the other hand, reported that this reaction occurs at 275-300°C.<sup>28</sup> Both reports agree on the radical mechanism and the production of  $\text{CO}_2$  during the reaction.

After their synthesis, the NP have a coating of oleic acid molecules, which are very apolar (oleic acid is a component of olive oil). The particles only disperse in apolar solvents (hexane, heptane, chloroform, dichloromethane, ...) at this point. For further use in aqueous applications, the surface has to be modified with a polar moiety. The following section will give an overview of different functionalization strategies and their main properties.

### 1.3 Surface functionalization

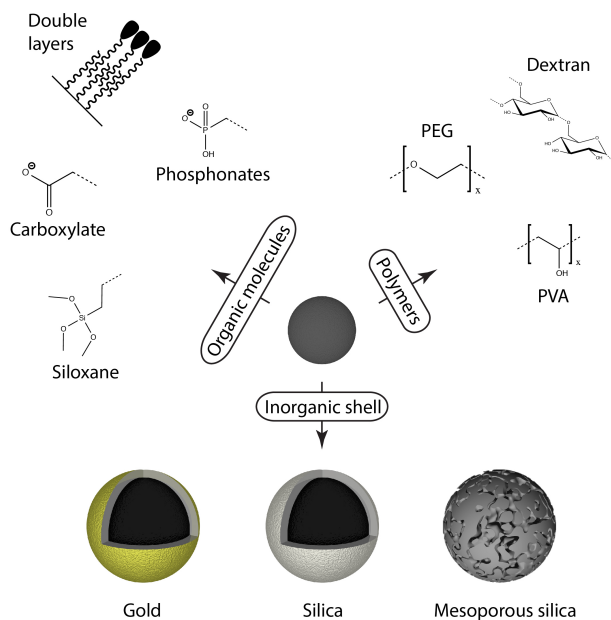


Figure 1.5: Overview of different ways to functionalize iron oxide NP: organic ligands (to form mono- or bilayers), polymers or inorganic shells.

Coating the surface of a nanoparticle is generally performed to improve the chemical or physical stability. Some NP, such as elemental Fe, Co or metal alloys, are very sensitive to oxidation by air. A surface coating protects the crystal from the environment and sustains the properties of the core. The physical stability of a nanoparticle should be regarded at a larger scale: the colloidal stability in the medium and prevention of aggregation. In general, the coating strategies can be divided into two groups: organic or inorganic shells

(see Figure 1.5). The organic shells include monomeric surfactants, polymers, double layers or proteins. Inorganic shells are usually based on silica ( $\text{SiO}_2$ ), carbon, metals (Au, Ag) or oxides.<sup>15</sup> The process of changing the initial ligand with a new molecule or shell is called *ligand exchange*. As an alternative, NP can be embedded in a matrix, such as a polymer, silica or composites. This prevents aggregation and oxidation, but the particles are fixed spatially and this limits their applicability.<sup>15</sup>

## Polymer coatings

The most common coatings described in literature are dextran, carboxymethylated dextran, sulfonated styrene, starch, polyvinyl alcohol (PVA) and polyethylene glycol (PEG).<sup>23,36</sup>

Dextran is a polymer, consisting of polysaccharides with varying chain length and branching and is often used because of its biocompatibility. It interacts via chelation or hydrogen bonding with the surface of iron oxide. Although these hydrogen bonds are weak, the polymer molecules have numerous hydroxyl groups and the total bonding energy hence becomes very large. PEG and PVA are very hydrophilic and water-soluble polymers. These coatings are biocompatible and provide the NP with excellent solubility and stability in aqueous environments.

Even though the resulting colloidal properties of these polymer-coated NP are often very good, the lack of control over the shell thickness and density of the layer makes this approach less favourable.<sup>37</sup> Most methods are based on a non-covalent interaction between the polymer and the surface, which limits the robustness and applicability. Physisorbed drug molecules can be lost before they reach the target site. Another issue arises when the coating of the particle is removed, since this results in aggregation and consequently adverse effects on cells or tissue.<sup>38</sup> These problems have been addressed by cross-linking the polymer layer, which increases the robustness but complicates the synthesis of the nanoparticles. Moreover, controlling the presence and availability of functional groups on the polymer layer is difficult and generally requires more advanced methods such as grafting-from or grafting-to.<sup>37,38</sup>

## Inorganic shells

The introduction of inorganic shells on iron oxide NP can be performed from two different points of view: protect the magnetic core from the surrounding environment or introduce a new property (such as plasmonic or catalytic

materials). The first is often achieved by the growth of a silica shell on the surface, which is inert and forms a dense protective layer. The latter, introducing a new property can be accomplished by the growth of a golden or silver shell. These materials have interesting properties such as plasmons, catalytic or antimicrobial activity.<sup>39–41</sup> An important advantage of inorganic shell formation is the high degree of control that, compared to polymers, can be achieved over the shell thickness and shape.

Silica coatings are well-established for magnetic NP, since it prevents aggregation, improves the chemical stability and lowers the toxicity by ion leaching. Moreover the shell is negatively charged, stabilizing the NP by coulombic repulsion. Three methods are developed to growth the shell: the Stöber process, silicic acid and emulsions methods.<sup>42–44</sup> The Stöber process is very well-known and relies on the hydrolysis and polycondensation of a silica precursor such as tetraethyl orthosilicate (TEOS).<sup>42</sup> Emulsions (micelles or inverse micelles) are of particular interest for modification of apolar iron oxide NP, since the shell is usually grown directly on top of the present oleic acid surfactant. In this case, extra surfactants are added to make the NP disperse better, such as Igepal CO-520 or cetyltrimethyl ammonium bromide (CTAB).<sup>45</sup> However, this complicates the workup of the resulting core-shell NP. More complex silica can be produced using a large excess of surfactants, resulting in mesoporous silica. These structures have a very large surface thanks to the pores and can be used for drug delivery.<sup>45</sup>

Coating iron oxide NP with a gold layer is not trivial since the two crystal structures do not match well. Recently, progress has been made by performing the reaction at higher temperatures, starting from an organometallic precursor (gold acetate) in an apolar medium.<sup>46</sup> Other approaches are often done in aqueous environments by chloroauric acid or seeded growth.<sup>41,47</sup> Post-functionalization by thiol-containing molecules is straightforward, thanks to the strong bond between thiols and gold. Moreover, the surface is chemically inert and has interesting optical properties.<sup>48</sup>

## Monomers and bilayers

Small organic molecules can also be used to form stabilizing layers on iron oxide NP. They can be chemically anchored or physically adsorbed to the surface, in a single or double layer. Well-known functional groups that interact strongly with the surface by forming a coordination bond are carboxylic acids, phosphates or catechols. Another class of molecules, siloxanes, are capable of forming a covalent bond with the nanoparticle's surface.<sup>23,49</sup>

Functionalization by a coordination bonding molecule is one of the most straightforward methods. Citric acid (citrate) is a widely used ligand in this

regard. Two of its carboxylates interact with the surface, leaving the third exposed to the solvent, providing a negative charge to the particle.<sup>50</sup> However, this type of bond is labile and is prone to break by increasing temperature, extreme pH or the presence of other ligands. Similarly, phosphonic acid (phosphonate) forms a coordination bond, albeit stronger than by a carboxylic acid.<sup>51</sup> This makes it possible to replace for instance oleic acid on the surface in a single step without complex two phase systems.<sup>52</sup> Those ligands show good chemical stability at neutral pH during several weeks.

Catechols-containing ligands are a recent development in surface chemistry.<sup>53–55</sup> These 1,2-dihydroxybenzene derivatives showed an exceptionally high complexation constant with metal ions ( $\log K \approx 30\text{--}40$ ), making the bond almost irreversible.<sup>56,57</sup> The concept of using catechols as highly versatile ligands is derived from nature itself, since the molecule is present in the adhesive proteins secreted by mussels for attachment to wet surfaces.<sup>55</sup> The large variety of commercially available catechol-containing molecules (dopamine, 3,4-dihydroxyhydrocinnamic acid, ...) has caused a large increase of publications about these ligands in recent years. A minor disadvantage of dopamine is its tendency to polymerize into polydopamine. This issue was addressed by the introduction of a nitro group onto the phenyl ring.<sup>58</sup>

Alternatively, the already existing oleic acid layer can be used to form a double layer. To achieve this, amphiphilic molecules (phospholipids) are added to the freshly prepared apolar NP, which will encapsulate the particle and form a double layer. This is stabilized by the hydrophobic interactions between the oleic acid and phospholipids.<sup>59</sup>

## Siloxanes

Some organic molecules, called silanes, have silicon atoms incorporated in their structure. A subgroup of these are the organosilanes, which have one or more organic groups. Siloxanes are member of this organosilane group, but they have at least one alkoxy bond present in their molecular structure. These molecules are of particular interest for the functionalization of iron oxide NP, since they can form a covalent bond with the surface, while introducing functional groups. They are frequently used for the modification of oxide surfaces (glass, metal oxides, ...) and hence a large variety of these siloxanes is commercially available.<sup>60–64</sup>

In the presence of water, one of the alkoxy groups (usually methoxy or ethoxy) splits off by an acid- or base-catalysed reaction (see Figure 1.6). This so-called silanol molecule can polymerize with another silanol molecule via a condensation

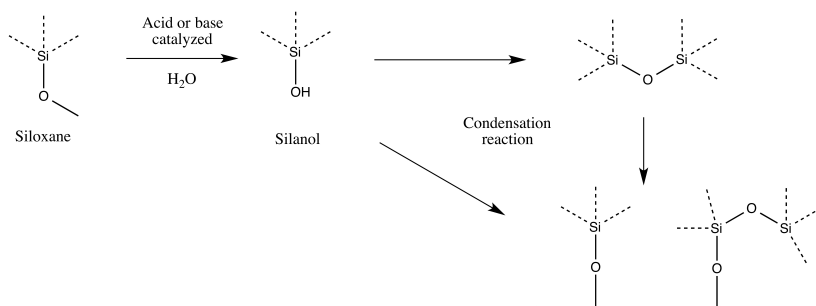


Figure 1.6: The alkoxy siloxane molecule is first hydrolyzed to a silanol molecule by an acid- or base-catalyzed reaction. This molecule can polymerize or react directly with the hydroxyls on the surface.

reaction or directly interact with the hydroxyl groups on the surface of the nanoparticle via a similar condensation reaction.<sup>65</sup>

## 1.4 Colloidal stability

In a colloidal system, with particles of similar sizes, several interaction forces have an influence on the overall stability of these particles. These forces, responsible for the behavior of NP in solution, usually are the electrostatic repulsion and van der Waals attraction. Moreover, hydration and steric repulsion can also have a significant impact if less charges are present. In the following section, the concepts that are applicable to the NP presented in this dissertation, will be discussed further in detail.

### DLVO theory

The most common way of stabilizing NP is by making use of electrostatic repulsion. This repulsion occurs when particles have a similar charge and is very effective in preventing particle aggregation. In Figure 1.7, this electrostatic repulsion is shown by the red curve. It quickly grows at smaller distance due to the close proximity of the charges. Besides this repulsion, an attractive force is also present in colloidal systems, the van der Waals forces. These dipole related forces are smaller and are more pronounced at smaller distances between the dipoles. It is the sum of the Keesom, Debye and London forces, respectively the attraction between two permanent dipoles, a permanent and induced dipole

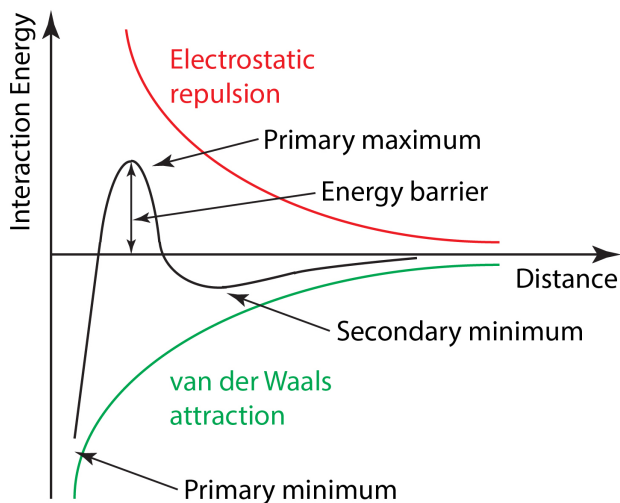


Figure 1.7: The DLVO theory (for a system with a high salt concentration) describes the sum of the van der Waals attraction and electrostatic repulsion. The primary minimum represent an irreversible aggregate, while the secondary minimum shows a flocculated state, which is reversible. An energy barrier has to be overcome to reach this irreversible aggregated state, which is related to the collision speed of the particles.

and the spontaneous oscillations of electrons that create temporary dipoles. Usually in colloidal systems, the London forces are most important. In Figure 1.7, the van der Waals force is shown by the green curve. The sum of both (see Figure 1.7, black curve) essentially explains the behavior of a colloidal system and can be used to determine whether it will be stable in time. This concept was developed by *Derjaguin, Landau, Verwey* and *Overbeek* and was hence called the *DLVO* theory.<sup>66,67</sup> It provides a framework that considers the total interaction energy of two NP to determine the stability of colloids. When two particles with similar charges approach each other, a small attractive force is present due to the van der Waals forces. This results in a minimum (secondary) where the particles are loosely packed together, called flocculation. So far the interactions are still reversible. If the particles would come even closer together, the repulsive force, due to their charges, creates a energy barrier that the particles have to cross. If the collision energy (from Brownian motion) is large enough, the particles can cross the barrier and end up in the primary minimum. This is the point of irreversible aggregation and minimal energy, and often results in precipitation. If the particles are highly charged, the barrier becomes very high and this would ensure colloidal stability since the particles

cannot end up in the primary minimum. This DLVO theory is dependent on many different parameters that determine the initial attraction of repulsion of two particles. For instance, at high charge densities, the overall force is repulsive, since the interaction is dominated by the double layer contribution. At small charge densities, the interaction is dominated by the attractive van der Waals force. In this work, the relation between a functional group and its zeta potential is discussed in Chapter 3, while in other chapters stability will be achieved by steric repulsion rather than electrostatic repulsion.

## Zeta Potential

Most oxide materials are charged by nature, since the presence of hydroxyls on their surface makes them partially pH responsive. This charge attracts ions with an opposite charge, that stick to the surface of the particle, forming the Stern layer. A second more diffuse layer is also formed, that has more mobile charges. The potential, caused by the surface charges, at the edge of the Stern layer is called the Stern potential, while the potential at the edge of the diffuse layer (slipping plane) is called the *zeta potential*. The latter is an important concept in colloid physics, since it gives a relatively good indication of the colloidal stability of a charged particle. It can be measured in an adapted dynamic light scattering experiment where the electrophoretic mobility of the particles is translated into a zeta potential value. If an absolute value higher than 25-30 millivolts (mV) is measured, the particles are said to be colloidally stable in time.<sup>68</sup> If the absolute value is lower than 25 mV, the system is probably not stable and aggregation will occur in time. However, this theory does not take any other repulsive forces, such as steric hindrance, into account. Therefore the value of the zeta potential is only important for highly charged particles, without presence of steric stabilizers. In this work, steric repulsion is far more important than electrostatic repulsion, hence the measurement of the zeta potential was often omitted due to its limited contribution. For example, a PEG coated nanoparticle will have a very low potential due to the absence of charged groups, insinuating colloidal instability, while these particles show exceptional stability in time. Nevertheless, this concept is generally accepted as one of the only ways to measure the stability of a nanoparticle dispersion.

## 1.5 Protein coronas

When NP enter a biological fluid (for instance blood), their surface is instantly covered by a layer of proteins, which is called a *protein corona* (see Figure 1.9). This newly formed corona alters the interfacial properties, size and aggregation

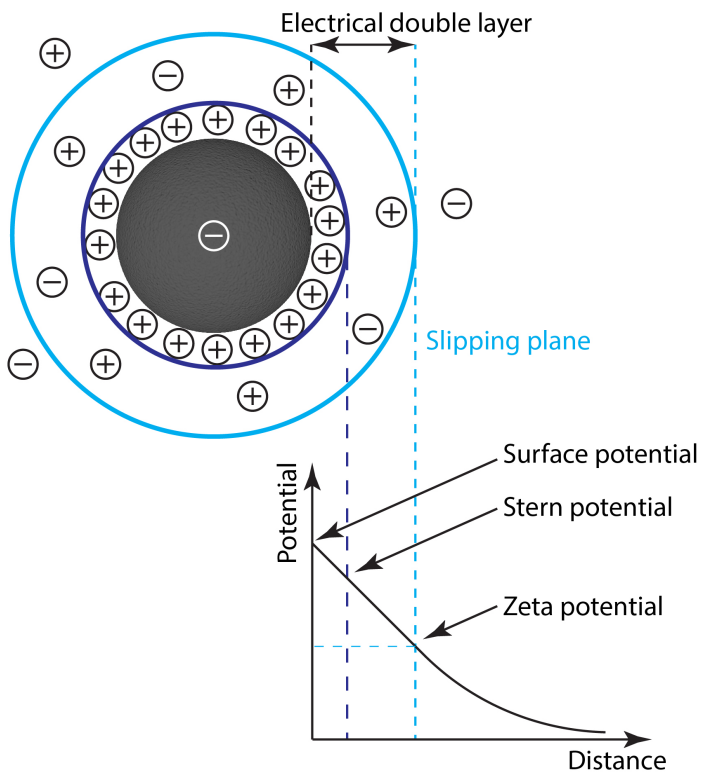


Figure 1.8: A negatively charged nanoparticle attracts a layer of positive ions, which are almost strongly bound, to its surface, called the Stern layer. The next layer is more diffuse and partially compensates the charge of the inner layers. The edge of the layer is called the slipping plane, which is the point where the zetapotential is measured.

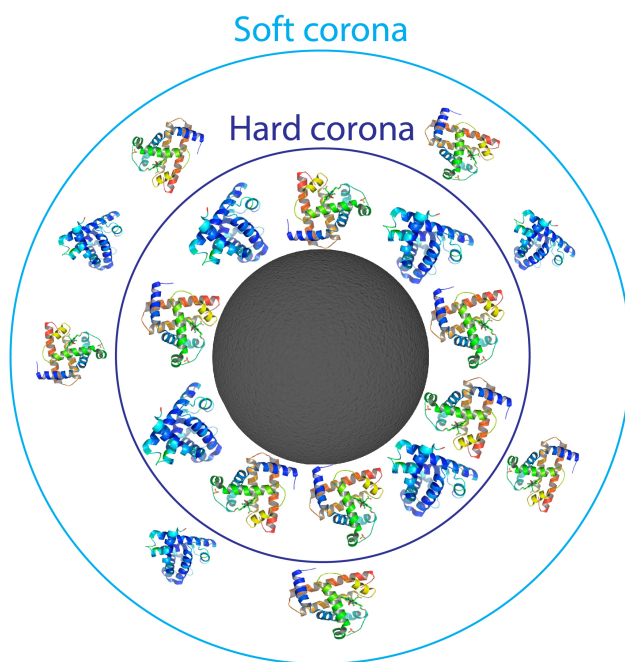


Figure 1.9: Two different protein layers are spontaneously formed around the nanoparticle: a hard corona on the surface and a soft corona as a second layer, which is more dynamic.

behavior of the nanoparticle. Moreover the NP gain a biological entity that is different from the initial synthetic identity. Their biological identity will determine whether NP can cross certain barriers or membranes and how the interaction with other biomolecules will occur.<sup>69–73</sup>

Two different types of coronae are formed around a nanoparticle: a hard and a soft one. The *hard corona* is defined as the first layer of proteins that are strongly interacting with the surface. The *soft corona* is the second layer of proteins, that have no direct contact with the surface, but have solely protein-protein interactions. Both layers show different kinetic behavior, with the soft corona having a faster exchange of proteins, while this is rather slow for the hard corona. The initial protein layer formation is thermodynamically driven, since it lowers the surface free energy of the nanoparticle. The protein composition of this layer depends fully on the concentration and nature of proteins in the surrounding liquid. For instance in blood, the high concentration of serum albumin will initially cause a high presence in the hard corona (kinetically

driven). But in time, less abundant proteins with higher affinity and slower kinetics might displace them (thermodynamically driven). Nevertheless, the protein corona is what a cell sees of a nanoparticle since it cannot directly interact with the nanoparticle's core and is hence a very important concept in nanoparticle science.<sup>71,74</sup>

## 1.6 Antibodies

The human body is defended by an adaptive immune system, that has evolved to recognize a great variety of antigens from bacteria, viruses or other pathogens. The antigen-recognizing molecules (on B-cells) are called the immunoglobulins (Ig) (or antibodies (Ab)) and are produced in a vast range of antigen specificities, even though each B-cell produces Ig of just one single specificity. They come in two forms, membrane-bound or secreted (which are structurally different), depending on the type of B-cell. These Ab serve two functions: binding to the molecules (from the pathogen) that initiated the immune response and to rally other cells and molecules to the pathogen to destroy it. For example, an antibody can bind to a virus, making it ineffective and marking it for destruction.<sup>75</sup>

### Structure

Ab are roughly Y-shaped proteins that have three portions of equal size, connected by a flexible linkage, called the hinge. The twofold purpose of an antibody is visible in its structure (see Figure 1.10). One part specifically binds the target antigen while another part influences recognition and removal mechanisms. The first part varies greatly between different Ab, and is hence called the *variable region* ( $V_L$  and  $V_H$ ), which is a substructure of the *antigen binding region* (Fragment antigen binding, Fab). The Fab fragment is build up from a complete light chain and part of the heavy chain. The large variability makes that Ab can bind to a wide range of pathogens and virtually any structure can be recognized. The second part, that can activate removal mechanisms, has less variation and is hence called the *constant region*. It was originally observed to crystallize easily and was called the *fragment crystallizable* (Fc). Five main classes of these constant fragments exist, which divides the Ab into classes, namely IgG, IgM, IgD, IgA and IgE. The immunoglobulin G (IgG) class is the most abundant in the human body.<sup>75</sup> A single pathogen can have many possible binding sites for Ab, called epitopes. As these Ab are produced by many different cells (1 cell = 1 type of antibody), they are called polyclonal. They are all targeting the same pathogen, but have a different variable region and bind to different epitopes. While this is advantageous for fighting infections

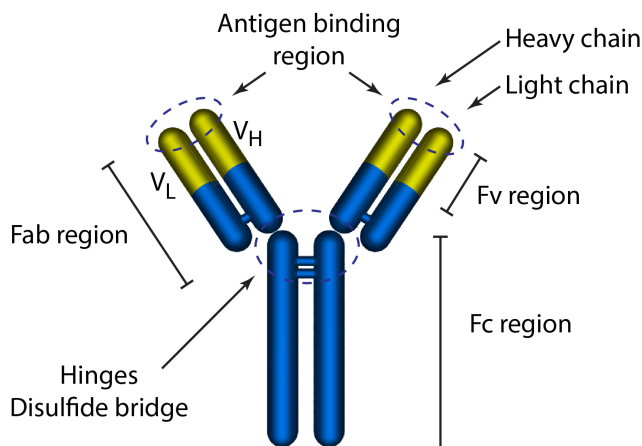


Figure 1.10: An antibody is roughly Y-shaped and has different regions with separate functions. The bottom Fc (Fragment crystallizable) part has no antigen binding properties, but is responsible for the activation of removal mechanisms. The top Fab (Fragment antigen binding) part is responsible for the interaction with the antigen and is build up from the complete light chain and part of the heavy chain. In between the two part, a flexible region is present, called the hinge.

in nature, the heterogeneity sometimes hinders their applicability in research. The following section will give more insight in the production of antibodies.<sup>75</sup>

## Production

Two main types of Ab can be obtained: mono- and polyclonal Ab. The latter were discussed in the previous paragraph, being a set of Ig produced by different B-cells, all targeting the same antigen but on different epitopes. Monoclonal Ab on the other hand represent a set of Ig that all target the same epitope and are produced by the same cell. This major breakthrough in the research and development of Ig was accomplished by Köhler and Milstein in 1975.<sup>76</sup> They fused the B-cells (that produce the Ab, but do not divide indefinitely) with immortal myeloma tumor cells. This resulting single hybrid cell is known as a hybridoma cell, which produces Ab and can divide indefinitely and grow well in cultures. These cells however are clones of each other and hence all secrete the same antibody, which is monoclonal.<sup>75,77,78</sup> Alternatively, the hybridoma cells can be injected into the abdomen of a mouse, where they will multiply and produce Ab, which is know as the *mouse ascites method*.

Table 1.2: Comparison of monoclonal and polyclonal antibodies, including their advantages and drawbacks.<sup>75,78</sup>

	Monoclonal	Polyclonal
Production	<i>in vitro</i> (hybridoma cells)	mostly <i>in vivo</i>
Target	one epitope	multiple epitopes
Cost	expensive	relatively cheap
Technology	highly complex	relatively easy
Production time	long (> 6 months)	short (2-3 months)
Batch to batch	identical	large variability
Scale	very large	limited
Cross-reactivity	very low	possible, depending on level of purification

Polyclonal antibodies on the other hand are acquired from the blood of an immunized animal. In short, a rabbit or goat is injected with a pathogen (or antigen (Ag)), after which the immune system is given time to produce an immune response in the form of Ab. After a second (or even third) boost with extra antigens, the blood from the animal is collected and purified.

Purification of Ab is usually performed via affinity column chromatography with proteins that strongly bind Ab, for instance protein A (*Staphylococcus aureus*), G (*Streptococcus* spp.) or other Ab. Depending on the starting material, derived from an *in vitro* culture of hybridoma cells or serum of an immunized animal, this process results in monoclonal Ab or the whole IgG fraction present in the serum. This fraction can later be purified further to collect all the Ab targeting a certain antigen. Again affinity column chromatography can be used to perform this purification step.<sup>77,79–82</sup> Instead, polyclonal Ab can also be prepared by mixing several monoclonal Ab together.

The main differences between the two types of Ab, mono- and polyclonal, are summed up in Table 1.2.

## 1.7 Coupling chemistry

The covalent attachment of proteins onto nanoparticles is a widely investigated research domain. Hundreds of methods have been described in scientific

literature, including zero-length, homobifunctional, heterobifunctional and even trifunctional cross-linkers. The following section will give a brief overview of the zero-length coupling options (no extra atoms after coupling) that require no modification of the protein itself, since this approach was used in this dissertation. A complete overview can be found in the book *Bioconjugate Techniques* written by G. T. Hermanson.<sup>83</sup>

The smallest possible coupling between two entities is via zero-length cross-linkers. These molecules are capable of connecting two molecules, without leaving behind extra atoms, intervening linkers or spacers. Definitely in the case of antibody coupling, the presence of linker molecules can induce possibly unwanted cross-reactivity. Moreover, the modification of Ab prior to coupling, such as cleavage of the disulfide bonds or oxidation of their carbohydrates, alters their structure and can have a negative impact on the affinity and stability of the protein.<sup>84,85</sup> Hence, the most common way of cross-linking Ab to a substrate is by means of their already present functional groups: carboxylic acids or amines.

## Carbodiimides

Carbodiimides are by far the most well-known mediators for the formation of amide linkages between amines and carboxylic acids. Similarly they can form phosphoramidate bonds between phosphates and amines. The carbodiimides can be divided into two classes: water soluble or insoluble. The first are of course the most common choice for coupling reactions involving proteins, since these are only stable in aqueous environments. The water insoluble carbodiimides on the other hand are frequently selected for peptide synthesis or coupling of molecules in organic solvents.

Essentially all carbodiimides react via the same reaction pathway, as shown in Figure 1.11. The diimide reacts with a carboxylic acid to form a highly reactive O-acylisourea intermediate. This molecule will then react with a primary amine to form an amide bond. Other nucleophiles, such as thiols or hydroxyls, can also attack the O-acylisourea molecule. This implies that hydrolysis by water is a major competing reaction, forming an isourea, setting the carboxylic acid free again, resulting in a net loss of diimide starting product (see Figure 1.11).<sup>86</sup> In aqueous environments, EDC is the most commonly used reagent. Another possibility is 1-cyclohexyl-3-(2-morpholinoethyl) carbodiimide (CMC). For organic solvents, dicyclohexyl carbodiimide (DCC) and diisopropyl carbodiimide (DIC) are often selected.<sup>83</sup>

The reaction between the O-acylisourea intermediate and an amine is unfortunately slow and hydrolysis in aqueous solutions is prone. If the amine

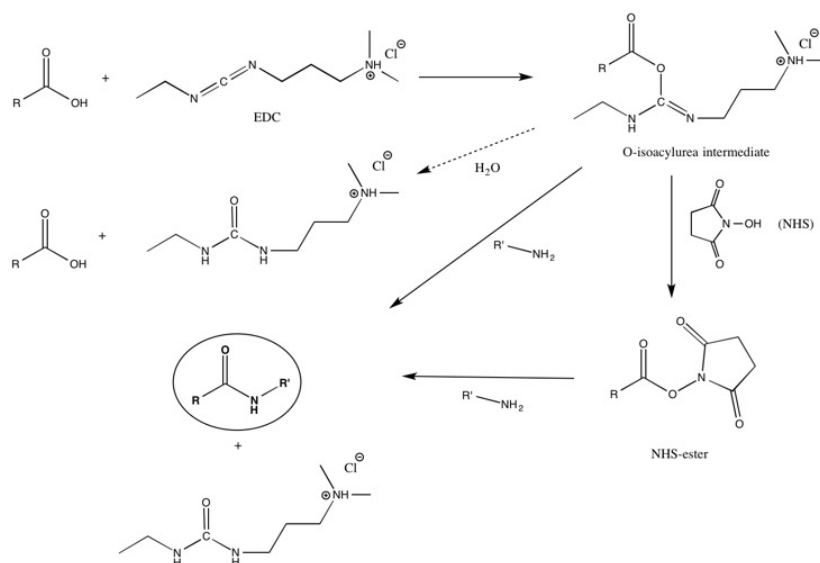


Figure 1.11: A typical reaction between a carbodiimide (1-ethyl-3-(3-dimethylaminopropyl)-carbodiimide hydrochloride (EDC)) and a carboxylic acid, starts with the formation of a O-isoacylurea molecule. This can reaction directly with an amine to form the amide product. Usually N-hydroxy succinimide (NHS) is added to form a NHS-ester, which is more stable. This ester will then react with the amine to form the amide product. An important side reaction is the hydrolysis of the intermediate, resulting in a net loss of EDC.

does not find the activated carboxylate before hydrolysis occurs, the coupling will fail. This situation is especially occurring in coupling reactions with proteins, since those are dissolved in water at relatively low concentrations. To solve this issue, NHS can be added to the reaction. This way a reactive NHS-ester can be formed (see Figure 1.11), that can react rapidly with amines. Moreover, this ester hydrolyses very slowly, allowing to purify the product at this stage. Overall, the addition of NHS to a coupling reaction increases the efficiency more than 20-fold, as investigated by Staros *et al.*<sup>87</sup> This improved efficiency has the unexpected consequence that the coupling might be too efficient and hence causes excessive cross-linking (and precipitation). Scaling the amount of EDC and NHS will solve this problem.

In this dissertation, carboxylic acid groups on the surface of the NP were coupled to amines on the Ab. The opposite reaction (with amines on the NP) could also have been performed. However this has a major disadvantage: proteins have both carboxylic acids and amines; activation of the carboxylic acids would

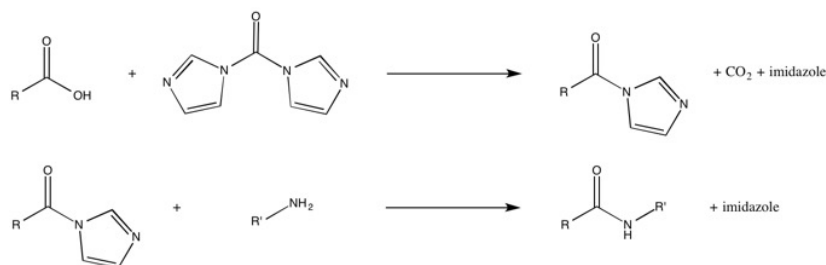


Figure 1.12: CDI reacts with a carboxylic acid group and form a N-acylimidazole with the liberation of CO<sub>2</sub> as the driving force. Next, this reacts with an amine to form the final amide bond.

lead to severe protein-protein cross-linking. The NP were designed to have only carboxylic acids and no amines, which can safely be activated by EDC and NHS. An extra advantage of the usage of EDC is the introduction of charges, which might help to stabilize the functionalized NP.

## N,N'-carbonyl diimidazole

N,N'-carbonyl diimidazole (CDI) is very efficient activator of carboxylic acids. It is capable of forming a zero-length bond between the acid and an amine, or a one-carbon-length bond between two amines (as a ureum), or a hydroxyl and an amine (as a N-alkyl carbamate). A carboxylic acid reacts with CDI and forms a N-acylimidazole compound that is highly reactive. This formation is very efficient and produces high yield thanks to the liberation of carbon dioxide as the driving force. The activated carboxylate can react with amines or hydroxyls to form amides or esters, respectively. Figure 1.12 shows the reaction of CDI to form an amide.<sup>83,88</sup>

The major disadvantage of CDI is that it is extremely sensitive to the presence of water. Hydrolysis will break down CDI instantly to CO<sub>2</sub> and imidazole. Therefore all reactions should be performed in dry solvents. An advantage is the very rapid activation of carboxylic acids, which also releases characteristic gas bubbles, which indicate a successful reaction. All excesses of CDI should be removed from the reaction mixture before the addition of the amine, since side reactions can occur at that point. Adding a small amount of water can be used for this. Hydrolysis of the activated carboxylate by water is a possible side reaction, but occurs much slower than the nucleophilic attack by a primary amine.<sup>88</sup>

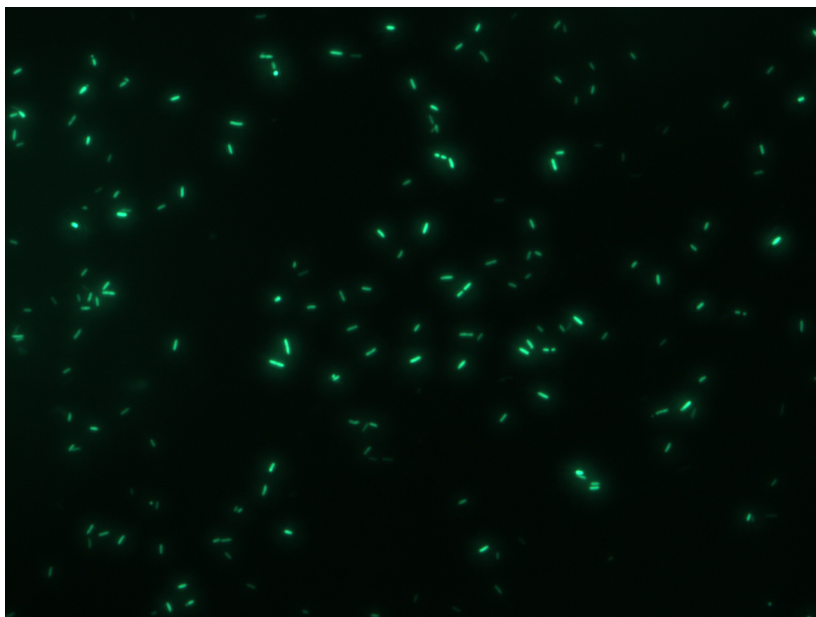


Figure 1.13: Fluorescence image of *L. pneumophila* bacteria (recombinant strain expressing the green fluorescent protein (GFP)), which are around  $2\text{ }\mu\text{m}$  long and  $0.5\text{ }\mu\text{m}$  wide. The rodlike shape is clearly visible.

## 1.8 *Legionella pneumophila*

The aim of this dissertation was to develop an NP-Ab system that targets *Legionella pneumophila* (*L. pneumophila*). These bacteria have a large social relevance and their detection in various aqueous environments (f.i. swimming pools, waste and cooling water) is mandatory by law. The following section will give more insight in the properties of these bacteria as well as their prevalence and detection.

### Ecology of *L. pneumophila*

The *Legionella* bacteria is a Gram-negative, aerobic, rodlike organism that is approximately  $0.5\text{ }\mu\text{m}$  wide and  $2\text{ }\mu\text{m}$  long (see Figure 1.13). It is ubiquitously present in fresh water and is the largest genus of bacteria that survives by parasitizing on free living single-celled protozoa.<sup>89</sup> They are remarkably acid-tolerant (able to withstand pH 2) and have been isolated from environmental

sources with pH of 2 to 8.<sup>90,91</sup> Moreover they have been found in sources as diverse as water on plants in rainforests, groundwater and even seawater.<sup>92</sup>

*Legionella* bacteria thrive at elevated temperature (30-40°C), in water with high (in)organic content and possible host protozoa.<sup>93</sup> This explains why the bacteria are so often found in artificial habitats, for instance warm water systems such as whirlpools, fountains, showers or air-conditioning units.<sup>91</sup> If more than 100,000 colony forming units (CFU) are found in 1 liter of water sample (in Belgium), the facility has to be closed until levels have dropped under 10,000 again.<sup>94,95</sup> This mandatory detection of the bacteria makes detection and pre-concentration techniques highly important.

The exact proliferation mechanism of *L. pneumophila* in protozoan hosts is complicated but is based on overcoming three major hurdles. First, the bacteria are phagocytosed by the host into a phagosome, which usually becomes a very inhospitable environment (phagolysosome). Secondly, they need nutrition and sustenance for growth, which has to be acquired through the vesicle that contains them. Thirdly, the surrounding phagosomes restrict the available space for continuous growth. The *L. pneumophila* bacteria overcome these issues by hijacking the host secretory system and membrane traffic (by dot/icm genes).<sup>96</sup> They camouflage their surrounding vesicle to obtain a steady supply of nutrients from the host and continue to grow.

## Legionellosis

An outbreak of a severe type of pneumonia during an American Legion Convention in Philadelphia led to the discovery and description of the Legionnaires' disease, named after the participants of the conference, in 1976.<sup>97</sup> More than 42 species of *Legionella* have been identified since the first outbreak. A less severe form of the disease is called the Pontiac fever. The Legionnaires' disease causes flu like symptoms, such as fever, headache, chills and muscle pains. It can cause large fatality rates of 40-80% among patients with lowered resistance (f.i. in hospitals). It can be treated by antibiotics such as clarithromycin and azithromycin.<sup>91</sup>

## Detection methods

For the detection of the *L. pneumophila* bacteria, 2 important steps should be considered: pre-concentration and the quantification itself. Since a standardized water sample for official *Legionella* enumeration has a volume of one liter, a pre-concentration step is crucial. No quantification technique is capable of

handling one liter samples directly and taking only small aliquots is not allowed by law.<sup>94</sup> Usually the sample is centrifuged or filtered to collect the harmful pathogens. However both techniques have serious drawbacks inherently related to their mechanism. Centrifugation can obtain high recovery values, but is not target specific and is very inconvenient for large sample volumes making it a very time consuming approach. Filtration can handle these large volumes, but is not specific either and has a profound influence on the cell viability and has issues with complex (dirty) samples.<sup>98</sup> Another technique, immunomagnetic separation, makes use of Ab and magnetic NP to have a target specific magnetic attraction of bacteria from aqueous environments. It is capable of achieving a purification from large volumes, has only limited effect on the cell viability and can be used in complex samples. This method will be developed further for the *L. pneumophila* bacteria in this dissertation.

For the quantification of the bacteria, multiple techniques have been developed: cell cultures, flow cytometry (FCM), enzyme-linked immunosorbent assay (ELISA), quantitative polymerase chain reaction (qPCR), hybridization (DNA or RNA), surface plasmon resonance (SPR) sensors or antibody staining.<sup>99,100</sup> Cell cultures are still considered as the golden standard for the enumeration of bacteria. However, the method is very time consuming, slow (7-10 days) and has issues with the presence of other bacteria if they grow faster than the target.<sup>101</sup> FCM makes use of the specific fluorescent signal and size of organisms for detection and quantification. Unfortunately the technique is expensive and impurities might hinder a correct enumeration.<sup>101,102</sup> qPCR is based on the polymerase chain reaction, in combination with fluorescent tags, for the quantification of target DNA (or RNA in the case of RT-qPCR). It is a fast method, with a low detection limit, but inhibitors (that are often present in an environmental water sample, f.i. metal ions, surfactants or polysaccharides) are a recurring problem. DNA- or RNA-hybridization approaches utilize complementary strands of DNA or RNA to detect the target bacteria. It is a technique with a high specificity, but can only handle relatively low concentrations and free DNA or RNA can result in false positive signals. SPR sensors measure the shift in the plasmon resonance of gold to determine the concentration of an analyte. It is very sensitive but can have problems with aspecific adsorption and false positive signals.<sup>103</sup> Antibody staining on the other hand employs fluorescent antibody conjugates to selectively stain target organisms. Cross-reactivity is a recurring issue with this technique and pre-concentration of the sample is advisable.<sup>100</sup>

The detection methods that were used for this dissertation will be explained in more detail in the appendix.

## 1.9 Objectives and outline

### Objectives and strategy

The increasing interest in functional nanomaterials has led to their implementation in various biomedical applications, either as a therapeutic agent or for diagnostic purposes.<sup>104–108</sup> NP with magnetic properties are well-known for their potential in magnetic resonance imaging (MRI), for which commercialization has been achieved (Feridex, Endorem). However, applications regarding selective magnetic purification are more scarce in scientific literature. These studies are often approached from either the synthetic or biomedical side, lacking an optimal design on the other side. A thorough nanoparticle synthesis and functionalization is often combined with a less comprehensive separation study and vice versa. Moreover the complexity of the syntheses often makes implementation in applications rather hard. In this dissertation a complete nanoparticle platform for magnetic purification of targeted organisms will be described that pays attention to all relevant properties, ranging from the nanoparticle's synthesis to their functionalization and testing their performance in several relevant applications, with an extra focus on reproducibility and low cost.

Three major material properties were identified as being crucial for the development of a **NP-based magnetic separation platform**. First, the synthesized core nanoparticle should be *well-defined, in terms of size and shape*. Moreover the reduction of batch-to-batch difference, and hence an improved reproducibility was an important rationale. Secondly, the available surface modification procedures of these particles had to be improved to meet two crucial requirements: a *fast and highly reproducible functionalization method that allowed covalent bonding of the ligand* to the surface. Thirdly, a new ligand had to be designed that combined all properties necessary for the intended applications. The *presence of a functional group and improved colloidal stability, combined with the possibility to covalently bind to the surface* of iron oxide were considered the primary requirements.

The synthetic method for nanoparticle production was chosen from dozens of possible approaches. Despite the complex setup and high temperatures, thermal decomposition of iron-oleate was selected mostly for its scalability, price, reproducibility and high nanoparticle quality.<sup>12</sup> For the surface functionalization less information was found in literature. Covalent surface modification is hardly described for oleic acid-coated magnetite NP and the available procedures were rather unreproducible during the initial tests. Therefore a new method was developed that was capable of introducing siloxane ligands covalently on the surface of iron oxide. The ligands required for the successful development of

the nanoparticle platform, needed several properties, such as improved colloidal stability of the NP and the possibility to perform subsequent coupling chemistry, combined with the presence of a siloxane group for covalent bonding to the surface. Since this product was not commercially available, a new synthesis was developed, keeping in mind that it should be highly reproducible, but also cost-effective (in terms of starting products) and easy to perform. Thiol-ene click chemistry was used in this regard and proved to be a valuable approach towards the synthesis of a highly effective new ligand.

## Outline

The **second chapter** will explain in more detail how the NP were synthesized and introduces the new functionalization procedure that was developed. Several characterization techniques were used at this stage to fully characterize the core material. The surface modification procedure was tested thoroughly by introducing multiple different siloxane molecules onto the surface of iron oxide NP. Moreover their colloidal stability in buffer systems was investigated, which was correlated with their zeta potential.

Because the commercially available siloxane ligands do not have the required functionalities, a new ligand molecule was designed and synthesized. **Chapter three** gives an overview about the synthetic details and how the ligand was introduced onto the NP. Furthermore, Ab were coupled to the molecule to underline its potential in biomedical applications. ELISA was introduced at this point as a new approach to quantify the amount of coupled proteins on the NP. The activity of these bioconjugated particles was tested by SPR measurements.

Functionalization of metal oxide surfaces by siloxanes is a well-established approach, even though some side reactions are generally ignored. Since functional groups on the siloxanes can interact with the surface itself, correct orientation is hard to control. In the **fourth chapter** a generalized methodology is presented that fully solves the issues related to the usage of functional siloxanes. Protective groups were used to ensure that no unwanted interactions could occur. To underline the potential of this approach, six different functional groups were introduced onto iron oxide NP. It was observed that the colloidal stability of the resulting product is far better compared to the traditional functionalization methods.

To prove that the developed ligands and in a broader sense the NP are capable of performing efficient and selective magnetic separations, we designed an experiment that supports this hypothesis. *L. pneumophila* bacteria were magnetically separated from an aqueous solution by making use of particles,

conjugated with Ab that target the bacteria. These experiments are explained in **chapter five**.

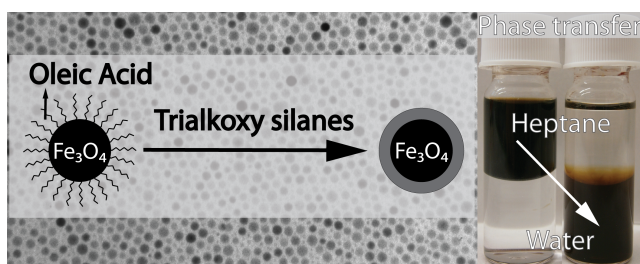
In the appendix, three techniques that are not standard in chemical sciences will be explained to support the reader.

The presented results summarize the development of a generic nanoparticle-based magnetic separation platform with excellent colloidal stability in complex environments, while being cost-effective and straightforward to perform.



## Chapter 2

# Functionalization of oleic acid-coated iron oxide nanoparticles



This chapter is based on the following publication with minor modifications:

**Bloemen M**, Brullot W, Luong TT, Geukens N, Gils A, and Verbiest T  
Improved functionalization of oleic acid-coated iron oxide nanoparticles for biomedical applications  
*Journal of Nanoparticle Research* 2012; 14: 1100–1109

Dr. W. Brullot performed the VSM experiments and analyzed the results. T. T. Luong helped with the zeta potential measurements.

## Abstract

Superparamagnetic iron oxide NP can provide multiple benefits for biomedical applications in aqueous environments, such as magnetic separation or MRI. To increase the colloidal stability and allow subsequent reactions, the introduction of hydrophilic functional groups onto the particles' surface is essential. During this process, the original coating is exchanged by preferably covalently bonded ligands, such as trialkoxy silanes. The duration of the silane exchange reaction, which commonly takes more than 24 hours, is an important drawback for this approach. In this paper we present a novel method, which introduces ultrasonication as an energy source to dramatically accelerate this process, resulting in high quality water-dispersible NP, around 10 nm in size. To prove the generic character, different functional groups were introduced on the surface, including polyethylene glycol chains, carboxylic acid, amine and thiol groups. Their colloidal stability in various aqueous buffer solutions as well as human plasma and serum was investigated to allow implementation in biomedical and sensing applications.

## 2.1 Introduction

For many years, iron oxide NP have been the subject of intensive research. These cost-effective and non-toxic particles are used nowadays in many applications, such as magnetic storage, drug delivery, biosensing, magnetic separation and contrast reagents for imaging techniques.<sup>23,109</sup> A common method to make such particles is co-precipitation, where iron (II+) and (III+) ions are dissolved in water and precipitated using ammonia or sodium hydroxide.<sup>110</sup> Drawbacks are the poor monodispersity and irregular shape of these particles. Recently, multiple methods have been published to synthesize very monodisperse NP in organic solvents. Sun *et al.* made high quality magnetite nanocrystals with small size distribution by thermal decomposition of iron (III) acetylacetonate in phenyl ether.<sup>14</sup> A similar method, reported by Park *et al.*, uses iron oleate as a precursor and oleic acid as a capping agent.<sup>12</sup> This results in NP with a hydrophobic coating, since the polar end groups are attached to the surface. Capping agents such as oleic acid are often used because they form a protective monolayer, which is strongly bonded. This is necessary for making monodisperse and highly uniform NP.<sup>111,112</sup> For biomedical applications in aqueous environments, this hydrophobic coating has to be replaced with a hydrophilic coating. The so-called ligand exchange is well-known for noble metal NP where for instance thiol groups attach strongly to the surface, thereby forming monolayers by self-assembly. A similar approach is possible for iron oxide NP by using polymers or  $\alpha$ -cyclodextrin.<sup>113–115</sup> Since these layers are often not covalently bonded to the surface, high ionic strength or extreme pH conditions might alter their interaction. An elegant alternative is silane chemistry, which is based on the reactivity of silanol molecules, formed by the hydrolyzation of alkoxy silane.<sup>116,117</sup> A high degree of control and reproducibility is possible, when the appropriate reaction conditions are chosen. The possibility to introduce a large variety of functional groups onto the surface of magnetic NP

makes this approach very valuable. Other advantages are the high stability and density of the formed silicon oxide layer. However, introducing silane molecules onto the surface of oleic acid-stabilized NP has only been scarcely reported so far. De Palma *et al.* described a method, which uses hexane as a solvent and acetic acid as a catalyst to form the reactive silanol molecules.<sup>118</sup> Larsen *et al.* published a protocol with toluene as the solvent and water being the catalyst; triethylamine was added to facilitate the reaction.<sup>119</sup> Kohler *et al.* also managed to introduce silanes but pre-treated the oleic acid coating with a mixture of 1M ammonium hydroxide in 1-butanol.<sup>120</sup> These methods have serious drawbacks, e.g. the extensive reaction time (24-72h) or pre-treatment procedure. In this chapter we present an improved nanoparticle functionalization method. The obtained superparamagnetic NP are thoroughly characterized by transmission electron microscopy (TEM), X-ray powder diffraction (XRD) and vibrating sample magnetometry (VSM). Infrared spectroscopy is used to confirm the presence of the functional groups on the surface after reaction with silane molecules. By performing this reaction in an ultrasonication bath, the reaction time is greatly reduced, while avoiding cross-linking thus maintaining the monodispersity. The colloidal stability of the resulting NP was extensively tested in different aqueous media at several pH's as well as in human serum and plasma, which demonstrates their applicability in biomedical applications. A large variety of functional groups were introduced to the surface, proving the generic character of the method.

## 2.2 Materials and methods

### Materials

Sodium oleate and iron (III) chloride hexahydrate (97%) were obtained from Sigma Aldrich, ethanol (absolute) and oleic acid from VWR and heptane and toluene from Fisher Scientific. Triethyl amine was ordered at Janssen Chimica. Acetone was purchased at Chem Lab. Methoxy (polyethyleneoxy) propyl trimethoxy silane (90%, 9-12 PE-units), 3-Mercapto propyl trimethoxy silane (95%), N-(Trimethoxysilylpropyl) ethylenediamine triacetic acid trisodium salt (45%) and 3-Amino propyl trimethoxy silane (97%) were obtained from ABCR. 1-octadecene (90%, technical grade) was purchased at Acros.

### Synthesis of NP

Superparamagnetic iron oxide nanoparticles were prepared using the method published by Park *et al.*, with minor modifications.<sup>12</sup> It consists of two separate reactions, first preparing an iron-oleate precursor, which is later on transformed into iron oxide nanocrystals. For the synthesis of the precursor, sodium oleate (36.5 g, 120 mmol) and iron (III) chloride hexahydrate (36.5 g, 120 mmol) were dissolved in a mixture of 80 mL ethanol, 60 mL MilliQ water and 140 mL heptane. This mixture was heated to reflux

at 70°C, for 4 hours under an argon atmosphere. Afterwards the upper heptane layer, which contains the iron-oleate, was separated using a separatory funnel and washed three times with 40 mL MilliQ water. As a final step, the heptane was evaporated using a rotavapor, resulting in a dark brown waxy solid. The iron oxide NP synthesis starts with mixing iron-oleate (36 g, 40 mmol) with oleic acid (5.7 g, 20 mmol) and 200 g of 1-octadecene in a 500 mL three-neck flask. This mixture was first heated to 100°C for 5 min to evaporate all remaining heptane. After fitting a reflux cooler, the mixture was heated further to 320°C and kept at that temperature for 30 min. Around 250°C, the decarboxylation of the oleate starts, producing a large amount of CO<sub>2</sub> gas. Afterwards the reaction mixture is cooled down to room temperature by removing the heat source. 500 mL of ethanol is added to precipitate the freshly prepared NP. Separation was done by centrifugation, after which the particles were washed three times with ethanol. After drying, the nanocrystals were dispersed in heptane (with one drop of oleic acid) in high concentration (100 mg/mL) for long-term storage.

## Functionalization

The new protocol presented here was partially based on a method published by Larsen *et al.*, but with important modifications.<sup>119</sup> In a typical functionalization experiment, 100 mg of iron oxide nanoparticles (in heptane, stock solution) were mixed with 50 mL of toluene. To this mixture, 2.5 mL of triethylamine, 0.05 mL of MilliQ water and 0.5 mL of the desired silane were added. The beaker was then placed in an ultrasonication bath for 5 hours. The temperature of the water inside this bath was kept at 50°C during the reaction. Afterwards, the volume of the reaction mixture was doubled by adding heptane to the solution, 50 mL in this case. The mixture was placed on a magnet to precipitate the functionalized nanoparticles. The supernatant was decanted and the particles were washed 3 times with acetone and precipitated by a magnet. After drying under reduced pressure for 15 min, the sample was weighed and dissolved in MilliQ water or the appropriate medium.

## Equipment & Characterization

The ultrasonication bath used in the particle functionalization was a Branson Model 5510 sonicator with a capacity of 10 liters. The built-in heating was never used. TEM measurements were performed on a 80 kV Zeiss EM-900 using 300 mesh Formvar coated copper grids. Distribution data were calculated using ImageJ. Oleic acid coated nanoparticles were dispersed in heptane and deposited onto the grid. Fourier transform infrared (FTIR) spectra were obtained by a Bruker Alpha FTIR spectrometer, equipped with a Platinum ATR module. Dynamic light scattering and zeta potentials were measured on a Brookhaven 90plus particle analyzer. The internal detector was positioned at 90 degrees. UV-VIS Spectrometry was performed on a Perkin Elmer Lambda 900 spectrometer. VSM experiments were conducted on a VSM Maglab setup from Oxford Instruments. XRD spectra were obtained in reflection (Bragg-Brentano geometry) by a Rigaku Rotaflex diffractometer, fitted with a Rigaku

RU-200B rotating Cu-anode ( $\lambda = 1.54 \text{ \AA}$ ) at a power of 4 kW. The diffracted X-rays were collected after Ni-filtering on a scintillation counter. Samples were deposited on a glass microscope slide from solution. Samples, to test the colloidal stability, were prepared by adding a concentrated nanoparticle dispersion (in water) to the appropriate medium. The protocol for collection of human plasma and serum is described in the supporting information at the end of this chapter. Absorbance values were measured at a wavelength of 1000 nm.

## 2.3 Results & Discussion

### Characterization of the core nanoparticle

Efficient surface modification of superparamagnetic NP is crucial for their application in biomedicine. Recent advances in high temperature syntheses already improved the shape and monodispersity of the core. As mentioned before, these particles are only soluble in apolar solvents, because of their oleic acid coating. To change the polarity of the layer to being hydrophilic, a ligand-exchange is essential. We preferred interaction with alkoxy silanes to polymers because of the covalent bond formation, resulting in more versatile and robust nanoparticles. The reaction mechanism is shown in Figure 2.1. After formation of the active silanol molecule, it reacts with the surface OH groups of the iron oxide nanoparticle. This results in the formation of a Fe-O-Si bond. Metal oxides are known to have reactive hydroxyl groups present on their surface, caused by the adsorption of water.<sup>19</sup> This is similar to functionalization of silicon oxide substrates.<sup>62</sup> The density and structure of the shell depends largely on the reaction conditions, being a combination of linear polymerization, network formation and covalent attachment to the iron oxide surface. Although chlorosilanes would react faster than alkoxy silanes, we opted for the latter. Chlorosilanes release hydrogen chloride upon reaction, which is incompatible with iron oxide. On top of that, their reactivity is often too high to allow sufficient control of the reaction. The nanoparticle synthesis published by Park *et al.* allowed us to make high quality spherical NP at large scale.<sup>12</sup> Figure 2.2 shows a TEM image of the oleic acid coated NP. As can be seen in the inset, the nanoparticle distribution is narrow. A mean size of 9.3 nm was calculated by a Gaussian fit, with a spread of  $\pm 1.6 \text{ nm}$  (one sigma).

Since superparamagnetism is an important property of the NP, VSM measurements were performed. Figure 2.3 shows the data of the oleic acid coated particles. The applied field was varied between four and minus four Tesla, while recording the remnant magnetization. No coercivity or magnetic remanence is observed, which is typical for superparamagnetic NP. The hysteresis loop can be fitted by a Langevin function to deduct the size of the magnetic core. In this case a core diameter of 10.5 nm was obtained. This value is comparable to the size determined by TEM measurements.

The crystal structure of the oleic acid coated iron oxide NP was determined via XRD (step size =  $0.05^\circ$ , dwell time = 40 sec). As Figure 2.4 indicates, the spectrum

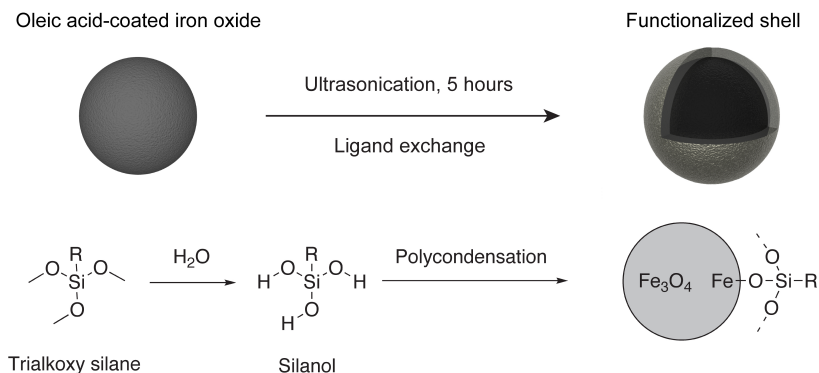


Figure 2.1: Overview of the chemical reactions during the functionalization of iron oxide NP with silanes. The formation of the silanol molecule occurs by reaction with water. Subsequent polycondensation renders a silane network on the surface of the nanoparticle.

closely resembles the reference spectrum of magnetite. However since the difference between maghemite and magnetite is very subtle in XRD, no conclusions about the exact composition can be drawn. Therefore, we can only state that the crystals produced in the synthesis are superparamagnetic iron oxide NP, consisting of magnetite, maghemite or a mixture of both. By using the Scherrer equation, the crystal size can be derived from the peak broadening in the spectrum.<sup>26</sup> Using MDI Jade, the (400) peak was fitted with a pseudo-Voigt function after polynomial background subtraction, resulting in a size of  $9.3 \pm 0.7$  nm. This value corresponds very well with the size determined by TEM measurements. Compared to previously reported functionalization methods, the method presented here has several advantages. (1) The reaction time is reduced to 5 hours compared to 24 or 72 h as described by Larsen *et al.* and De Palma *et al.*<sup>118,119</sup> (2) By using a sonicator, crosslinking of particles during the reaction is strongly reduced thereby maintaining the monodispersity of the NP. In this case the exact mechanism is unknown but in general, sonication of a solution introduces microbubbles, which subsequently implode. These implosions generate high temperatures inside and around the cavity, as well as a shock wave upon collapse. The surrounding liquid quickly disperses the heat, allowing the use of fragile organic materials.<sup>121,122</sup> (3) Another advantage is the elevated concentration of NP (2 mg/mL) during the synthesis, which reduces the amount of solvent needed. The functionalization procedure was performed with four different trialkoxy silanes. PEG, carboxylic acid, amine and thiol groups were introduced on the surface for various reasons. Thiol and amine groups are excellent anchor points for subsequent coating with a gold layer, by e.g. reduction of a gold containing salt. This is particularly useful in biomedical applications where the plasmonic response of gold is used to heat the environment or to release drugs at a specific location.<sup>48,104</sup> PEG chains on

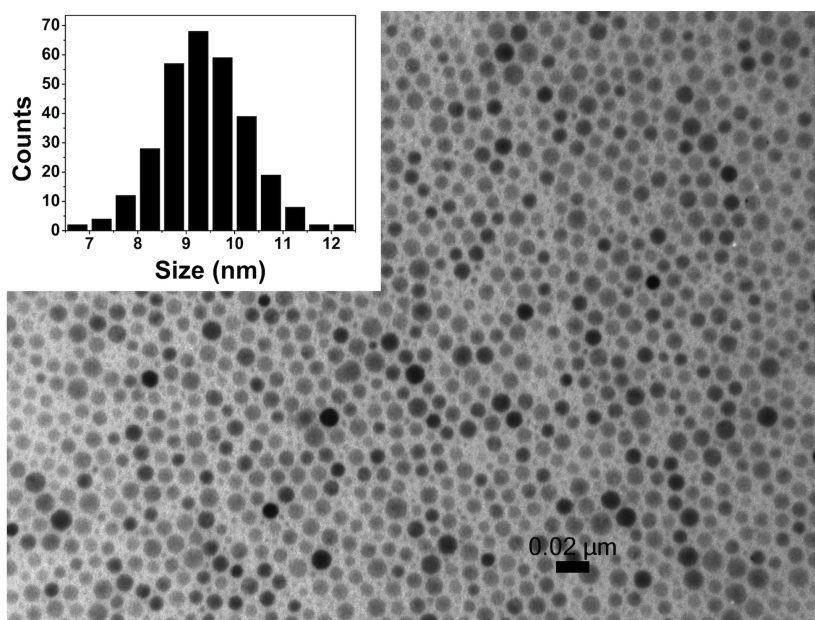


Figure 2.2: TEM image of oleic acid-stabilized iron oxide NP. The scale bar represents 20 nm. The inset shows the size distribution:  $9.3 \pm 1.6$  nm

the surface, on the other hand, provide the NP with excellent dispersibility in water. These particles can be used to form magnetic fluids for applications like magnetic hyperthermia or thermo-ablation.<sup>123</sup> The introduction of carboxylic acid and amine groups can be utilized for bioconjugation of proteins to the NP. Typical chemical coupling reagents like EDC-NHS or glutaraldehyde, link these functional groups to the target protein via an amide or imine bond. These bioconjugates are often used for detection and magnetic separation.

Successful modification of the NP' surface was confirmed by FTIR measurements. Table 2.1 gives an overview of the vibrations measured on the oleic acid and silane coated particles. For the unmodified iron oxide cores, the characteristic bands of the asymmetric stretching, symmetric stretching and scissoring of  $\text{CH}_2$  are visible at 2919, 2850 and 1436  $\text{cm}^{-1}$ , respectively.<sup>112,124,125</sup> The stretching of the  $\text{C}=\text{O}$  double bond is clearly shown by the peak at 1709  $\text{cm}^{-1}$ . This was expected since the peak resembles free oleic acid, indicating that a significant amount of unbound surfactant is present, which can be related to the storage conditions. The presence of a peak at 1462  $\text{cm}^{-1}$ , coming from in-plane OH bending, supports this idea. Zhang *et al.* reported that the  $\text{C}=\text{O}$  peak shifts to 1541 and 1639  $\text{cm}^{-1}$  when the molecule is attached to a ferrite surface.<sup>112</sup> The carboxylic acid groups are then present in a  $\text{COO}^-$  conformation. If the spectrum is magnified, these vibrations are also visible

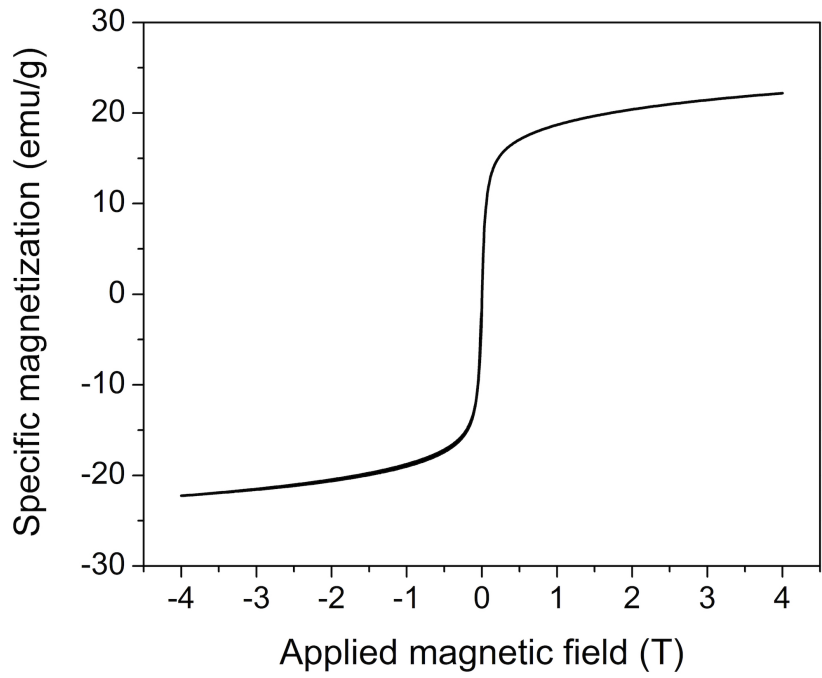


Figure 2.3: VSM signal of the NP, showing a hysteresis curve. The data points are fitted by a Langevin function to determine the magnetic core size.

Table 2.1: Overview of the different vibrations, related to the different coatings around the nanoparticle. The original spectra can be found in the supporting information (see Figures 2.6, 2.7, 2.8, 2.9, 2.10) at the end of this chapter.

Surface of Fe <sub>3</sub> O <sub>4</sub>	IR vibrations (cm <sup>-1</sup> )
Oleic acid	3005 (HC=), 2919 (CH <sub>2</sub> ), 2850 (CH <sub>2</sub> ), 1709 (C=O), 1635 (COO <sup>-</sup> ), 1541 (COO <sup>-</sup> ), 1462 (OH), 1436 (CH <sub>2</sub> ), 598 (Fe-O)
COOH silane	3600-3000 (OH), 2932 (CH <sub>2</sub> ), 1612 (COO <sup>-</sup> ), 1452 (CH <sub>2</sub> ), 1396 (COO <sup>-</sup> ), 1113 & 1089 & 1007 (Si-O), 585 (Fe-O)
PEG silane	3600-3000 (OH), 2860 (PEG CH <sub>2</sub> ), 1643 (H <sub>2</sub> O), 1454 & 1349 & 1297 & 1250 & 1047 & 947 (CH <sub>2</sub> -O-CH <sub>2</sub> ), 1198 (O-CH <sub>3</sub> ), 620 (Fe-O)
NH <sub>2</sub> silane	3004 (OH & NH <sub>2</sub> ), 2922 (CH <sub>2</sub> ), 2850 (CH <sub>3</sub> ), 1543 (NH <sub>3</sub> <sup>+</sup> ), 1400 (CH <sub>3</sub> COOH), 1224 (Si-C), 1073 (Si-O-R), 773 (NH <sub>2</sub> ), 617 (Fe-O)
SH silane	3600-2500 (OH & CH <sub>2</sub> ), 2600-2550 (SH), 1645 (H <sub>2</sub> O), 1430 (CH <sub>2</sub> ), 1035 (Si-O), 590 (Fe-O)

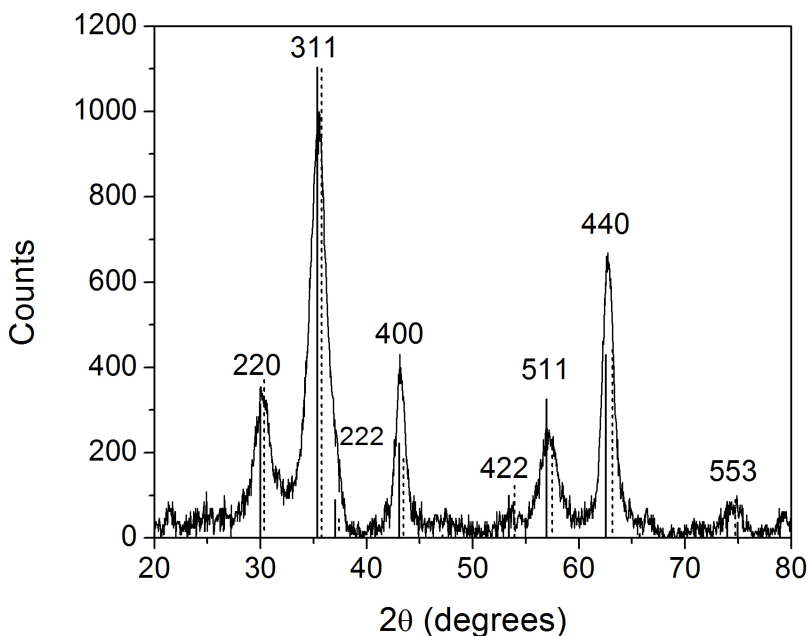


Figure 2.4: X-ray powder diffraction spectrum of the oleic acid-coated iron oxide NP. The solid and dashed vertical drop-down lines represent the peak positions of a reference magnetite and maghemite spectrum, respectively (AMCSD 0007824 and 0007899).

in our case at  $1541$  and  $1635\text{ cm}^{-1}$ , although they are fairly small. The wavenumber separation (of  $94\text{ cm}^{-1}$ ) between those two peaks is an indication for how the oleate and the iron atoms on the surface interact. Because the difference is smaller than  $110\text{ cm}^{-1}$ , a chelating bidentate interaction can be derived from the spectrum. The iron oxide core itself shows a characteristic vibration at  $598\text{ cm}^{-1}$ , related to the Fe-O bond.<sup>112</sup> The presence of carboxylic acid groups, after functionalization, is proven by the vibrations at  $1612$  and  $1396\text{ cm}^{-1}$ . These correspond to the asymmetric and symmetric stretching of the  $\text{COO}^-$  group, respectively. Other important features are the  $1113$ ,  $1089$  and  $1007\text{ cm}^{-1}$  bands due to the stretching of the Si-O bond.<sup>126,127</sup> The PEG silane shows distinct bands caused by the ether functions in the chain, to which several peaks between  $1454$  and  $947\text{ cm}^{-1}$  can be attributed. The high hydrophilicity of the PEG chain is expressed by the presence of a water peak in the spectrum. Even after extensive drying this peak remains, indicating that the water is trapped by hydrogen bonding.<sup>118</sup> Several papers already reported that more information about the structure of the PEG layer on the nanoparticle's surface can be derived from the FTIR spectrum. Compared to these reports, the conformation of the PEG layer is partially crystalline and partially amorphous. Small shoulders at

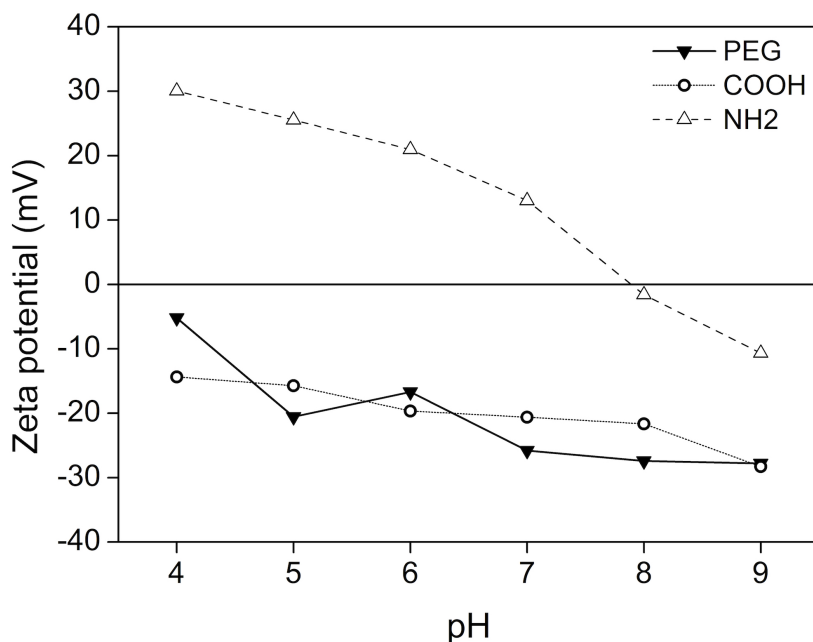


Figure 2.5: Zeta potential values for PEG, carboxylic acid and amine coated nanoparticles in various pH solutions. Every data point was derived from 10 measurements by the software.

1244, 1460 and  $1470\text{ cm}^{-1}$  are present in the spectrum, indicating crystalline parts in the coating. On the other hand, also the amorphous bands are visible, at 948, 1140 and  $1250\text{ cm}^{-1}$ .<sup>128,129</sup> For the amino silane coated nanoparticles, the most important peaks are visible at 3004, 1543 and  $773\text{ cm}^{-1}$  corresponding to the protonated amines. Because this protonation was done by adding acetic acid, a peak at  $1400\text{ cm}^{-1}$  appears. Mercapto silane coated particles show a broad band above  $2500\text{ cm}^{-1}$ , consisting of a combination of OH,  $\text{CH}_2$  and SH vibrations. Also a small peak caused by the presence of water is visible. Typical peaks for Si-O and Fe-O also appear, at 1035 and  $590\text{ cm}^{-1}$ , respectively.

## Colloidal stability

Further experiments were only conducted on the PEG, COOH and amine coatings, since the thiol particles were only stable in water for a very short time, regardless the pH. In general, the stability of NP dispersed in aqueous media can be expressed by the zeta potential. Theoretically, it refers to the potential difference between the slipping plane in the electronic double layer and the bulk potential. If the potential

Table 2.2: Overview of the stability of the nanoparticles in buffer solutions: (+) stands for excellent dispersibility and stability in time (minimum 1 week), ( $\pm$ ) corresponds to colloidal solutions that are stable for <4 days, (-) stands for dispersions which are stable for only a short period of time (between 5 and 10 hours). Concentration of nanoparticles in solution was 0.25 mg/mL. Criterion for stability was the absence of visible aggregation or precipitate.

Coating	CH <sub>3</sub> COOH/CH <sub>3</sub> COONa			CH <sub>3</sub> COOH/CH <sub>3</sub> COONa			MES/HCl		
100%	pH 4			pH 5			pH 6		
	0.1 M	0.05 M	0.025 M	0.1 M	0.05 M	0.025 M	0.1 M	0.05 M	0.025 M
NH <sub>2</sub>	+	+	+	+	+	+	$\pm$	$\pm$	$\pm$
PEG	+	+	+	$\pm$	$\pm$	$\pm$	$\pm$	$\pm$	$\pm$
COOH	$\pm$	+	+	+	+	+	+	+	+

Coating	NaH <sub>2</sub> PO <sub>4</sub> /Na <sub>2</sub> HPO <sub>4</sub>			TRIS/HCl			Glycine/NaOH		
100%	pH 7			pH 8			pH 9		
	0.1 M	0.05 M	0.025 M	0.1 M	0.05 M	0.025 M	0.1 M	0.05 M	0.025 M
NH <sub>2</sub>	-	-	-	-	-	-	-	-	-
PEG	+	+	+	+	+	+	+	+	+
COOH	+	+	+	+	+	+	+	+	+

has an absolute value higher than 25-30 mV it is generally accepted that the particles are electrostatically stable.<sup>68</sup> Although colloidal stability is related to electrostatic and steric repulsion, zeta potential measurements usually give a good indication. Figure 2.5 shows the combined data of the PEG-, carboxylic acid- and amine-coated NP. A clear downward trend for the zeta potential of NH<sub>2</sub> is visible when the pH increases. This can be related to the lowering of the surface charge due to deprotonation of the amine at high pH. A similar but reverse trend can be observed for COOH, since the acid becomes protonated at low pH, thereby losing its negative charge. The zeta potential would eventually approach zero at a pH lower than 4. For PEG-coated particles the zeta potential shows similar behavior, even though polyethylene glycol chains have no pH responsive groups. The incorporation of ions into the PEG layer can explain this trend, taking into consideration that sodium hydroxide and hydrogen chloride were added to adjust the pH of the solution.<sup>130,131</sup> Nevertheless, the PEG coated particles were stable over the entire pH range, indicating that their stability is caused by steric repulsion rather than electrostatic repulsion. For the COOH-coated nanoparticles, solutions of pH 4 and 5 showed extensive aggregation and consequent precipitation. A similar effect was observed for the amine-coated particles, this time for dispersions of pH 7 to 9. The profound impact of the pH on the stability of COOH and NH<sub>2</sub> coatings shows that electrostatic repulsion is crucial for these types of dispersions.<sup>118,124,125</sup>

To study the effect of buffer solutions onto the colloidal stability, various dispersions with different salt concentrations were prepared. To our knowledge, no extensive studies have been conducted on magnetic nanoparticle dispersions in different buffer media at different pH's and concentrations.<sup>132,133</sup> Nevertheless this information can be very valuable for subsequent reactions or applications of the nanoparticles. Five

commonly used buffer reagents were chosen, covering the entire pH range between 4 and 9. These included sodium acetate, 2-(N-morpholino)-ethanesulfonic acid (MES), sodium hydrogen phosphate, 2-amino-2-hydroxymethyl-propane-1,3-diol (TRIS) and glycine. The concentration of the reagents ranged from 0.1 M to 0.025 M; while the particle concentration was fixed at 0.25 mg/mL. Table 2.2 provides an overview of the stability in different buffer solutions, each having 3 different concentrations. Carboxylic acid coated NP show excellent stability in different buffers above pH 4, which can be related to the presence of charged carboxylate groups on their surface, providing sufficient electrostatic repulsion. For the NH<sub>2</sub> coated particles, the instability can be explained by the lack of charged functional groups. This is partially caused by the pH, which is too high for sufficient stabilization. On top of that, the high ionic strength and ion size largely influence the zeta potential. These results are in perfect agreement with the zeta potential measurements and the observed correlation between the presence of surface charges and colloidal stability. The particles with polyethylene glycol chains on their surface show good stability in phosphate, glycine and TRIS based buffer solutions. The instability in MES and acetate buffer however is somewhat unexpected, since the zeta potential measurements showed that PEG provides mainly steric hindrance, rather than electrostatic repulsion. Ion adsorption onto the coated surface is expected to be the cause of this instability.

If superparamagnetic NP are used as for example a MRI contrast reagent, colloidal stability in (human) serum or plasma is crucial. To prove the value of the presented functionalization method, nanoparticle dispersions in both serum and plasma were prepared and their stability was monitored in time by absorption measurements (see supporting information at the end of this chapter). Human blood has a pH of 7.4, which will strongly influence the stability of the nanoparticles as was shown in previous paragraphs. Similar as for the dispersions in buffer solutions, three different coatings were tested, respectively amine, carboxylic acid and PEG functional groups. These NP were dispersed in serum and plasma at a concentration of 1 and 0.25 mg/mL. In accordance to the previous results, amine groups on the surface cannot provide sufficient electrostatic repulsion at pH 7.4, which resulted in a rapid decline of the absorbance. On the contrary, carboxylic acid groups and PEG chains should be able to provide sufficient stabilization in these conditions. This was observed in both cases, since the absorbance remained constant during the entire experiment, which lasted 48 hours. These results indicate that the PEG and carboxylic acid coated nanoparticles can be of great importance for future in vivo experiments.

An important remark about the use of NP in biomedical applications is their possible toxicity towards cells. Although many conflicting results were published about the toxicity of superparamagnetic iron oxide NP, a study by Mahmoudi *et al.* showed that the surface coating as well as the cell type itself has a large influence on the possible toxic effects.<sup>17,117</sup> They state that the introduction of a functional surface coating lowers the toxicity. Tartaj *et al.* reported that the size, shape and magnetic dipole moment of the particle also play a role in in vivo experiments.<sup>134</sup> Properties of nanoparticles like longer sedimentation times, higher surfaces areas and smaller magnetic dipole-dipole interactions might facilitate their use. Nevertheless a study of the adverse effects towards their environment is necessary for every specific application.

## 2.4 Conclusions

Oleic acid-coated NP were functionalized by reaction with trialkoxy silanes. The reaction takes place in an ultrasonication bath, which reduces the reaction time and prevents crosslinking. The successful coating procedure of the NP' surface was proven by FTIR measurements. Multiple techniques (TEM, XRD, VSM) proved the composition of the magnetic core. The obtained functionalized NP can be dispersed in various aqueous environments, including human serum and plasma. Their stability under these conditions was addressed by zeta potential and absorbance measurements, showing a strong relation between the colloidal stability and the pH of the solution. Although PEG coated NP also exhibit this dependency, steric hindrance is expected to be more prominent here. In general, the generic method described here allows the introduction of various functional groups on the surface of the NP. This is particularly useful for subsequent coupling reactions to fluorescent probes, proteins or substrates. Therefore, we believe that this type of superparamagnetic NP can be of major importance for future research and applications in biomedicine.

## 2.5 Supporting information

### Protocol human plasma and serum

Human serum and plasma were obtained by the following method: a blood sample from a healthy volunteer was collected in heparinized tubes (BD Vacutainer Systems) and spun at room temperature at a speed of 1300 g for 20 minutes in a swinging bucket centrifuge, with plasma harvested and stored at -20°C until assayed. For serum preparation, a blood sample from the same healthy volunteer was collected in SST Serum Separation Tubes (BD Vacutainer Systems), inverted five times and allowed to clot at room temperature for 30 minutes before centrifugation in a swinging bucket centrifuge for 20 minutes at 1300 g; the resultant serum was collected and stored at -20°C until assayed.

### FTIR spectra

Following figures show the FTIR spectra of the coated NP. Oleic acid (Figure 2.6), carboxylic acid (Figure 2.7), PEG (Figure 2.8), amine (Figure 2.9) and thiol (Figure 2.10) coatings were measured.

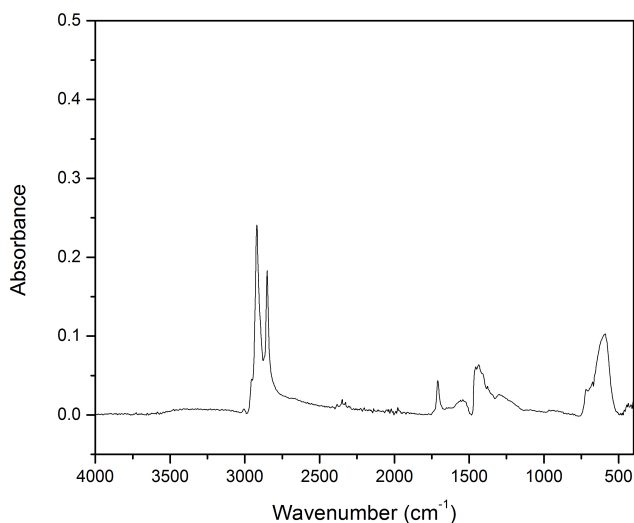


Figure 2.6: Infrared spectrum of oleic acid coated NP.

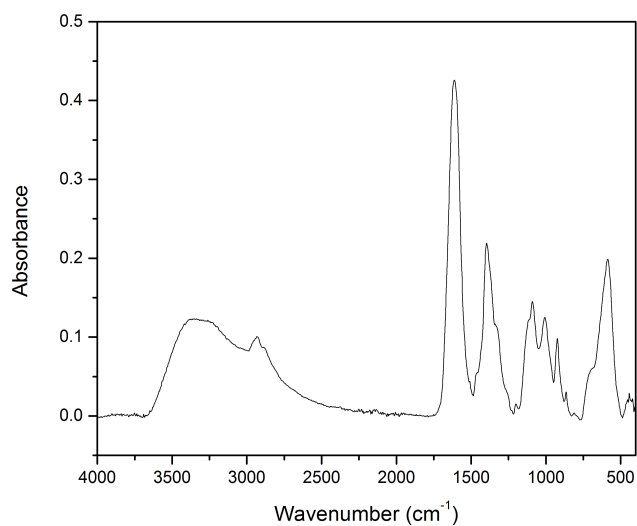


Figure 2.7: Infrared spectrum of NP coated with carboxylic acid groups.

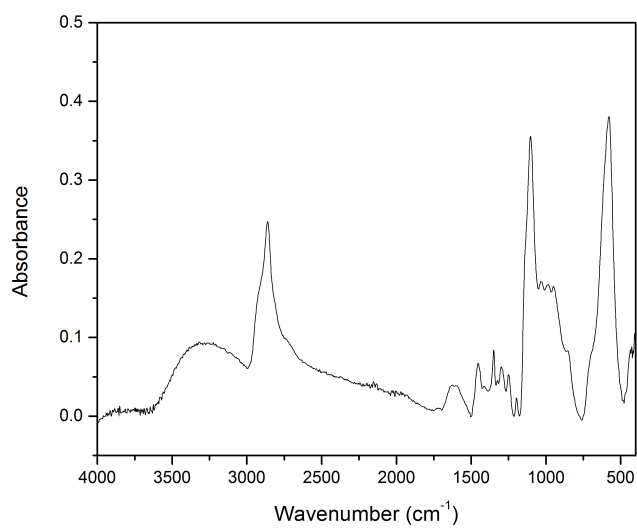


Figure 2.8: Infrared spectrum of NP coated with PEG chains.

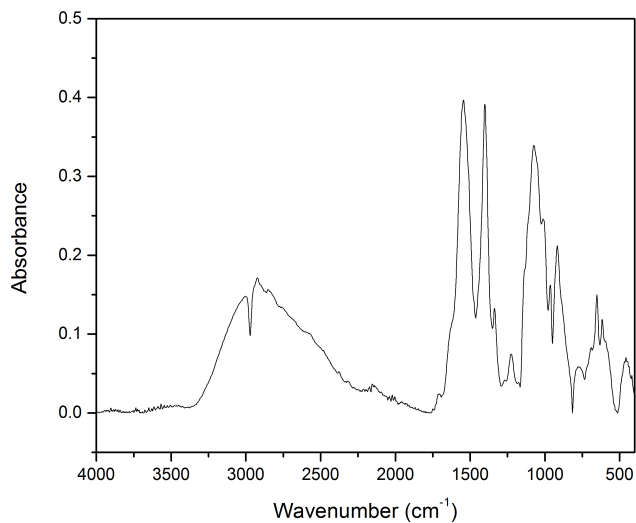


Figure 2.9: Infrared spectrum of NP coated with amine groups.

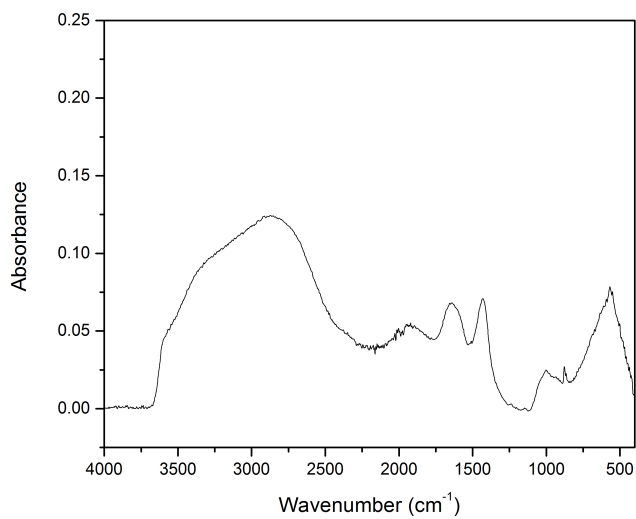


Figure 2.10: Infrared spectrum of NP coated with thiol groups.

## Absorbance spectra

The following figures combine the absorbance data of the amine (Figure 2.11), carboxylic acid (Figure 2.12) and PEG (Figure 2.13) coated NP respectively. The concentration of the NP was 1 or 0.25 mg/mL in serum or plasma, as indicated in the legend. Absorbance values were measured at a wavelength of 1000 nm. At pH 7.4, the amine functionalized NP are not colloidal stable, resulting in a decrease in absorbance over time. The COOH and PEG coated particles on the other hand show excellent stability in these complex environments.

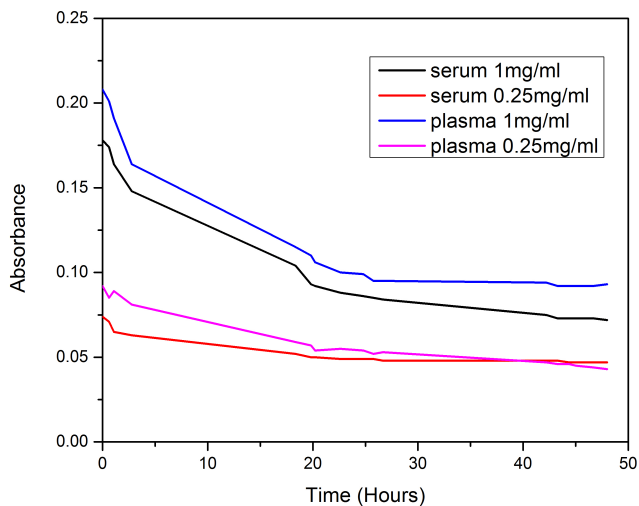


Figure 2.11: Absorbance data of the amine coated NP. The concentration of NP in serum or plasma was 1 or 0.25 mg/mL.

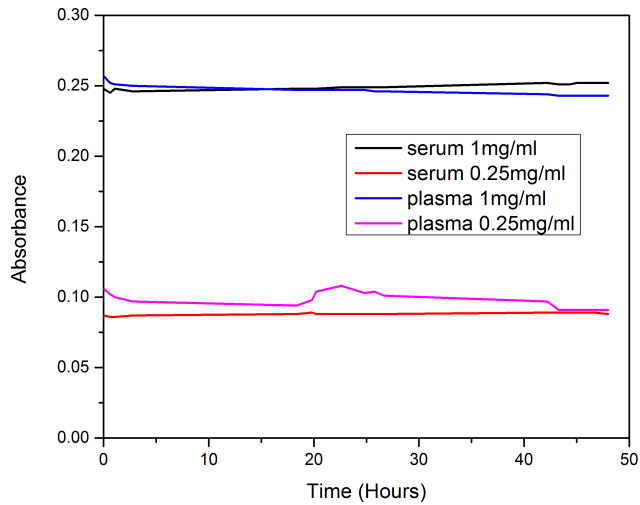


Figure 2.12: Absorbance data of the carboxylic acid coated NP. The concentration of NP in serum or plasma was 1 or 0.25 mg/mL.

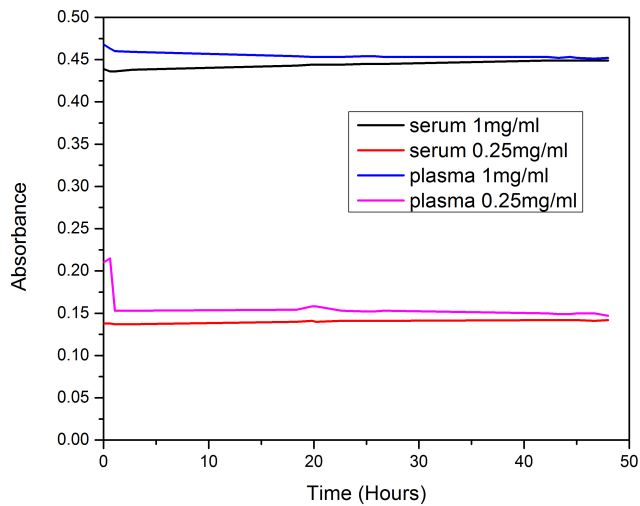
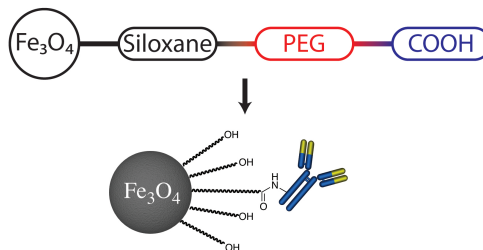


Figure 2.13: Absorbance data of the NP coated with PEG chains. The concentration of NP in serum or plasma was 1 or 0.25 mg/mL.

## Chapter 3

# Heterobifunctional PEG ligands for bioconjugation reactions



This chapter is based on the following publication with minor modifications:

**Bloemen M**, Van Stappen T, Willot P, Lammertyn J, Koeckelberghs G, Geukens N, Gils A, and Verbiest T

Heterobifunctional PEG ligands for bioconjugation reactions on iron oxide nanoparticles

*PLoS ONE* 2014; 9: e109475

T. Van Stappen performed the enzyme-linked immunosorbent assays and analyzed the results. Dr. P. Willot and Prof. dr. G. Koeckelberghs helped with the interpretation of the NMR and mass spectrometry results. Prof. dr. J. Lammertyn and his team were responsible for the SPR measurements and the data analysis.

## Abstract

Ever since iron oxide nanoparticles have been recognized as promising scaffolds for biomedical applications, their surface functionalization has become even more important. We report the synthesis of a novel polyethylene glycol-based ligand that combines multiple advantageous properties for these applications. The ligand is covalently bound to the surface via a siloxane group, while its polyethylene glycol backbone significantly improves the colloidal stability of the particle in complex environments. End-capping the molecule with a carboxylic acid, introduces a variety of coupling chemistry possibilities. In this study an antibody targeting plasminogen activator inhibitor-1 was coupled to the surface and its presence and binding activity was assessed by enzyme-linked immunosorbent assay and surface plasmon resonance experiments. The results indicate that the ligand has high potential towards biomedical applications where colloidal stability and advanced functionality is crucial.

## 3.1 Introduction

The potential of iron oxide NP in biomedical applications is widely recognized: they can act as MRI contrast agents, superparamagnetic carriers for drugs or are used in hyperthermia treatments.<sup>6,48,134–137</sup> By improving the synthesis of these particles, their quality and availability has largely increased.<sup>12,14,33,138–140</sup> When NP are used in biomedical applications, two requirements are often necessary. First, their colloidal stability in complex environments is crucial. If the particles become unstable in for instance blood, they will precipitate, possibly triggering severe inflammatory responses.<sup>141–143</sup> Secondly, they should possess accessible anchor points for molecules or proteins to be coupled onto. This allows NP to selectively interact with certain targets or to carry drugs close to a desired location. However, functionalization of their surface has proven to be non-trivial. Although multiple different approaches have been developed, most of them lack a certain degree of control.<sup>23</sup> Coating their surface with functional polymers is a straightforward method, but has cross-linking issues and allows little control over the thickness of the layer and orientation of functional groups.<sup>144</sup> Since they are not covalently attached to the surface, they could potentially detach, which would make the particles precipitate. Growing an additional silica layer on the iron oxide core, on the other hand, has several advantages: the shell thickness can be well controlled and it is chemically inert.<sup>145</sup> However, the diameter of such NP increases by several nanometers, which is often not desired for biomedical applications.<sup>146</sup> This problem was circumvented by the introduction of functional siloxane molecules on iron oxide NP. They also form a silicon dioxide shell, albeit very thin, and they contain a functional group, which can have several advantages or uses later on.<sup>119,147</sup> Even though multiple variants of these silanes are commercially available, they often do not have the desired structure or properties. This can easily be related to the complicated handling of siloxane molecules. Since they react with water and are relatively intolerant to heat, modification reactions have to be limited in time and workup. Tucker-Schwartz *et al.* recently published an

easy method to avoid this direct modification of the siloxanes, by adopting thiol-ene click chemistry.<sup>148</sup> Their approach allows to synthesize a very complex molecule first and attach a siloxane group as the final step. Click chemistry is a concept rather than a specific reaction, which comprises fast reactions with very high yields and non-aggressive by-products.<sup>149,150</sup> In addition the reaction should be modular and have relatively simple reaction conditions. Very well-known examples are copper mediated azide-alkyne cycloadditions, thiol-ene and Diels-Alder reactions.<sup>150,151</sup> We developed a new ligand, based on a PEG backbone, and transformed it into a siloxane by straightforward thiol-ene click chemistry. By modifying the end-group of the backbone, functional groups were easily introduced onto the nanoparticle's surface. The high purity and straightforward synthesis of the ligand makes this method very valuable for large scale and reproducible functionalization of iron oxide NP. This universal method requires only basic knowledge of organic chemistry and can be widely applicable by scientists without a substantial chemistry background. To investigate the full potential of the ligand, several Ab were coupled to its anchor groups (carboxylic acids) and their activity was assessed via fiber optic SPR experiments. As a model system, an antibody (MA-33H1F7) targeting the serine protease inhibitor (serpin) plasminogen activator inhibitor-1 (PAI-1) protein was selected.<sup>152</sup> This protein is an important factor in the plasminogen-plasmin system since it inhibits plasminogen activators, tissue-type plasminogen activator and urokinase, which are involved in clot formation and degradation processes in blood.<sup>153</sup> These Ab were coupled to the NP by using popular EDC-NHS chemistry and their presence was investigated by ELISAs. To assess their potential in biomedical applications, their colloidal stability was tested in undiluted human plasma and serum. The results indicate that the developed ligand has high potential because of its elegant synthesis, its positive influence on the colloidal stability of the nanoparticle as well as its properties for antibody coupling chemistry.

## 3.2 Materials and methods

### Materials

2,2-dimethoxy-2-phenylacetophenone (DMPAP, 99%), 4-dimethylamino pyridine (DMAP, >99%), succinic anhydride (>99%), 1-Ethyl-3-(3-dimethylaminopropyl) carbodiimide (EDC) and mercaptopropyl trimethoxysilane (95%) were purchased from Sigma Aldrich. Allyl-PEG10-OH was obtained from Polysciences, Inc. Triethylamine was ordered at Janssen Chimica. N-hydroxy succinimide (NHS, 98+%) was obtained from Alfa Aesar. 2-(N-morpholino)ethanesulfonic acid monohydrate (MES) was purchased at Fluka. The monoclonal antibodies (host: mouse) used in this study are MA-33H1F7 (target: human PAI-1/t-PA complex) and MA-T12D11 (target: human Thrombin Activatable Fibrinolysis inhibitor (TAFI)), supplied by the Therapeutic and Diagnostic Antibodies group of the KU Leuven.<sup>152</sup> All ultrasonication steps were performed in a Branson 5510 sonicator bath. FTIR spectra were measured using a Bruker Alpha FT-IR spectrometer equipped with a Platinum ATR module.

## Synthesis of carboxylic acid-terminated PEG

In a 50 ml flask, allyl-PEG10-OH (1 eq, 4,00 mmol, 1.992 g) was mixed with succinic anhydride (1.1 eq, 4.40 mmol, 440 mg) and 4-dimethylaminopyridine (DMAP) (0.02 eq, 0.08 mmol, 9.7 mg). This mixture was stirred and heated to 50°C for 16 hours. The resulting product was purified twice by precipitation in cold diethyl ether, centrifugation and drying in vacuum.  $^1\text{H}$  NMR (300 MHz,  $\text{CDCl}_3$ ):  $\delta$  (ppm) 2.65 (s, 4H), 3.6-3.7 (m, 38H), 4.02 (d, 2H), 4.26 (t, 2H), 5.16-5.30 (m, 2H), 5.8-6.0 (m, 1H).  $^{13}\text{C}$  NMR (75 MHz,  $\text{CDCl}_3$ ):  $\delta$  (ppm) 29.2, 29.5, 63.8, 68.9, 69.3, 70.5, 72.2, 117.1, 134.7, 172.1. MS (chemical ionization, isobutane):  $m/z = 499$  (ester fragment,  $\text{M}^+ - \text{C}_4\text{O}_3\text{H}$ ), 101 (ester fragment,  $\text{M}^+ - \text{C}_{23}\text{O}_{11}\text{H}_{46}$ )

## Thiol-ene click chemistry

To form the siloxane-terminated PEG molecule, allyl-terminated PEG (mixture of modified and unmodified, 1 mmol) was mixed with (3-mercaptopropyl) trimethoxysilane (1 eq, 1 mmol, 185.7  $\mu\text{L}$ ) and 2,2-dimethoxy-2-phenyl-acetophenone (DMPAP) (0.05 eq, 0.05 mmol, 12.8 mg). This mixture was stirred for 1 hour in a UV chamber, equipped with 3 LEDs (365 nm, output power 200 mW). If smaller quantities are used, a small amount of chloroform can be added to improve the stirring.<sup>148</sup> The product was used without further purification.  $^1\text{H}$  NMR (300 MHz,  $\text{CDCl}_3$ ):  $\delta$  (ppm) 0.76 (t, 2H), 1.70 (m, 2H), 1.85 (m, 2H), 2.55 (m, 4H), 2.64 (s, 4H), 3.57 (s, 9H), 3.5-3.8 (m, 40H), 4.26 (t, 2H)

## Nanoparticle surface functionalization

The synthesis of iron oxide NP as well as the introduction of siloxanes onto their surface was performed as reported in Chapter 2. In general, 1 mmol of siloxanes is mixed with 100 mg of  $\text{Fe}_3\text{O}_4$  NP in 50 mL of toluene. To this mixture 2.5 mL of triethylamine and 50  $\mu\text{L}$  of water are added. The solution was placed in an ultrasonication bath for 5 hours, after which 50 mL of heptane was added to precipitate the particles. Afterwards, they were attracted magnetically and washed 3 times with acetone. Finally the particles were dried in vacuum and dispersed in MilliQ water (with a concentration up to 20mg/mL).

## Protein coupling

The concentrated nanoparticle solution was diluted in 50 mM MES buffer, pH 5.5, to reach a final concentration of 3 mg/mL. 0.75 mg EDC and 0.75 mg NHS was added to 1ml of this solution and shaken for 20 minutes to activate the carboxylic acids. The antibodies were diluted in 2 mL of the same MES buffer after which both solutions were mixed and shaken for 1 hour. To separate the particles from the

solution, a Miltenyi Biotec MS magnetic column was used. After rinsing the column with MilliQ water, the nanoparticle dispersion was run through the column, which was placed inside a circular magnet. The column was washed 2 times with 1 mL of sodium phosphate buffer (20 mM, pH 7). To elute the particles, the column was removed from the magnet and 1 mL of phosphate buffer was used as eluent.

## ELISA

In the ELISA assay, recombinant PAI-1 is coated on the plate and free binding sites are blocked with bovine serum albumin. Samples are applied in different dilutions as well as a standard curve of MA-33H1F7.<sup>152</sup> After incubation, horseradish peroxidase (HRP) conjugated rabbit anti-mouse IgG (Sanbio B.V., Uden, The Netherlands) is applied, followed by an o-phenylenediamine (OPD) induced colorimetric reaction. The intensity of the color is directly correlated with the amount of bound MA-33H1F7. Sample values are calculated using the standard curve.

## SPR measurements

An optical fiber was first coated with a gold layer, which was subsequently covered with a self-assembling monolayer (SAM). This thiol- and carboxyl-terminated molecule was obtained from Dojindo molecular technologies. The SAM was activated by a solution containing 0.4 M EDC and 0.1 M NHS in a 50 mM MES buffer (pH 6.0) for 20 minutes. Afterwards the fiber was brought into a solution containing the antigen, PAI-1 (24  $\mu\text{g/mL}$ ) for 25 minutes. Finally the fiber was transferred into a blocking solution (0.1 % tween and 0.05 % BSA). All subsequent experiments were performed with 1 mg/mL nanoparticle solutions.

## 3.3 Results & Discussion

### Ligand Design

The novel PEG-siloxane ligand was designed bearing two important characteristics in mind: having one accessible functional group and providing excellent colloidal stability to the nanoparticle. To ensure the first property, a PEG-oligomer end-capped with an allyl functionality was modified with succinic anhydride. This reaction was performed without solvent, since the anhydride dissolves in PEG at elevated temperatures. DMAP was added, as a catalyst, to speed up the reaction.<sup>154</sup> The available hydroxyl group at the end of the PEG chain reacts with the anhydride, resulting in a free carboxylic acid (see Figure 3.1). This product was purified once by precipitating it in diethyl ether, which removed traces of the catalyst and excess anhydride.

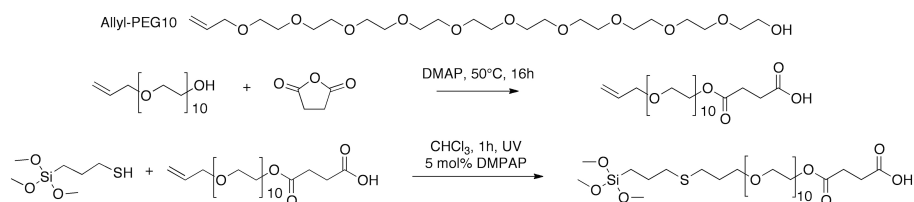


Figure 3.1: Allyl-terminated polyethylene glycol was modified by reaction with succinic anhydride. DMAP catalyzes this reaction. Subsequently the allyl functionality is reacted with a thiol-containing siloxane molecule, by thiol-ene click chemistry, which yields the final carboxylic acid-terminated PEG-siloxane.

The second step of the ligand synthesis involved a click chemistry reaction. We opted for this approach, since working with siloxanes is difficult. They react with moisture and are not resistant to prolonged heating.<sup>148</sup> The thiol-ene click chemistry, on the other hand, is fast and takes place at room temperature. Another great advantage of this approach is that the final siloxane molecule can be added directly to the functionalization solution, without additional workup. Any traces of the radical initiator or its by-products are inert in this reaction. Even though the functionalized PEG molecule could provide sufficient steric hindrance, which ensures colloidal stability of the nanoparticle, we chose to mix modified and unmodified PEG siloxanes during the functionalization step.<sup>147</sup> Thus, the nanoparticle is covered with a complete PEG shell, where the modified chains are sterically available, since they are longer. From the FTIR data (data in the supporting information at the end of this chapter, Figures S1 and S2) was derived, that even though the chain length of the ligand is sufficiently short to enhance the stacking of the molecules (crystalline domains), a small percentage is coiled (amorphous domains).<sup>147</sup> Because only a small part of the ligands have a carboxylic acid functionality, the overall pH sensitivity is reduced. The end result (idealized) is shown in Figure 3.2: carboxylic acid groups are now available as anchor points for future reactions. By FTIR measurements, the presence of modified PEG chains was observed (data in the supporting information at the end of this chapter, Figures S1 and S2). All further experiments were conducted on nanoparticles coated with 90% unmodified and 10% modified PEG siloxanes (molar percentages). These functionalized NP show excellent colloidal stability in multiple different environments. Similarly to Chapter 2, we tested the stability in undiluted human serum and plasma (data in the supporting information at the end of this chapter, Figure S3).<sup>147</sup> The nanoparticles ( $8.6 \pm 0.6$  nm, TEM data in the supporting information at the end of this chapter, Figure S5), coated with mixed siloxanes, clearly showed the properties of both PEG and carboxylic acids. In particular they show enhanced stability in pH ranges above 5, where the carboxylic acids are charged (picture in the supporting information at the end of this chapter, Figure S4). In media like serum or plasma, no precipitation was observed, even after 25 hours at room temperature without agitation. NP were also coated with 100% modified PEG siloxanes, but these particles had significantly lower colloidal stability in these acidic environments (pH 5-6), due to the

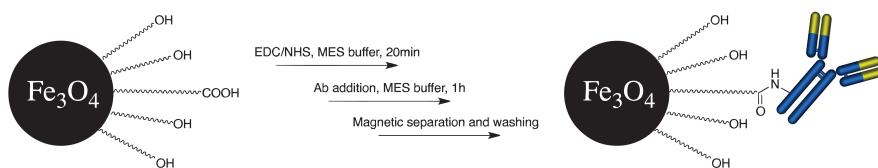


Figure 3.2: The available carboxylic acid groups are activated with EDC-NHS chemistry. The resulting NHS ester reacts with amine groups of the antibody in a MES buffer. Finally the particles are recovered from the supernatant by a magnetic column.

lack of stabilizing charges. Steric stabilization by the PEG chains was not sufficient in this case, since too much carboxylic acids were present. We therefore decided to focus on nanoparticles with mixed siloxane coatings.

## Bioconjugation

Covalent attachment of the selected Ab onto the NP was performed via a standard EDC-NHS coupling.<sup>155</sup> The mechanism is based on the activation of the carboxylic acid with EDC, which forms an unstable acylisourea intermediate. This intermediate reacts with NHS to form a stable ester that exhibits enhanced stability in aqueous environments. Although this extra step is not strictly necessary, it greatly improves the binding efficiency, by reducing the occurrence of side reactions on the acylisourea intermediate. All reactions were performed in a slightly acidic buffer (MES 50mM, pH5.5), which improves the final coupling reaction on two domains. First, the low pH enhances the activation of the carboxylic acid by EDC.<sup>83</sup> Secondly, the formed NHS ester has substantially lower hydrolysis rates below pH 7.<sup>83</sup> Further protein crosslinking (second, third, ... layer) is reduced by the slow reaction rate of the partially protonated amines.<sup>83</sup> A slower reaction rate was preferred in this procedure, since the formation of a protein corona is also a thermodynamically favorable process.<sup>70</sup> A higher reaction rate could result in coating the NP with multiple layers of proteins and crosslinking between different NP. Afterwards the conjugated NP were purified by a magnetic column, which has a very large surface area, since normal attraction with a magnet was too time-consuming. This was necessary because of the excellent colloidal stability of the NP in the buffer, which dramatically slows down the attraction rate. If the NP were precipitated by a highly concentrated salt solution, it was difficult to redisperse them afterwards. Using a magnetic column also enabled us to wash the particles while they were retained on the column. After removing the magnetic field from the column, the particles were easily collected by eluting with a PBS buffer. In this study, we opted for two different Ab: MA-33H1F7, targeting PAI-1, and MA-T12D11, targeting TAFI, as the negative control.<sup>152,156</sup>

Multiple methods are available to determine the concentration of proteins on NP; however not all are appropriate when iron oxide is involved. Colorimetric methods like

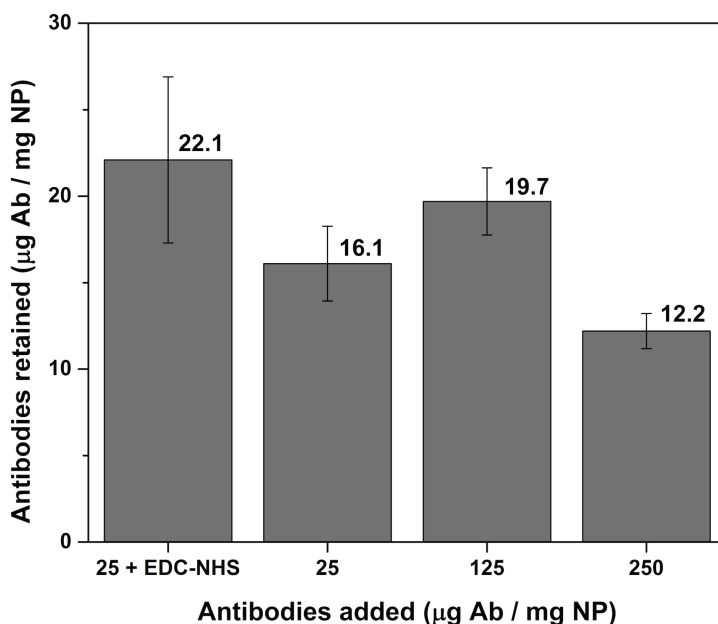


Figure 3.3: If EDC-NHS coupling reagents are added to the mixture of NP and Ab, slightly more proteins are retained on the Ab. This indicates that a small level of crosslinking occurs. When a large amount of Ab (without coupling reagents) is added, no significant difference is observed, which shows that only a hard corona remains on the NP after washing. All error bars are shown as the percentage error on the total value.

the Bradford assay are influenced by the strong light absorption of the black NP, which makes the results difficult to interpret.<sup>157</sup> FTIR spectroscopy can only confirm the presence of proteins but is not appropriate for assessing the concentration. We opted for an ELISA assay in this case, whereby the remaining proteins in the supernatant and washing fractions were determined. This way, the amount of proteins on the surface of the NP can easily be calculated. As a comparison, NP and Ab were also mixed in the absence of coupling reagents, so only aspecific adsorption could occur (protein corona formation).<sup>70,158</sup> Hence this would set a benchmark for the protein concentration of the hard corona formation (without possible protein crosslinking).<sup>73,159</sup> When the concentration of proteins was increased ten times (see Figure 3.3), the amount of adsorbed proteins does not change significantly. This indicates that the washing steps remove all proteins, except the hard corona, which is more strongly attached to the surface.<sup>73,159,160</sup> Since all three experiments without coupling reagents (including error bars) give a similar value, we learned that the hard protein corona corresponds to 15-20 micrograms of proteins per milligram nanoparticles, which is similar to literature for particles of comparable size and shape.<sup>106,161-165</sup> When we added the coupling

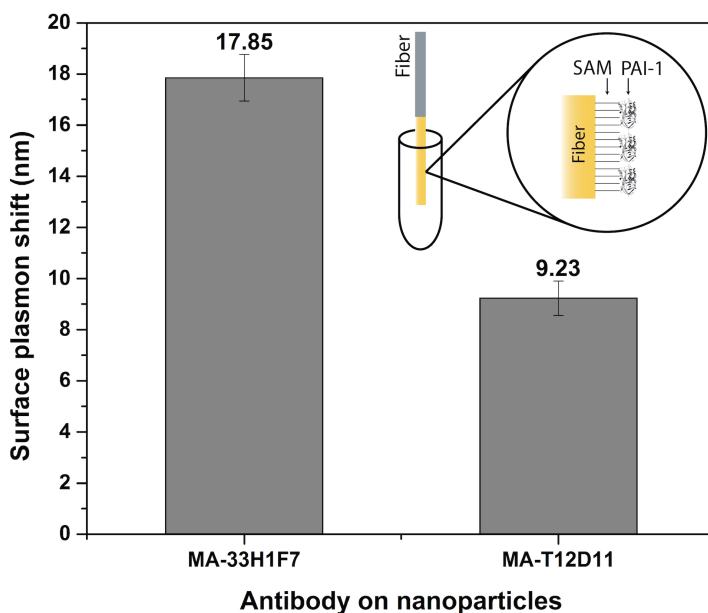


Figure 3.4: A multimode optical fiber was coated with a gold layer, a self-assembling monolayer (SAM) and the appropriate Ag (PAI-1), as shown in the inset. The SPR shift caused by the NP, coated with MA-33H1F7 or MA-T12D11, is clearly visible.

reagents (25 + EDC-NHS), we obtained a result that was comparable, but slightly higher in value. This indicates that a small amount of crosslinking is occurring, which can be expected for EDC-NHS reactions involving proteins. However the coating of the nanoparticles is close to the optimal value (solely the hard corona), which underlines the quality of the coating and the coupling procedure.

## Activity assessment

Although an ELISA can determine the loading capacity, it is incapable of assessing the activity of the coupled antibodies on the spherical nanoparticles. To investigate the ability of the Ab to recognize their Ag, the nanoconjugates were brought into contact with a PAI-1-coated SPR optical fiber. By looking at the shift in the plasmon wavelength, the interaction between Ab and Ag can be assessed. A standard multimode optical fiber was coated with a gold layer and a self-assembling monolayer with carboxylic acid end-groups.<sup>166</sup> To these groups, PAI-1 was coupled via EDC-NHS chemistry (Figure 3.4). When the nanoparticles were brought into contact with the fiber, they induced a shift in the plasmon resonance relative to their binding efficiency. The binding, as a whole, is the sum of two separate interactions: the protein corona

effect and the antibody-antigen (Ab-Ag) bond. The first is caused by the aspecific interaction between the Ab and the Ag, similar to the formation of a second (soft) corona, this cannot be avoided and hence is viewed as a background in the signal. The latter, however, is specific for each Ab-Ag couple. In this experiment, one can clearly see the difference in SPR shift, caused by the Ab-Ag interaction. An extra shift of more than 8 nm was measured by the SPR-fiber setup when comparing the NP, coated with MA-33H1F7 (targeting PAI-1) or MA-T12D11 (targeting TAFI). This result ensures that, although the Ab are coupled in a random fashion, their activity is retained and they are still partially sterically accessible. We hypothesize that a large fraction of the Ab indeed lose their activity due to an unfavorable direction of bonding. However, the strongly curved, large surface of the NP allows a high overall antibody loading capacity that partially compensates for the losses in activity. Future experiments will focus on employing a more directional coupling strategy, which will give us more insight in this complex relation.

The excellent colloidal stability of the NP, coated with the PEG-ligand, will allow to use the particles for various biomedical applications. Since the ratio of functional ligands can easily be adjusted, a library of mixed-monolayer nanoparticles can be synthesized for future experiments. Similarly, the core size of the NP can be varied, to control the overall size of the bioconjugates. This can have an important influence on their cell uptake or retention time *in vivo*.<sup>167,168</sup> Moreover, they can serve as a platform for the bioconjugation of proteins for multiple applications like selective magnetic separation or MRI contrast agents.

### 3.4 Conclusions

In order to fully customize the surface coating of iron oxide NP, a PEG building block was modified with carboxylic acid groups and afterwards attached to a siloxane via thiol-ene click chemistry. These ligands were introduced onto the NP' surface, which significantly improved the colloidal stability in complex environments. To prove their added functionality, Ab were coupled to the carboxylic acid end-groups. An ELISA was performed to indirectly determine the amount of coupled proteins, while SPR experiments confirmed their activity. Because these ligands provide excellent colloidal stability and can also act as an anchor point for coupling via a simple modification, they have high potential in future nanoparticle design for biomedical applications.

## 3.5 Supporting information

### Thiol-ene click chemistry

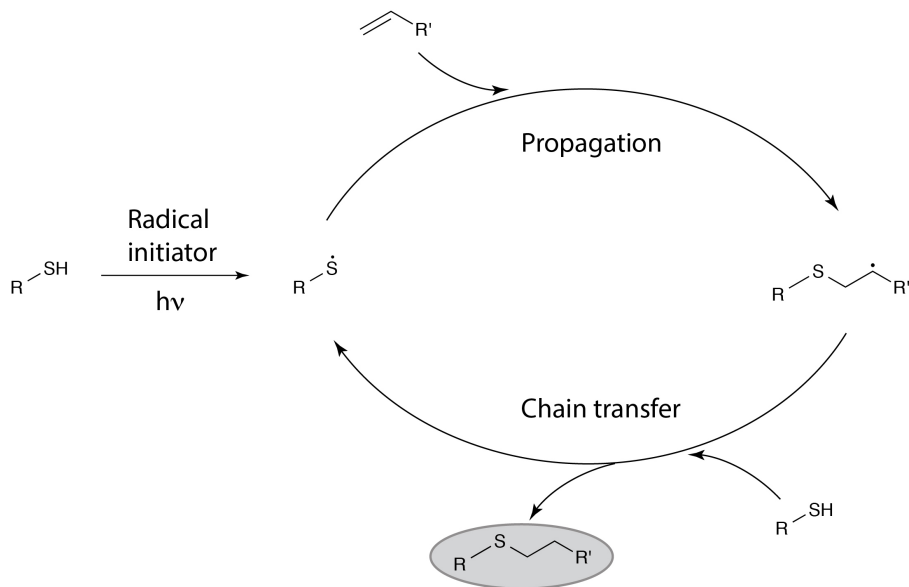


Figure 3.5: Scheme of the thiol-ene click chemistry reaction, after the formation of a thiyl radical by the initiator, a propagation step forms the bond to the alkene. A chain transfer reaction forms the new radical on another thiol-containing molecule.

An ideal thiol-ene reaction is an alternation of a radical propagation and chain transfer reaction. The propagation step involves the addition of a thiyl radical to a double bond, while the chain transfer step involves the abstraction of a hydrogen radical from the thiol by the carbon-centered radical. Ideally, no polymerization reactions, chain growth by propagation of the carbon radical onto another double bond, occur. It has been proven that the thiol-ene kinetics are largely dependent on the electron density of the double bond and steric hindrance.<sup>151,169,170</sup> Because of the fast kinetics, limited side reactions and high yields, the thiol-ene reaction is categorized under click chemistry reactions. Other typical examples are copper mediated azide-alkyne cycloadditions, Diels-Alder reactions or ring openings of strained heterocycles.<sup>150</sup>

## FTIR spectra

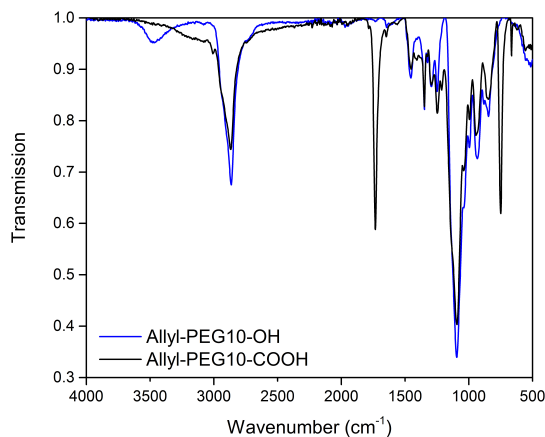


Figure 3.6: FTIR spectrum of the original allyl-PEG<sub>10</sub>-OH ligand and the modified version. The ester peak at  $1725\text{ cm}^{-1}$  is clearly visible after the ring opening of the anhydride, while the  $\text{-OH}$  peak around  $3500\text{ cm}^{-1}$  disappears.

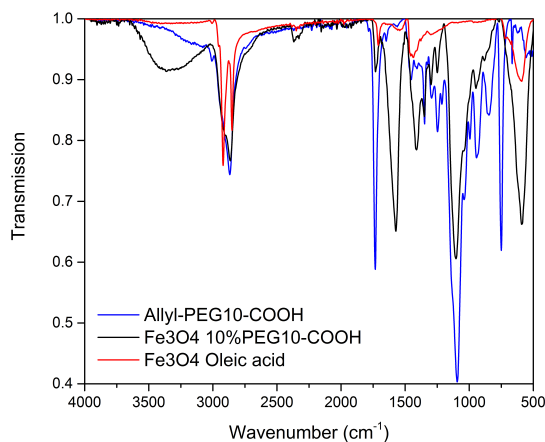


Figure 3.7: FTIR spectrum of the allyl-PEG<sub>10</sub>-COOH ligand, the oleic acid-coated and the modified iron oxide NP. The ester peak is still clearly visible at  $1725\text{ cm}^{-1}$ , as well as the different PEG vibrations between  $1250$  and  $1500\text{ cm}^{-1}$ . The presence of the iron oxide NP is confirmed by the Fe-O and Si-O vibrations at respectively,  $590$  and  $1100\text{ cm}^{-1}$ .

Colloidal stability data

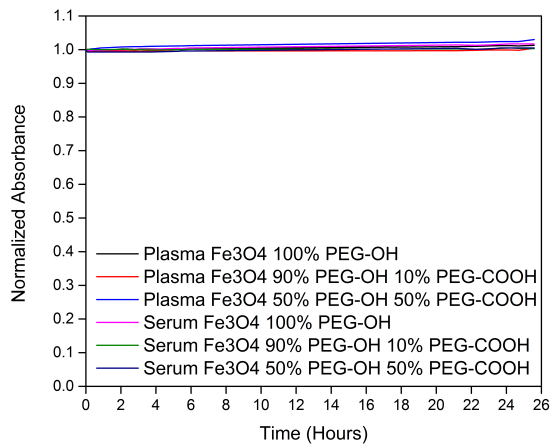


Figure 3.8: Absorbance of nanoparticle dispersions in plasma and serum. To verify the stability of the functionalized NP in complex environments; the absorbance of dispersions in plasma and serum was measured at 1000 nm. The particles were dispersed at 1 mg/mL and the absorbance was monitored for 25 hours. A significant decrease of the absorbance would indicate colloidal instability and precipitation of the NP.

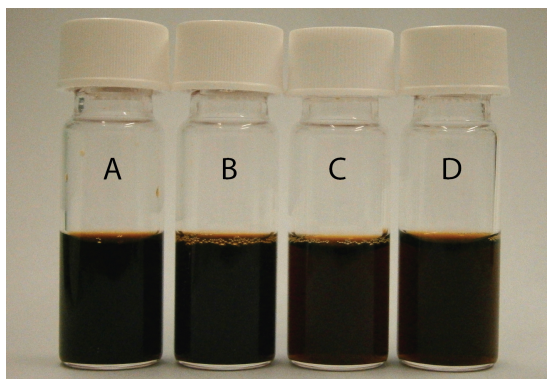


Figure 3.9: The colloidal stability of the nanoparticle dispersions is excellent, even after 1 year of storage. The samples (5 mg/mL in water, pH 7) shown above have the following coatings (molar percentages): **A**, 100% PEG<sub>10</sub>-OH; **B** 10% PEG<sub>10</sub>-COOH 90% PEG<sub>10</sub>-OH; **C**, 25% PEG<sub>10</sub>-COOH 75% PEG<sub>10</sub>-OH; **D**, 50% PEG<sub>10</sub>-COOH 50% PEG<sub>10</sub>-OH

## TEM data

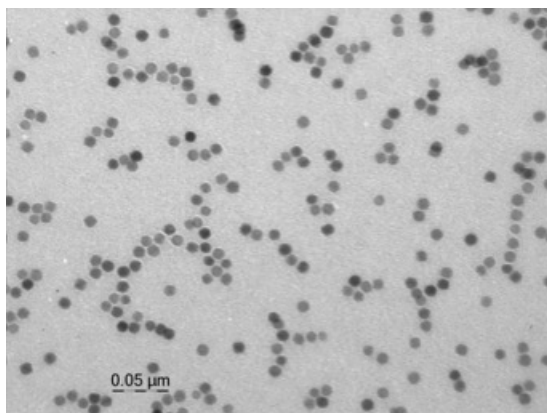
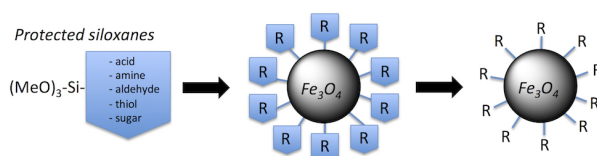


Figure 3.10: TEM image of the iron oxide NP ( $8.6 \pm 0.6$  nm). Their size was determined by ImageJ software.

## Chapter 4

# Two-step directional surface modification via protected siloxanes



This chapter is based on the following publication with minor modifications:

**Bloemen M**, Sutens B, Brullot W, Gils A, Geukens N and Verbiest T  
Two-step directional surface modification of iron oxide nanoparticles via protected siloxanes  
*ChemPlusChem* 2014; 80: 50-53

B. Sutens helped with the click chemistry reactions and particle functionalization. Dr. W. Brullot performed the nanoparticle multilayer experiments and interpreted the results.

## Abstract

Successful surface modification of iron oxide NP is crucial for their usage in applications. However, ligand exchange methods introducing siloxanes have a few drawbacks. We herein present a novel approach for surface modification of iron oxide NP by making use of siloxanes, synthesized by thiol-ene click chemistry, with protected functional groups. Afterwards the ligands were deprotected to liberate their functionality. This approach solves the issues related to ligand orientation and colloidal stability during surface modification.

## 4.1 Introduction

There is an increased interest in the development of iron oxide NP with customized surface functionalization, which can be used in magnetic storage devices, ferrofluids, drug delivery, contrast agents or hyperthermia applications.<sup>26,104,109,171–174</sup> Multiple protocols have already been published for obtaining high quality monodisperse spherical NP.<sup>12,14,175,176</sup> These particles are often coated with apolar alkyl chains, like oleic acid or oleylamine, that serve as surfactants during the synthesis. However, for most applications they have to be replaced by other ligands, which make the NP dispersible in water or introduce functional groups. This so-called ligand exchange process can be performed with different molecules. Polymers and phospholipid double layers are often used, since they are very versatile and can be easily introduced.<sup>144,177</sup> Catechol-containing molecules are another option, but their synthesis is rather complicated.<sup>55,178,179</sup> Moreover, these ligands are not covalently coupled to the surface. Valuable alternatives are silica or siloxane shells that are very robust and can be well defined. Since siloxane molecules can have functional groups, they are often the molecules of choice for functionalization of metal oxide surfaces.<sup>120,127,147,180</sup> However, these functionalities induce a few issues for iron oxide NP surface modification. Firstly, the colloidal stability of the NP during the modification process is crucial; if NP precipitate from the reaction solution this will have a negative effect on the coating procedure's performance. Secondly, multiple popular functional groups (carboxylic acids, amines, ...) can also interact with the surface of the NP itself. This way, the molecule can be oriented upside-down, with the siloxane groups pointing outwards, which results in crosslinking and excessive layer thickness.<sup>181–183</sup> Another challenging property of siloxanes is their tendency to crosslink through the presence of small amounts of water or prolonged exposure to heat. This requires the reactions to be limited in time and influences the available workup methods. Tucker-Schwartz et al. reported the synthesis of siloxanes by using thiol-ene click chemistry, which can produce complex molecules on a large scale with minimal impurities.<sup>148</sup>

In this chapter, we made use of thiol-ene click chemistry to synthesize various different siloxanes with protected functional groups. These were introduced onto the surface of iron oxide NP and deprotected later on. This novel approach solves the issues of wrong ligand orientations and colloidal stability issues. By adopting the thiol-ene

click reactions; we were able to synthesize various siloxanes that are not commercially available, without elaborate organic synthesis steps. Initially apolar NP could be dispersed in an aqueous phase after coating with protected polar siloxanes and subsequent deprotection of their functional groups. The presented concept is generic and is in no way limited to the ligands that are discussed in this manuscript.

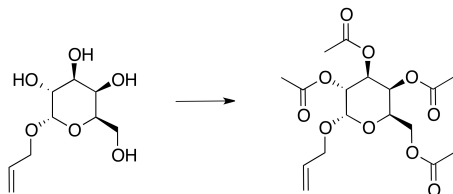
Finally, the amine functionalized NP were used as a building block in a layer-by-layer synthesis of nanoparticle multilayers to prove their efficiency in these complex systems. Such magnetic-plasmonic nanoparticle multilayers can be used for fundamental research to unravel interactions at the nanoscale (magnetoplasmonics) and for applications in sensing, optical switching and designing optical components. To be used for such research, nanocomposites need to have large nanoparticle filling fractions, a minimum of potentially disturbing organic content and partial transparency.<sup>184</sup> Layer-by-layer nanocomposites are mainly synthesized using polymers or polyelectrolytes as ‘glue’ interlayers between nanoparticle layers, which inherently limits nanoparticle filling fractions and can introduce unwanted noise. Recently, a novel synthesis method for such nanoparticle multilayers was developed that uses short bifunctional molecular linkers to connect the subsequent nanoparticle layers.<sup>184</sup> No polymers or polyelectrolytes are used in this method. To produce gold-magnetite nanoparticle multilayers, aminosiloxanes are ideal molecules as they can strongly bind to gold through the amino functionality and to magnetite through the siloxane moiety.

## 4.2 Materials and methods

### Materials

Allyl  $\alpha$ -D-galactopyranoside (97%), 4-dimethylaminopyridine (DMAP, >99%), tert-butyl acrylate (98%), 2,2-dimethoxy-2-phenylacetophenone (DMPAP, 99%), tert-butyl N-allylcarbamate (98%), acrolein dimethyl acetal (98%), mercaptopropyltrimethoxysilane (95%), trimethoxy(7-octen-1-yl)silane (80%, technical grade) and trifluoroacetic acid (TFA, 99%) were purchased from Sigma Aldrich. S-allyl thiopropionate (99%) was bought from ABCR GmbH & Co. 1-thioacetic acid (98%) was obtained from Acros Organics. Triethylamine (99%) and tetrabutyl ammonium hydrogen sulphate (98%) were purchased from Janssen Chimica. Acetic anhydride (pro analysis) and sodium hydroxide were obtained from Riedel de Haën. All ultrasonication steps were performed in a Branson 5510 sonicator bath. FTIR spectra were measured using a Bruker Alpha FT-IR spectrometer equipped with a Platinum ATR module. CHN data were obtained by a CE Instruments EA-1110 elemental analyzer.

### Acetylation of allyl $\alpha$ -D-galactopyranoside

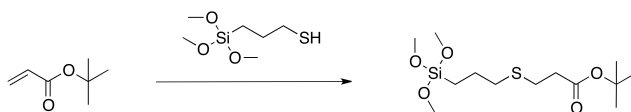


The acetylation of the sugar starts with adding allyl  $\alpha$ -D-galactopyranoside (440 mg, 2 mmol) to a mixture of 4-dimethylaminopyridine (12.2 mg, 0.1 mmol) and acetic anhydride (3.78 mL, 40 mmol). This solution was stirred overnight at a temperature of 80°C. The resulting mixture was added to an excess dichloromethane in a separatory funnel and washed three times with 40 mL MilliQ water. Afterwards, the solution was washed with 50 mL of 1M NaOH and potassium carbonate until the pH was neutral. The resulting solution was dried with magnesium sulfate and filtered. The product (620 mg, 83 %) was obtained after removing the dichloromethane under reduced pressure.  $^1\text{H}$  NMR (300 MHz,  $\text{CDCl}_3$ ):  $\delta$  (ppm) 2-2.2 (s, 12H), 4.15-4.25 (m, 5H), 5.1-5.5 (m, 6H), 5.8-6.0 (m-1H).

## Thiol-ene click chemistry

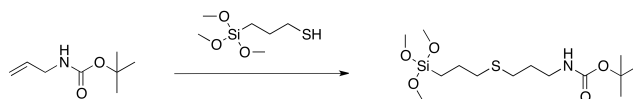
The synthesis of the functionalized trimethoxysiloxanes was done in a UV chamber, equipped with 3 LEDs (365 nm, output power 200 mW), following the method published by Tucker-Schwartz *et al.*<sup>148</sup> All products were used in the subsequent nanoparticle functionalization protocol without further purification.

### Siloxane-acrylate (1)



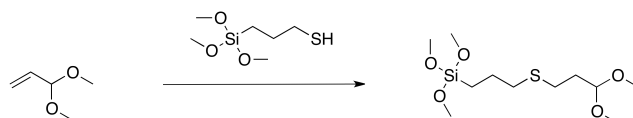
For the synthesis of the siloxane-acrylate, tert-butyl acrylate (73.24  $\mu\text{L}$ , 0.5 mmol) was added to 3-mercaptopropyltrimethoxysilane (93  $\mu\text{L}$ , 0.5 mmol), 2,2-dimethoxy-2-phenylacetophenone (12.8 mg, 0.05 mmol) and 0.5 mL chloroform. This mixture was placed next to a UV-light for 1 hour on top of a stirring plate.  $^1\text{H}$  NMR (300 MHz,  $\text{CDCl}_3$ ):  $\delta$  (ppm) 0.78 (t, 2H), 1.46 (s, 9H), 1.59 (m, 2H), 2.5 (t, 2H), 2.6 (t, 2H), 2.75 (t, 2H), 3.57 (s, 9H).

### Siloxane-carbamate (2)



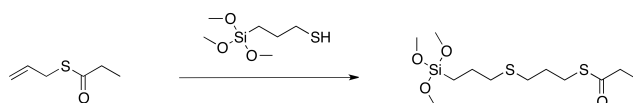
Tert-butyl N-allylcarbamate (78,6 mg, 0.5 mmol) was added to a mixture of 3-mercaptopropyltrimethoxysilane (93  $\mu$ L, 0.5 mmol) and 2,2-dimethoxy-2-phenylacetophenone (12.8 mg, 0.05 mmol) in 0.5 mL chloroform. This mixture was placed next to a UV-light for 1 hour on top of a stirring plate.  $^1\text{H}$  NMR (300 MHz,  $\text{CDCl}_3$ ):  $\delta$  (ppm) 0.75 (t, 2H), 1.49 (s, 9H), 1.65 (m, 2H), 1.74 (m, 2H), 2.55 (t, 4H), 3.2 (t, 2H), 3.57 (s, 9H).

### Siloxane-acrolein (3)



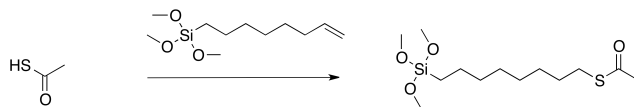
The synthesis of the siloxane-acrolein starts with adding acrolein dimethyl acetal (59.24  $\mu$ L, 0.5 mmol) to 3-mercaptopropyltrimethoxysilane (93  $\mu$ L, 0.5 mmol), 2,2-dimethoxy-2-phenylacetophenone (6.4 mg, 0.05 mmol) and 0.5 mL chloroform. Secondly, the mixture was placed next to a UV-light for 1 hour on top of a stirring plate.  $^1\text{H}$  NMR (300 MHz,  $\text{CDCl}_3$ ):  $\delta$  (ppm) 0.76 (t, 2H), 1.7 (m, 2H), 1.89 (q, 2H), 2.56 (t, 4H), 3.34 (s, 6H), 3.57 (s, 9H), 4.5 (t, 1H).

### Siloxane-thiol-propionate (4)



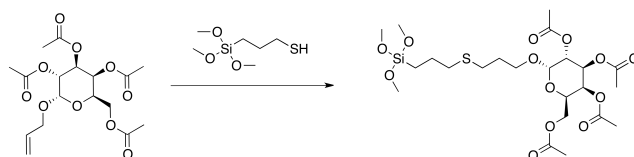
S-allyl thiopropionate (67.5  $\mu$ L, 0.5 mmol) was added to a mixture of 3-mercaptopropyl trimethoxysilane (93  $\mu$ L, 0.5 mmol) and 2,2-dimethoxy-2-phenylacetophenone (6.4 mg, 0.025 mmol) in 0.5 mL chloroform. This mixture was placed next to a UV-light for 1 hour on top of a stirring plate.  $^1\text{H}$  NMR (300 MHz,  $\text{CDCl}_3$ ):  $\delta$  (ppm) 0.76 (t, 2H), 1.18 (t, 3H), 1.7 (m, 2H), 1.85 (m, 2H), 2.56 (m, 6H), 2.95 (t, 2H), 3.57 (s, 9H).

### Siloxane-C8-thiol-acetate (5)



1-thioacetic acid (35.23  $\mu\text{L}$ , 0.5 mmol) was added to trimethoxy(7-octen-1-yl)silane (125.35  $\mu\text{L}$ , 0.5 mmol) and 2,2-dimethoxy-2-phenylacetophenone (6.4 mg, 0.025 mmol) in 0.5 ml chloroform. This mixture was placed next to UV-light for 1 hour on top of a stirring plate.  $^1\text{H}$  NMR (300 MHz,  $\text{CDCl}_3$ ):  $\delta$  (ppm) 0.64 (t, 2H), 1.3-1.5 (m, 10H), 1.58 (m, 2H), 2.36 (s, 2H), 2.85 (t, 2H), 3.57 (s, 9H).

### Siloxane-acetylated-sugar (6)



Tetra-acetyl allyl  $\alpha$ -D-galactopyranoside (194 mg, 0.5 mmol) was added to a mixture of 3-mercaptopropyltrimethoxysilane (93  $\mu\text{L}$ , 0.5 mmol) and 2,2-dimethoxy-2-phenylacetophenone (6.4 mg, 0.025 mmol) in 0.5 ml chloroform. This mixture was placed next to a UV-light for 1 hour on top of a stirring plate.  $^1\text{H}$  NMR (300 MHz,  $\text{CDCl}_3$ ):  $\delta$  (ppm) 0.76 (t, 2H), 1.72 (m, 2H), 1.85 (m, 2H), 2-2.2 (s, 12H), 2.56 (t, 2H), 2.6 (t, 2H), 3.52 (t, 2H), 3.57 (s, 9H), 3.8 (m, 1H), 4.15+4.25 (t, 2H), 5.1-5.5 (m, 4H).

## Nanoparticle synthesis and functionalization

The NP were synthesized and functionalized, following the methods described in chapter 2 and 3. The functionalized NP were dispersed in the appropriate solvent (chloroform or THF, for deprotection) with a concentration of 5 mg/mL.

### Deprotection of the functional group

The deprotection of the functionalized particles can be divided in two different methods. The first method includes the deprotection of the tert-butyl acrylate (**1**), tert-butyl N-allylcarbamate (**2**) and the acrolein dimethyl acetal (**3**) with a 1:1 mixture of trifluoroacetic acid (TFA) and dichloromethane. Secondly, grinded sodium hydroxide and tetrabutyl ammonium hydrogen sulphate were used to deprotect the thiopropionate (**4**), the thioacetate (**5**) and the tetra-acetyl  $\alpha$ -D-galactopyranoside (**6**), as reported by Crouch et al. with minor modifications.<sup>185</sup>

### **TFA/CH<sub>2</sub>Cl<sub>2</sub>**

5 mg functionalized particles (in CHCl<sub>3</sub>, 5 mg/mL) were added to a flask with 1.5 mL dichloromethane and 2.5 mL trifluoroacetic acid. The flask was put on a shaker overnight at room temperature. The particles were then magnetically separated and washed three times with acetone. Finally the NP were stored in MilliQ water, with a concentration of 5mg/mL.

### **Grinded NaOH/Bu<sub>4</sub>NHSO<sub>4</sub>**

For the deprotection with grinded NaOH and Bu<sub>4</sub>NHSO<sub>4</sub>, 1 mg functionalized particles (in THF, 5 mg/mL) were mixed with grinded NaOH (16 mg, 0.4 mmol), Bu<sub>4</sub>NHSO<sub>4</sub> (3.2 mg, 0.08 mmol) and 1 mL tetrahydrofuran. The resulting solution was placed in the ultrasonication bath for 5 hours. Afterwards, the particles were magnetically separated and washed three times with THF and acetone. Finally the NP were stored in MilliQ water, with a concentration of 5 mg/mL.

### **Layer-by-layer**

Nanoparticle multilayers incorporating gold and amine-functionalized magnetite NP on glass substrates were synthesized as published elsewhere.<sup>184</sup> Briefly stated, first gold NP with a size of approximately 9.2 nm and a strong plasmon resonance centered on 530 nm were produced using an aqueous citrate reduction procedure.<sup>186</sup> Synthesis of the nanoparticle multilayers started by cleaning glass microscope slides (16x16 mm<sup>2</sup>) with NoChromix cleaning solution (7 g/100 mL NoChromix in MilliQ water, add 100 mL sulfuric acid 97%) for 1 h. These cleaned substrates were then functionalized with amino propyl trimethoxy silane (1 vol% in MeOH, 1 h) and rinsed with MeOH and water. A first metal nanoparticle layer was added by putting the functionalized substrate in 10 mL of a metal NP dispersion while shaking (350 rpm) for 1.5 h and rinsing with water and MeOH afterwards. By putting the sample in 10 mL of a 0.4 mg/mL dispersion of functionalized iron oxide NP in MeOH for 1 h, a layer of these NP could be added on top of the gold nanoparticle layer. After rinsing the sample with methanol and water, adding extra nanoparticle layers was possible by repeating the previous steps.

## **4.3 Results & Discussion**

### **Methodology**

To rule out unwanted interactions between the functional group of siloxane molecules and the surface of the iron oxide NP, we developed a strategy that involves the synthesis

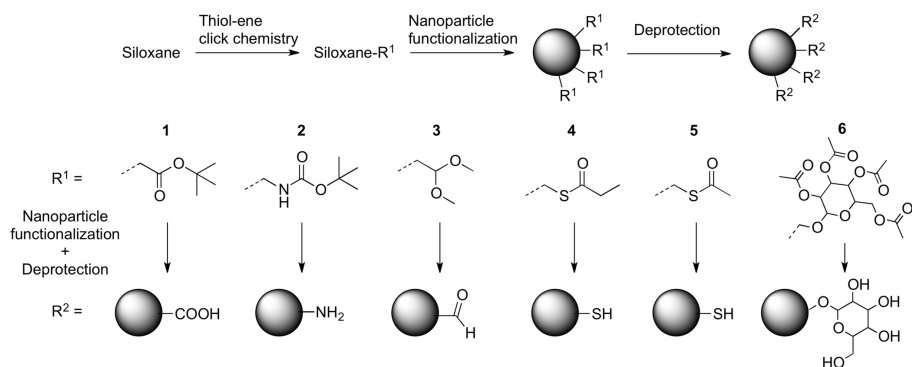


Figure 4.1: Six different siloxanes, with protected groups, were synthesized by click chemistry for subsequent introduction on the surface of iron oxide NP. Later on, the ligands were deprotected to make the desired functional group available. This results in free carboxylic acids (**1**), amines (**2**), aldehydes (**3**), thiols (**4**, **5**) or sugars (**6**) on the surface of the nanoparticle. All experimental information can be found in the supporting information at the end of this chapter.

of protected siloxanes and their subsequent deprotection after surface functionalization (see Figure 4.1). This method has a three major advantages: first, it protects functional groups that can interact directly with the surface, like carboxylic acids (**1**) or amines (**2**).<sup>181–183,187,188</sup> Hence, only the siloxane side of the molecule can interact with the surface of the nanoparticle, which ensures proper directionality. Secondly, groups that would not survive the functionalization procedure in the ultrasonicator (such as aldehydes) can be introduced (**3**). They would hydrolyze, by the presence of water at elevated temperatures. Thirdly, it is possible to introduce functionalities that provide insufficient colloidal stability (due to polarity) during the functionalization step, like thiols (**4**, **5**) or sugars (**6**). The ligand exchange reaction was performed in toluene, since this solvent has the perfect water content (0.3–0.4%) for silanization reactions.<sup>189</sup> Unfortunately, this method is limited to siloxanes that dissolve properly in toluene and provide sufficient colloidal stability to the nanoparticle. Our approach eliminates the restrictions due to polarity of the ligands, because most protective groups, such as tert-butyl esters, are apolar (see Figure 4.1). The apolar groups stabilize the particle in toluene, which improves the functionalization by keeping the nanoparticle in dispersion (avoiding precipitation).

To our knowledge, none of the siloxanes shown in Figure 4.1 is commercially available, so we opted for the straightforward approach of thiol-ene click chemistry to synthesize the different compounds. Because this click reaction is fast and gives high yields, side reactions of the trimethoxy groups are limited.<sup>151</sup> Multiple different molecules with an allyl functionality are readily available since they are vinyl-monomers, which are often used in polymerization reactions.

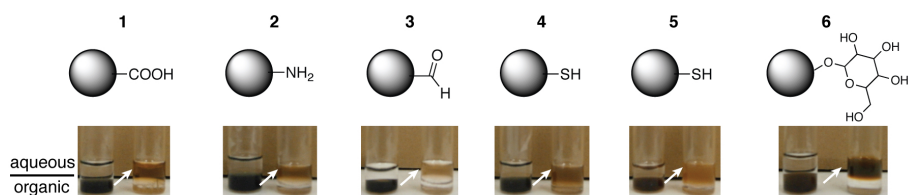


Figure 4.2: The transfer from the organic (lower phase) to the aqueous phase (upper phase) is clearly visible after the deprotection of the ligands on the NP.

Deprotection of all ligands was achieved by typical protocols with minor modifications, more specific the duration of the reaction.<sup>190</sup> Similar to dendrimer chemistry, long reaction times are necessary to ensure that full deprotection has occurred.<sup>191</sup> This is caused by the limited rotational freedom of the ligands and the corresponding steric hindrance. Therefore, we prolonged the TFA and sodium hydroxide deprotection protocols to 16 and 5 hours respectively. The deprotection reaction for compounds **4**, **5**, **6** was performed in an ultrasonicator, which raises the temperature to approximately 55°C and improves the solubility of all reagents. Figure 4.2 shows the phase transfer that occurs after the ligands are deprotected. After the initial ligand exchange, the NP are apolar and hence they only disperse in the bottom organic phase. The successful introduction of the ligands on the surface is supported by FTIR measurements (data in supporting information at the end of this chapter). The characteristic peaks of the different functional groups are clearly visible in the spectra of the NP samples. After deprotection, the NP become polar and can be dispersed in the upper aqueous phase. Since no particles are visible in the organic phase after deprotection, we can conclude that the polarity of the particles has switched from apolar to polar, indicating a successful deprotection. CHN analyses also supported the deprotection of the functional groups (data in supporting information at the end of this chapter, Table 4.1). However this approach is no guarantee for colloidal stability of the NP in the aqueous phase. Aldehydes (**3**) and thiols (**4**, **5**) possess no charges (or can form disulfide bridges) in a pH range between 4 and 10 and they are therefore very susceptible to precipitation. This is visible in Figure 4.2 as a slightly turbid aqueous phase.

NP with charged carboxylic acids and amines are often used in nanotoxicity experiments to test the effect of the surface charges on the cellular uptake.<sup>17</sup> Thiol-coated NP, on the other hand, are valuable for their interaction with noble metals, like gold or silver. Sugar molecules are biocompatible; which makes these sugar-coated NP interesting for biomedical applications. Unlike typical sugar-containing polymers like dextran, the presented approach results in a very thin surface layer, with a directional bonding.<sup>192</sup>

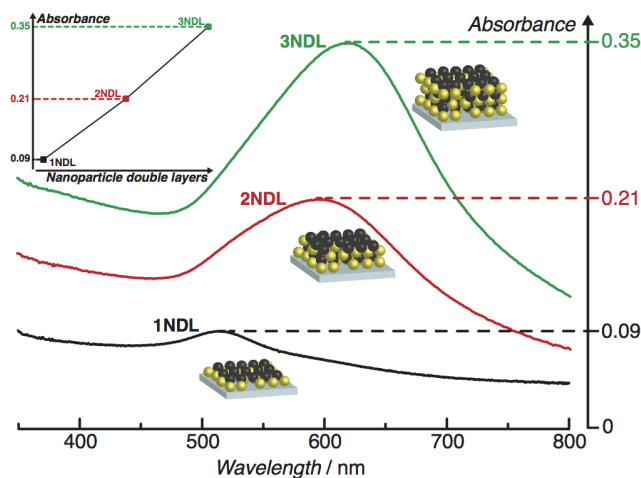


Figure 4.3: Due to plasmon hybridization the plasmon resonance broadens and red-shifts with each added nanoparticle double layer (NDL). The absorbance at maximal intensity increases linearly with the number of added nanoparticle layers, demonstrating that the layer-by-layer procedure was successful (inset).

## Nanoparticle multilayers

To demonstrate their efficiency in more complex systems, amine-functionalized iron oxide NP, together with gold NP were incorporated in nanoparticle multilayers. To produce gold-magnetite nanoparticle multilayers, amino-siloxanes are ideal molecules as they can strongly bind to gold through the amino functionality and to magnetite through the siloxane moiety. Such multilayers, in which nanoparticle layers are layer-by-layer constructed through short molecular linkers, have large nanoparticle filling fractions and interesting linear, nonlinear and magneto-optical properties.<sup>184</sup> They can be applied for research into e.g. plasmon influenced (magneto-) optical effects and active plasmonics through magnetism.

When adding multiple gold and magnetite nanoparticle layers, the plasmon resonance of gold NP broadens and red-shifts due to plasmon hybridization (see Figure 4.3).<sup>184</sup> The linear increase of the absorbance at maximal intensity demonstrates the success of the layer-by-layer process. In contrast to previously used amine-functionalized iron oxide NP, the NP presented in this work are monodisperse and have a well defined surface functionalization. This is an asset for layer-by-layer processes as it might improve packing of subsequent nanoparticle multilayers.

## 4.4 Conclusions

We developed a new approach for efficient functionalization of iron oxide NP by using protected siloxanes as ligands. Six different protected ligands, with a large variety of functional groups (including carboxylic acids, amines, thiols, aldehydes and sugars), were prepared by thiol-ene click chemistry and subsequently introduced onto the surface of the NP by a ligand exchange reaction. By protecting the functional group, a directional bonding of the ligand on the iron oxide surface was ensured. Moreover, this approach allows the introduction of very polar or reactive functional groups. After deprotection of these groups, all samples were dispersible in aqueous solutions, indicating a successful surface functionalization. To highlight the potential of the NP, they were incorporated in nanoparticle multilayers, a very promising material where well-defined surface properties are crucial.

## 4.5 Supporting information

### FTIR spectra of synthesized compounds

This section combines all FTIR spectra of the synthesized protected siloxanes. These spectra serve as a reference for subsequent nanoparticle functionalization.

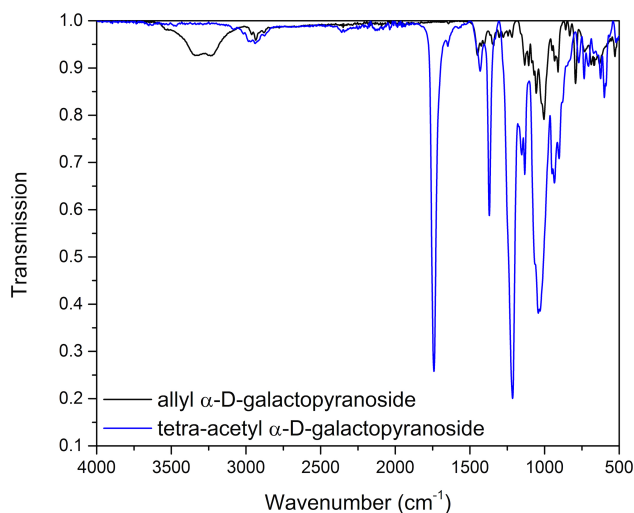


Figure 4.4: Spectrum of allyl  $\alpha$ -D-galactopyranoside and the acetylated end-product. The broad OH vibrations at  $3200\text{--}3500\text{ cm}^{-1}$  are clearly replaced by the ester peak at  $1720\text{ cm}^{-1}$ .

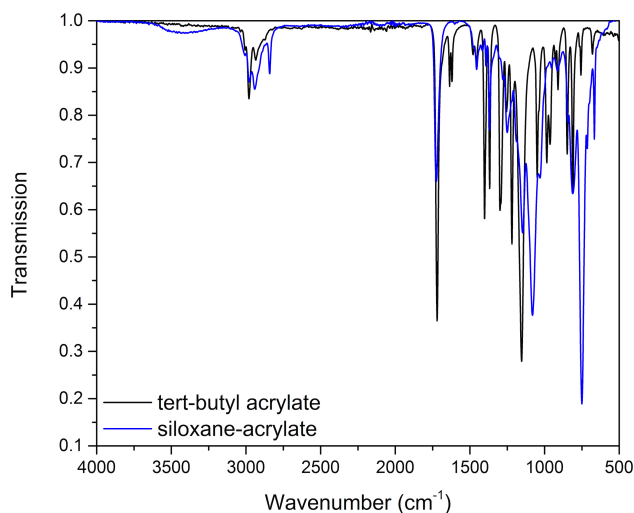


Figure 4.5: Spectrum of the tert-butyl acrylate and the siloxane-acrylate (**1**) end-product. Characteristic peaks of this product are the Si-O vibration at  $1100\text{ cm}^{-1}$  and the ester peak at  $1720\text{ cm}^{-1}$ .

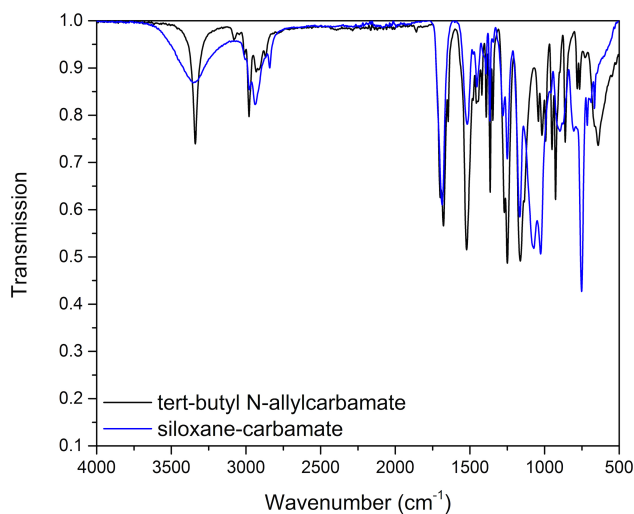


Figure 4.6: Spectrum of the tert-butyl N-allylcarbamate and the siloxane-carbamate (**2**) end-product. Characteristic peaks of this product are the Si-O vibration at  $1100\text{ cm}^{-1}$ , the ester peak at  $1720\text{ cm}^{-1}$  and the amine band at  $3100\text{--}3500\text{ cm}^{-1}$ .

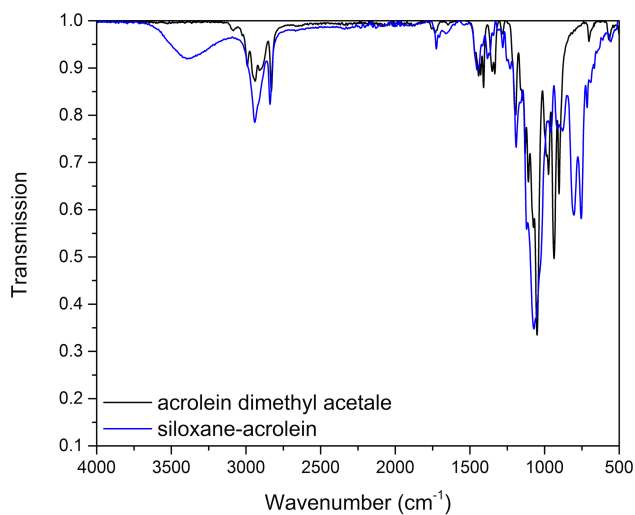


Figure 4.7: Spectrum of the acrolein dimethyl acetale and the siloxane-acrolein (**3**) end-product.

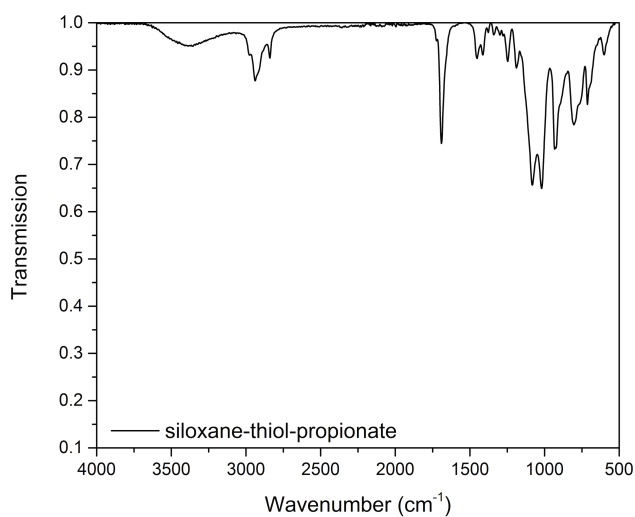


Figure 4.8: Spectrum of the siloxane-thiol-propionate (**4**) compound. S-allyl thiopropionate was not measured because of its odor and the related safety issues. Characteristic peaks of this product are the Si-O vibration at 1100 cm<sup>-1</sup> and the ester peak at 1720 cm<sup>-1</sup>.

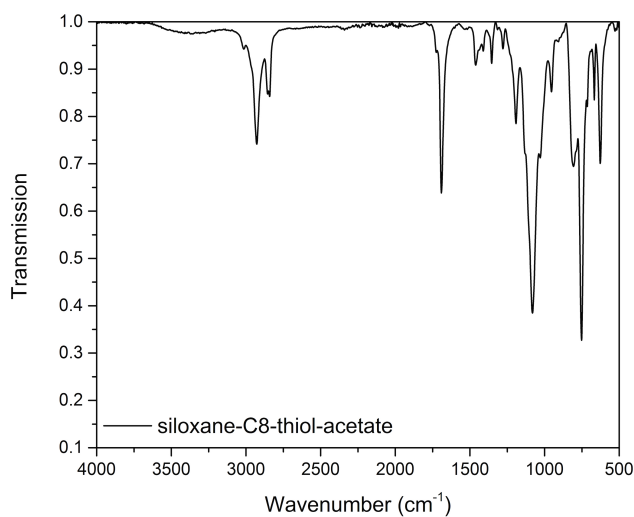


Figure 4.9: Spectrum of the siloxane-C8-thiol-acetate (**5**) compound. 1-thioacetic acid was not measured because of its odor and the related safety issues. Characteristic peaks of this product are the Si-O vibration at  $1100\text{ cm}^{-1}$ , the ester peak at  $1720\text{ cm}^{-1}$  and the C-H vibrations at  $2920\text{--}2930\text{ cm}^{-1}$ .

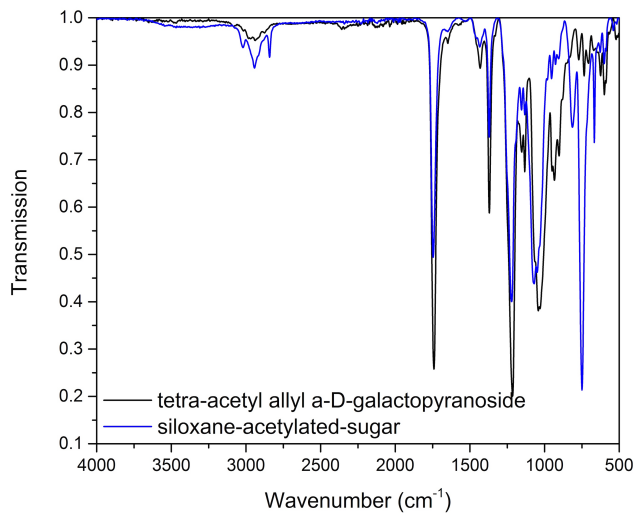


Figure 4.10: Spectrum of the tetra-acetyl allyl  $\alpha$ -D-galactopyranoside and the siloxane-sugar (**6**) end-product. Characteristic peaks of this product are the Si-O vibration at  $1100\text{ cm}^{-1}$  and the ester peak of the four protective acetyl-esters at  $1720\text{ cm}^{-1}$ .

## FTIR spectra of functionalized nanoparticles

This section shows all spectra of the protected siloxanes and the NP samples, functionalized with those protected siloxanes. In all spectra, a substantial overlap between both spectra can be observed, indicating a successful functionalization of the NP. Characteristic vibrations of iron oxide can be seen at  $580\text{--}620\text{ cm}^{-1}$  (Fe-O).

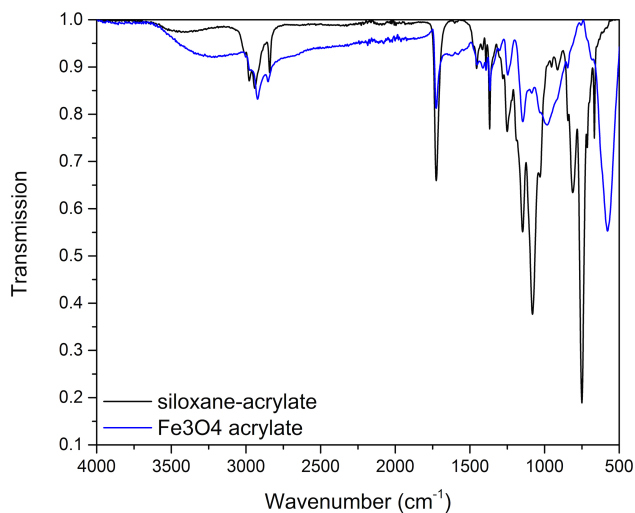


Figure 4.11: Spectrum of siloxane-acrylate (**1**) functionalized iron oxide NP.

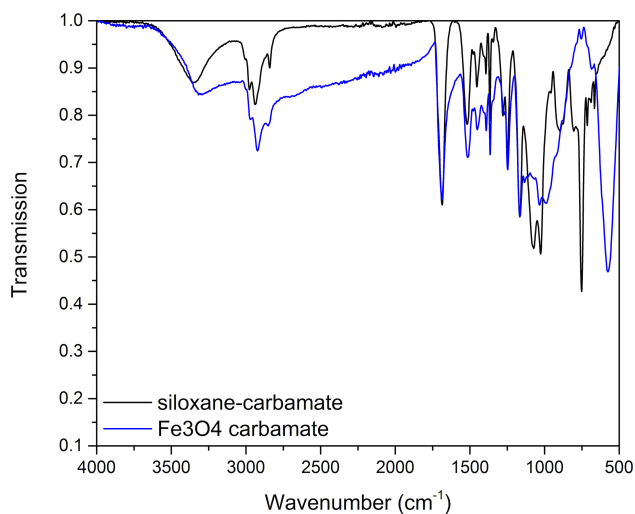


Figure 4.12: Spectrum of siloxane-carbamate (**2**) functionalized iron oxide NP.

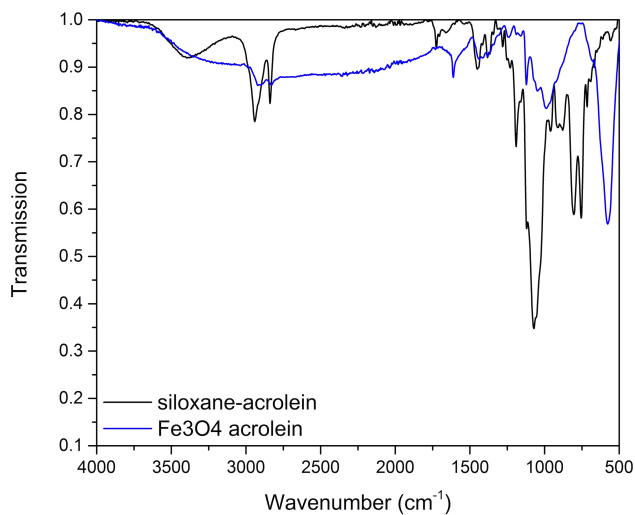


Figure 4.13: Spectrum of siloxane-acrolein (**3**) functionalized iron oxide NP.

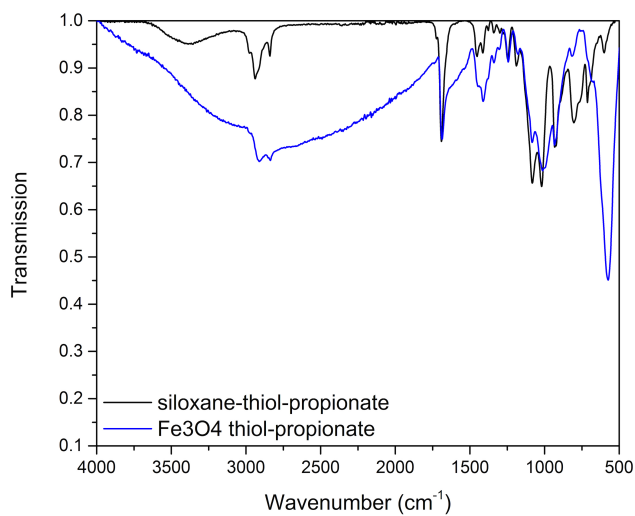


Figure 4.14: Spectrum of siloxane-thiol-propionate (4) functionalized iron oxide NP.

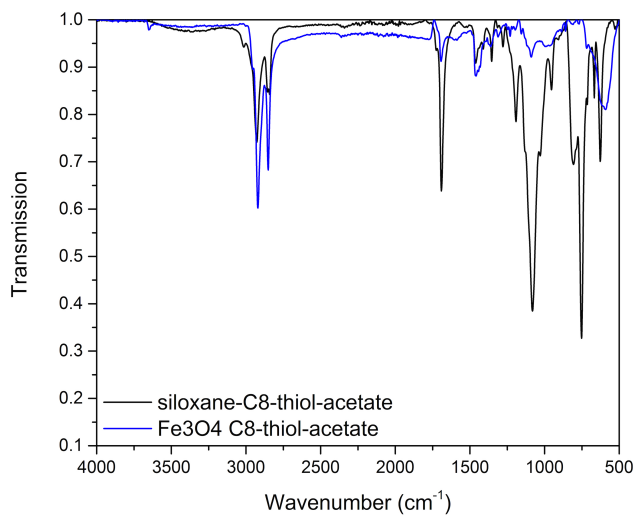


Figure 4.15: Spectrum of siloxane-C8-thiol-acetate (5) functionalized iron oxide NP.

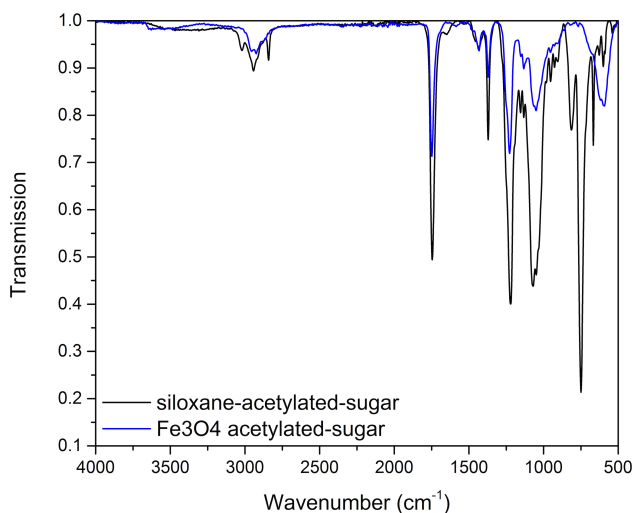


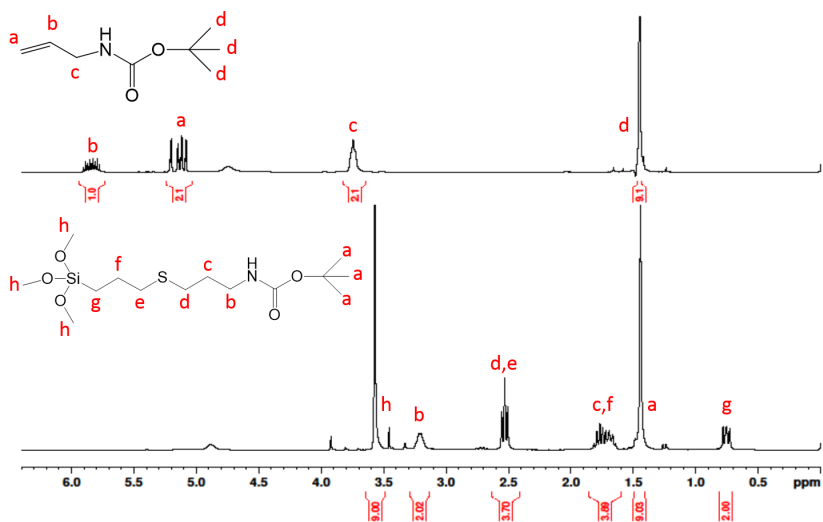
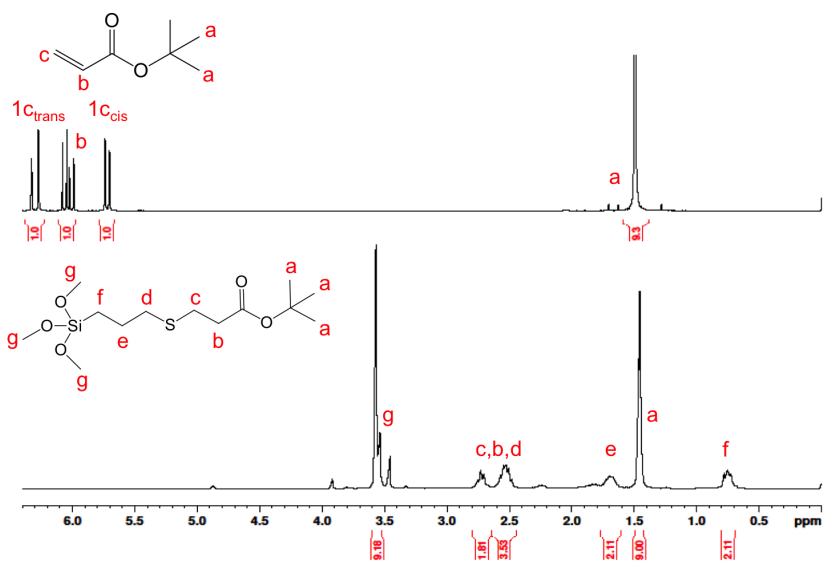
Figure 4.16: Spectrum of siloxane-acetylated-sugar (**6**) functionalized iron oxide NP.

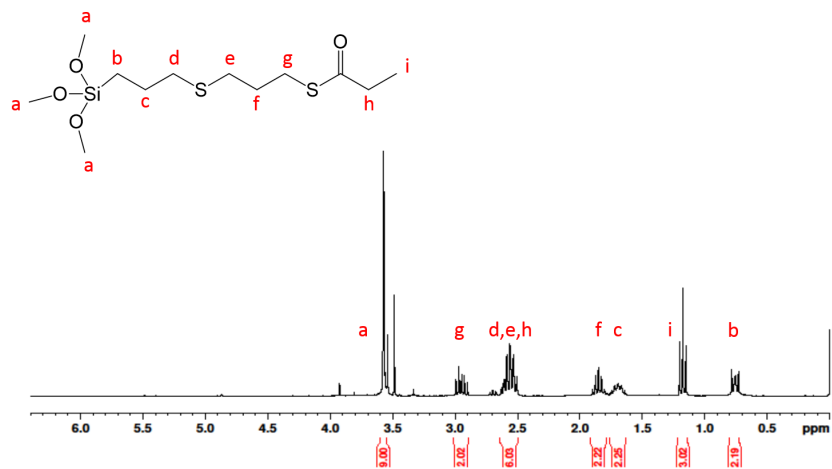
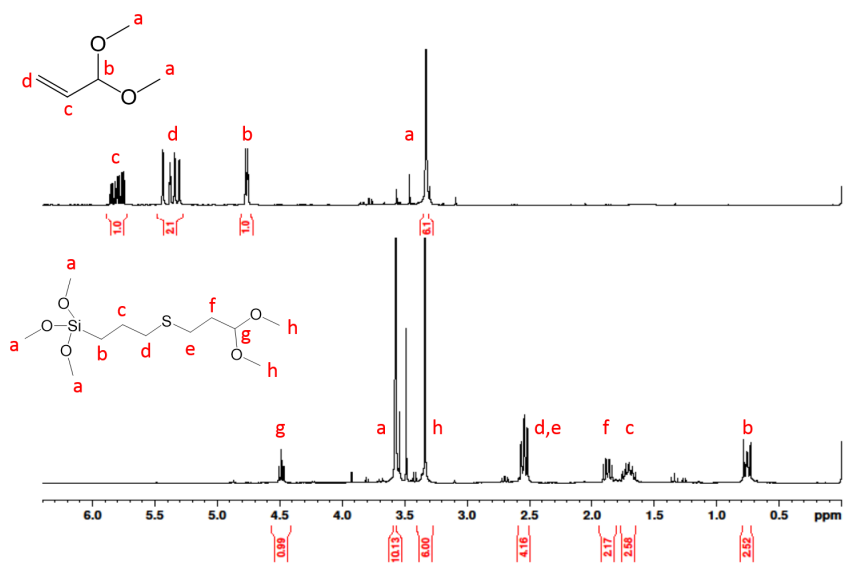
## <sup>1</sup>H-NMR spectra of synthesized compounds

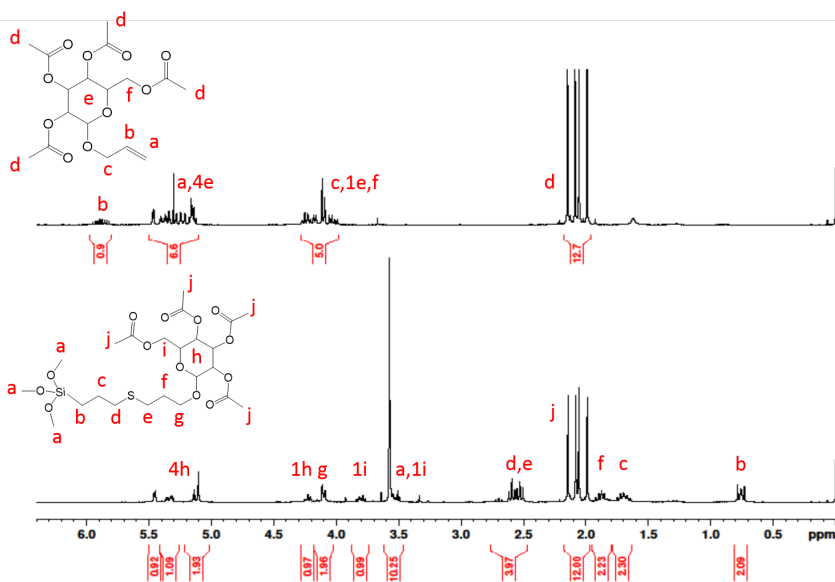
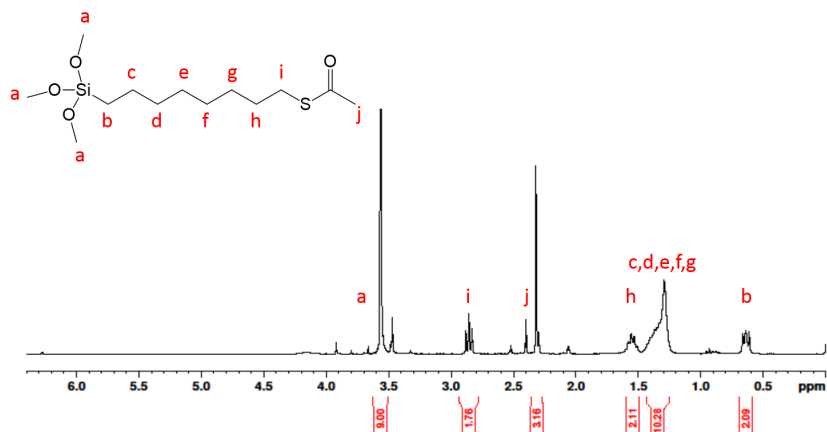
In this section, all <sup>1</sup>H-NMR spectra of the synthesized protected siloxanes are shown. The peaks of the double bond (5.0-6.5 ppm) disappear after the click chemistry, indicating a successful reaction. Due to safety restrictions, the precursors for the protected thiol siloxanes (**4**, **5**) were not measured. We refer the reader to a manufacturer's website, where these spectra can be found.

S-allyl thiopropionate: <http://www.sigmaaldrich.com/catalog/product/aldrich/w332909>

1-thioacetic acid: <http://www.sigmaaldrich.com/catalog/product/aldrich/t30805>







## CHN analysis derived data

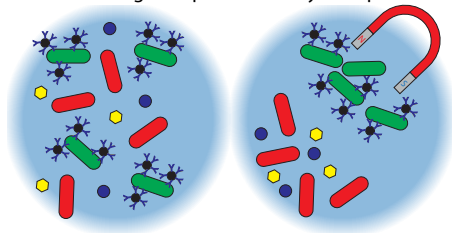
Table 4.1: Comparison of the weight percentage of surface groups on the functionalized nanoparticle. After deprotection, the overall percentage lowers, since carbon and hydrogen atoms are removed in this process. The thiol ligands (**4**, **5**) show an opposite trend, but this can be attributed to the formation of thiolate-tetrabutylammonium ion pairs (caused by deprotection process and sample preparation), hence largely increasing the carbon content. Even though a similar deprotection protocol is followed for the sugar ligand (**6**), this effect is absent here since no ion pairs can be formed.

Sample name (Fe <sub>3</sub> O <sub>4</sub> -ligand)	Surface group w% (protected)	Surface group w% (deprotected)
Fe <sub>3</sub> O <sub>4</sub> - <b>1</b>	24.98	9.12
Fe <sub>3</sub> O <sub>4</sub> - <b>2</b>	43.30	12.66
Fe <sub>3</sub> O <sub>4</sub> - <b>3</b>	20.68	15.59
Fe <sub>3</sub> O <sub>4</sub> - <b>4</b>	24.00	32.96
Fe <sub>3</sub> O <sub>4</sub> - <b>5</b>	23.99	37.15
Fe <sub>3</sub> O <sub>4</sub> - <b>6</b>	62.34	38.32

## Chapter 5

# Design of nanoparticles for efficient magnetic isolation of aquatic pathogens

Selective magnetic purification by nanoparticles



This chapter is based on the following publication with minor modifications:

Antibody-modified iron oxide nanoparticles for efficient magnetic isolation and flow cytometric determination of *L. pneumophila*

**Bloemen M**, Denis C, Peeters M, De Meester L, Gils A, Geukens N and Verbiest T  
*Microchimica Acta* 2015; *accepted*

C. Denis prepared the cell cultures and performed the DNA extraction and qPCR experiments. M. Peeters provided assistance during the antibody purification process.

## Abstract

Multifunctional nanoparticles are becoming increasingly important since they combine interesting properties like fluorescence, magnetism or plasmonic effects. We designed a superparamagnetic nanoparticle that is capable of selectively separating targeted bacteria from an aqueous solution. By covalently functionalizing the surface of the particle with a heterobifunctional polyethylene glycol ligand, functional groups for antibody coupling were introduced. Polyclonal antibodies, targeting *Legionella pneumophila* bacteria, were coupled to the particles and these bioconjugates were tested for their magnetic separation properties. Flow cytometry measurements showed high efficiency in this regard. Furthermore the targeted bacteria were purified from a complex mixture of microorganisms. The results indicate that the presented multifunctional nanoparticles are capable of selectively attracting pathogens from a complex mixture, with a high efficiency, which can be of great interest for pre-concentration protocols in water quality monitoring.

## 5.1 Introduction

Iron oxide NP have become popular since they were applied in various fields like MRI, hyperthermia or drug delivery carriers.<sup>45,171,173,193,194</sup> For most applications, magnetite ( $\text{Fe}_3\text{O}_4$ ) is the preferred species of iron oxide, because of its interesting magnetic properties.<sup>26</sup> If the NP size ranges between 5 and 25 nm, they exhibit superparamagnetic behavior. This is highly valuable because it combines the large magnetic moment of a ferromagnetic material, with the convenient handling of a paramagnet, which has no net moment without an external magnetic field.<sup>195</sup> Consequently these NP are excellent materials for performing magnetic separation of target ions, molecules or cells from solution.<sup>196–198</sup> However two more properties of the material are crucial for these applications: their colloidal stability in the medium and their selectivity towards the target. To achieve the first requirement, multiple solutions have been reported. Typically the surface of the NP is coated with a polymer, silica or organic ligands, to introduce functionalities and improve its colloidal properties.<sup>41,144,179,199</sup> Recently we reported a strategy to efficiently functionalize the surface of iron oxide NP with a heterobifunctional PEG ligand and couple Ab to this layer.<sup>200</sup> Depending on the target: organic ligands, Ab or nanobodies with a high affinity can be introduced to acquire selective targeting.<sup>108,198,201–205</sup> Xu *et al.* reported that these NP-Ab bioconjugates can help in the separation of cancer cells from blood.<sup>198</sup> However, to our knowledge, no references are present in literature of studies describing a full cell separation study with multiple cell detection techniques. In this manuscript we focus on the magnetic separation of *Legionella pneumophila* serogroup 1 bacteria from aqueous solutions. These gram-negative bacteria are a widespread problem in cooling towers, air-conditioning systems, fountains and showers.<sup>206</sup> They are known to cause the Legionnaires' disease or legionellosis, a serious form of pneumonia.<sup>207</sup> Their detection is mandatory in all publicly accessible water system, like swimming pools, but also in cooling circuits and wastewater. Different methods,

such as filtration, centrifugation or immunomagnetic isolation by microparticles, are currently available to separate these bacteria from their aqueous environment for subsequent quantification.<sup>98,208–210</sup> However all these methods have some specific drawbacks. Filtration has a profound influence on cell viability and centrifugation is less appropriate for large volumes. Moreover these methods are not target specific; so all organisms are retained, including possible inhibitors that might complicate further quantification. Immunomagnetic isolation by microparticles is target specific, but the efficiency is low and cell damage might occur due to the localized excessive magnetic forces.<sup>210</sup> After isolation, quantification of the bacteria can be performed by traditional plate counting or quantitative real-time polymerase chain reactions (qPCR). Even though the culturing method is still considered as the standard, it is very time-consuming and inconvenient. qPCR is substantially faster but is very susceptible to inhibitors, such as metal salts, surfactants or polysaccharides.<sup>211</sup> In comparison to microparticles, the proposed NP have a more than 100 times larger surface to volume ratio, which allows binding more Ab to the nanoparticle's surface. Moreover more particles can interact with the cells, resulting in a larger net magnetic moment, hence lowering separation time. On top of that, the magnetic forces are more evenly spread across the cell's surface, which will increase the amount of intact organisms that can be collected. In this manuscript we report the design of a functionalized iron oxide (Fe<sub>3</sub>O<sub>4</sub>) nanoparticle with customized PEG ligands and Ab. These particles were tested extensively on their ability to specifically attract and separate *Legionella pneumophila* serogroup 1 bacteria from an aqueous solution. To underline the efficiency, the targeted bacteria were also separated from a mixture of bacteria (*L. pneumophila* and *Escherichia coli*). Negative control experiments reported in literature often make use of NP without a targeting ligand (f.i. an antibody). The recent scientific discussions about protein coronas have shown that the interaction between the nanoparticle's surface and another entity is largely dependent on its coating.<sup>159</sup> Therefor we opted for a negative control composed of iron oxide NP, conjugated with a non-*Legionella* targeting antibody (targeting murine PAI-1).

## 5.2 Materials and methods

### Materials

Allyl-PEG<sub>10</sub>-OH was obtained from Polysciences, Inc. DMPAP (99%), DMAP (99%), EDC, succinic anhydride (99%) and mercaptopropyltrimethoxysilane (95%) were purchased from Sigma Aldrich. NHS (98+%) was purchased from Alfa Aesar. Triethylamine was obtained from Janssen Chimica. MES was purchased at Fluka. All ultrasonication steps were performed in a Branson 5510 sonicator bath.

## Antibody purification

“New Zealand White” rabbits were immunized with *Legionella pneumophila* serogroup 1 and murine PAI-1.<sup>212</sup> After collecting the serum, the full IgG fraction was purified using protein A ProSep beads.<sup>213</sup> These polyclonal fractions were used without additional enrichment towards the target protein and denoted as Ab that target *L. pneumophila* (pAb Leg) and Ab that target murine PAI-1 (pAb mur PAI-1; negative control).

## Synthesis of the ligands, nanoparticles and functionalization procedure

The heterobifunctional PEG ligand was synthesized as described in Chapter 3.<sup>200</sup> Allyl-PEG<sub>10</sub>-OH (1.1 eq, 4.00 mmol, 1.992 g) was mixed with succinic anhydride (1.1 eq, 4.40 mmol, 440 mg) and 4-dimethylaminopyridine (DMAP) (0.02 eq, 0.08 mmol, 9.7 mg). This mixture was stirred and heated to 50°C for 16 hours. The product (**2**) was purified twice by precipitation in cold diethyl ether, centrifugation and drying in vacuum. <sup>1</sup>H NMR (300 MHz, CDCl<sub>3</sub>):  $\delta$  (ppm) 2.65 (s, 4H), 3.55–3.75 (m, 38H), 4.02 (d, 2H), 4.26 (t, 2H), 5.15–5.32 (m, 2H), 5.85–5.95 (m, 1H). <sup>13</sup>C NMR (75 MHz, CDCl<sub>3</sub>):  $\delta$  (ppm) 29.2, 29.5, 63.8, 68.9, 69.3, 70.5, 72.2, 117.1, 134.7, 172.1. MS (chemical ionization):  $m/z$  = 499, 101.

To introduce the siloxane onto the heterobifunctional PEG molecule, allyl-terminated PEG (1 mmol in total, mixture of modified (0.1 mmol) and unmodified (0.9 mmol)) was mixed with (3-mercaptopropyl) trimethoxysilane (1 eq, 1 mmol, 185.7  $\mu$ L) and 2,2-dimethoxy-2-phenylacetophenone (DMPAP, 0.05 eq, 0.05 mmol, 12.8 mg). This mixture was stirred during 1 hour in a UV reactor, equipped with 3 LEDs (365 nm, output power 200 mW). The product (**3**) was used without further purification. <sup>1</sup>H NMR (300 MHz, CDCl<sub>3</sub>):  $\delta$  (ppm) 0.76 (t, 2H), 1.70 (m, 2H), 1.85 (m, 2H), 2.55 (m, 4H), 2.64 (s, 4H), 3.57 (s, 9H), 3.55–3.75 (m, 40H), 4.26 (t, 2H). The synthesis of iron oxide NP and coating their surface with siloxanes was performed as described in Chapter 2 and 3.<sup>200,214</sup> In general, 1 mmol of siloxanes was mixed with 100 mg of Fe<sub>3</sub>O<sub>4</sub> NP in 50 mL of toluene. To this mixture triethylamine (2.5 mL) and 50  $\mu$ L of water were added. The solution was placed in an ultrasonication bath for 5 hours, after which 50 mL of heptane was added to precipitate the particles (dispersion becomes turbid). Afterwards, they were attracted magnetically and washed 3 times with acetone. Finally the particles were dried in vacuum and dispersed in MilliQ water (with a concentration up to 20 mg/mL).

## Antibody coupling

The concentrated nanoparticle solution was diluted in 50 mM MES buffer, pH 5.5, to reach a final concentration of 3 mg/mL. 0.75 mg EDC and 0.75 mg NHS was added to 1 mL of this solution and shaken for 20 minutes to activate the carboxylic acids. The antibodies (75  $\mu$ g) were diluted in 2 mL of the same MES buffer after which

both solutions were mixed and shaken for 1 hour. To separate the particles from the solution, a Miltenyi Biotec MS magnetic column was used. After rinsing the column with MilliQ water, the nanoparticle dispersion was loaded onto the column, which was placed inside a circular NdFeB magnet. The column was washed 2 times with 1 mL of sodium phosphate buffer (20 mM, pH 7). To elute the particles, the column was removed from the magnet and 0.5 mL of phosphate buffer and subsequently 0.5 mL of MilliQ were used as eluent.

## Bacterial strains and growth conditions

Recombinant strains of *E. coli* and *L. pneumophila* serogroup 1 expressing the red fluorescent protein (RFP) and green fluorescent protein (GFP) genes respectively, were used to test strain specificity and efficacy of the iron oxide nanoparticles. The transformed bacteria were cultivated in the presence of appropriate antibiotics (10  $\mu$ g of kanamycin/mL for RFP and 5  $\mu$ g/mL chloramphenicol for GFP) to ensure plasmid maintenance. Briefly, *Legionella* bacteria were cultured by standard procedures at a temperature of 37°C on buffered yeast extract agar containing  $\alpha$ -ketoglutarate (BCYE- $\alpha$ ) supplemented with L-cysteine and ferric pyrophosphate.<sup>215</sup> *E. coli* bacteria (LMG2092T, RFP labelled and kindly given by Prof. N. Boon, UGent, Belgium) were grown in Luria broth (LB) medium supplemented with kanamycin (10 mg/mL) and incubated overnight at 30°C.

## Magnetic separation of bacteria

Separate *L. pneumophila* and *E. coli* solutions were prepared by spiking Ringer's Solution (Oxoid) with scraped bacteria from the culture plates following the preparation of 10-fold dilution series. In general, 4 different concentrations of *Legionella* bacteria (1E7, 1E6, 1E5 and 1E4 cells/mL) were tested in either monospecies suspensions or mixed suspensions with added *E. coli* bacteria. In general, 300  $\mu$ L of each bacteria solution was mixed with 250  $\mu$ L of NP solution (0.5 mg NP). Then, this mixture was placed on a rotator at room temperature for 1 hour and afterwards separated by a magnetic column. The supernatant was collected and the column was washed with 1 mL of MilliQ water. To elute the NP and bacteria, the column was removed from the magnet and 1 mL of MilliQ was used as an eluent (see Figure 5.3 B-C).

## Flow cytometry

Cell numbers of *L. pneumophila* and *E. coli* were determined by flow cytometry using an Attune®Acoustic Focusing Cytometer (Life Technologies, Gent, Belgium) equipped with a 488 nm laser, a forward scatter (FSC) diode detector, and a photomultiplier tube (PMT) SSC detector. The instrument was checked for stable fluidic alignment using Performance tracking beads (Life Technologies). Bacterial fractions expressing GFP and RFP fluorescence were detected using, respectively, the BL-1 (530/30 nm)

and BL-3 (640 LP) detector. The different fractions of the separation experiment were fixed with 4% paraformaldehyde (PFA) and were diluted 100-fold. The collection rate of the instrument was 25  $\mu\text{L}/\text{min}$  and a total of 50  $\mu\text{L}$  was analyzed per sample.

## Quantitative PCR

For the specific detection of *L. pneumophila*, a TaqMan qPCR designed by P. Declerck and J. Behets was used.<sup>216</sup> DNA was extracted using the QIAGEN DNeasy Blood & Tissue Kit. The primers were based on the macrophage infectivity potentiator (mip) gene and were: LPQF (5'-TTCATTTGYTGYTCGGTTAAAGC) and LPQR (5'-AWTGGCTAAAGGCATGCAAGAC). The mip-specific TaqMan probe was 5'-GCGCCACTCATAG labeled with a 6-carboxyfluorescein (FAM) reporter dye at the 5' end and a non-fluorescent quencher at the 3' end. The probe was conjugated to a minor groove binder (MGB) to improve real-time PCR specificity and sensitivity.

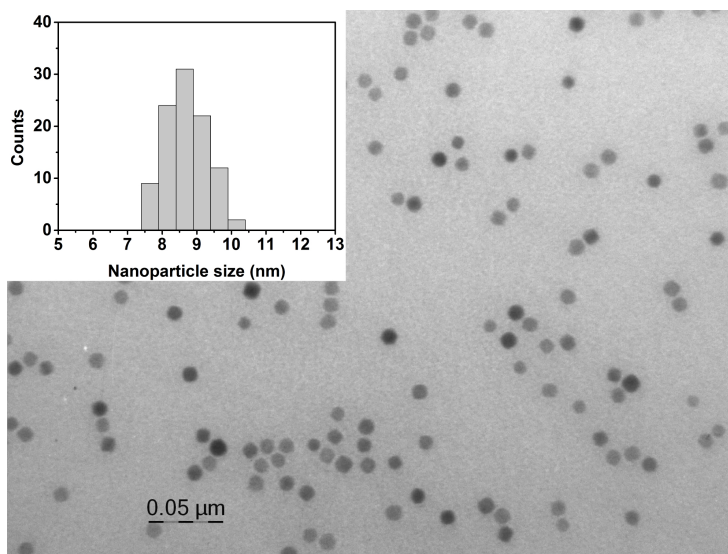


Figure 5.1: The synthesized iron oxide (magnetite) nanoparticles are  $8.6 \pm 0.6 \text{ nm}$  in size and are spherical.

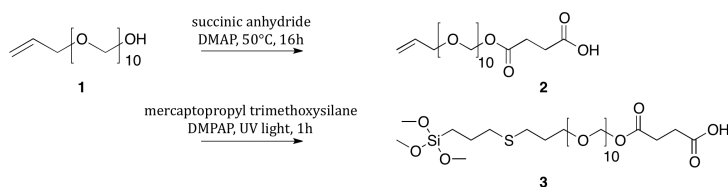


Figure 5.2: The allyl-PEG<sub>10</sub> molecule is modified first by an anhydride ring opening on the hydroxyl group, resulting in a carboxylic acid group. Secondly the allyl group is used in a thiol-ene click chemistry reaction to attach the siloxane.

## 5.3 Results & Discussion

### Synthesis and characterization of the bioconjugates

The procedure to synthesize the nanoparticles was carefully selected for its ability to produce particles at a large scale with good monodispersity.<sup>12</sup> Even though these characteristics are not strictly necessary for magnetic separation experiments, it does improve the reproducibility of surface functionalization and antibody coupling. The iron oxide nanoparticles (magnetite, Fe<sub>3</sub>O<sub>4</sub>) that were prepared are 8.6 nm wide in diameter, with a narrow size distribution of 0.6 nm (see transmission electron microscopy data, Figure 5.1). The large scale at which these nanoparticles are produced (>10 grams) ensures that batch-to-batch differences during experiments can be fully excluded.

Even though the functionalization of iron oxides is a well-known research topic, multiple recent advances have been reported.<sup>174</sup> We choose siloxane surface chemistry in this regard, since it provides the particles with several important properties. First of all, the ligand coating is covalently attached to the surface, which improves its resistance to the environment, merely extreme pH, heat or high ionic strength. Secondly, the ligand can be designed with a specific application in mind. In this case, a PEG backbone was preferred for its excellent solubility in aqueous environments. Moreover, the ligand was altered to have one functional carboxylic acid end-group, which concentration on the nanoparticle can be tailored by mixing with unaltered ligands. As shown in Figure 5.2, the ligand is prepared by a two-step reaction involving an anhydride ring opening reaction and a thiol-ene click chemistry reaction. The latter is very convenient for siloxane chemistry since it occurs fast and without notable side reactions. The product can be used without any further purification, which reduces the chance of cross-linking and hydrolysis of the siloxane group.

The presence of a carboxylic acid group on the ligand implies that pH will have an influence on the charge of the functionalized nanoparticle. To reduce this potential issue, the modified ligand was mixed with unmodified ligands (siloxane-PEG<sub>10</sub>) during the nanoparticle functionalization procedure. A fixed ratio of 10% modified to 90%

unmodified ligands was maintained throughout the experiments. Since the subsequent coupling to antibodies will use the present functional groups to form amide bonds, the influence of pH will be limited, which is necessary to ensure colloidal stability in complex environments (such as buffer solutions).

After functionalization of the NP' surface, Ab were covalently coupled onto their carboxylic acid groups. A well-known EDC-NHS approach was preferred for its reproducibility and simplicity.<sup>83</sup> One major drawback of this method is the non-directional bonding that occurs. Since a protein contains multiple free amines, the orientation of the protein can hardly be controlled. Hence a high percentage of the Ab will lose their activity because of a non-optimal orientation (as shown in Figure 5.3 A). The polyclonal Ab used in this study are the whole IgG fraction of leporine serum, derived from *L. pneumophila* immunized rabbits. This IgG usually contains 1 to 5% of target specific Ab. It is technically possible to purify this further to a monospecific polyclonal fraction, but this is very time consuming. Moreover, the target species are bacteria, which makes the purification even more complex. It would require a column coated with whole *L. pneumophila* bacteria, not just membrane proteins, to ensure that no epitopes would be ignored. Therefore, in this study, the full IgG fraction was used during the coupling experiments, maximizing the range of targeted epitopes. We argue that the gain of having monospecific polyclonal Ab is small if the bonding is non-directional anyway. A directional (but much more complex) bonding strategy could definitely profit from this on the other hand.<sup>83,217</sup>

## Magnetic isolation results

The bioconjugated iron oxide NP were added to monospecies spiked *L. pneumophila* solutions (1E7, 1E6, 1E5 and 1E4 cells/mL) and incubated for 1 hour while rotating the test tubes. No precipitation was observed, which is a strong indication that the custom functionalized surface is coping well with the complex environment and is keeping the particle colloiddally stable. The dispersion was loaded onto a magnetic column (inside a circular magnet) and the supernatant was collected. After a washing step, the column was removed from the magnet and eluted to collect the nanoparticle-bacteria complexes. This fraction was split to perform all different characterization techniques.

Flow cytometry was selected as the main characterization technique because of its ability to quantify fluorescently labeled bacteria with high accuracy. Since the *L. pneumophila* strain was labeled with a GFP marker, detection and quantification was straightforward. The results show that as expected the type of antibody, coupled to the nanoparticle, has a profound influence on the magnetic separation behavior. Table 5.1 shows the amount of bacteria found in the different fractions that were magnetically separated from an initial solution of 5E6 bacteria per milliliter. The presence of Ab targeting the bacteria clearly has a positive influence on the separation capabilities of the NP. In the supernatant of the negative control (pAb mur PAI-1), the concentration of cells is more than 150 times higher. While the opposite can be seen in the NP-cell fraction, where the negative control performs more than 10 times

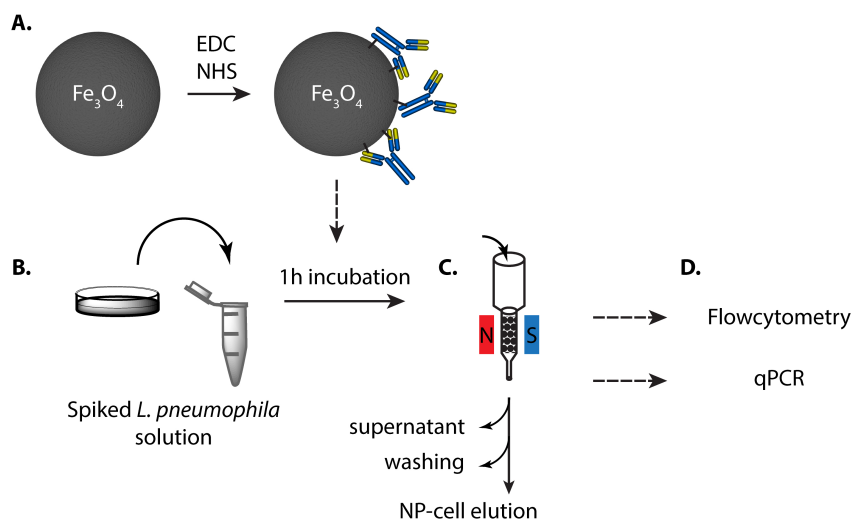


Figure 5.3: Schematic overview of the cell separation procedure. First, the functionalized NP were conjugated to the corresponding Ab via an amide bond, induced by EDC-NHS coupling chemistry (A). Secondly, *L. pneumophila* solutions were prepared (B), which were brought into contact with the NP and magnetically separated (C). Finally, the different collected fractions were characterized by flowcytometry and qPCR (D).

worse. Moreover, the final fraction is underestimated by the flow cytometer, since small clusters of bacteria are formed after interaction with NP. Hence multiple cells are shown as one event only. Experimental data revealed that the underestimation is approximately a factor 2-3 (see supporting information, Figure 5.5). The background of the flow cytometer, used in these experiments, is approximately  $3\text{E}3$  cells/ml; this number was not subtracted from the experimental values, since this was a systematic error and the influence on the end results is minimal. However, due to this substantial background signal, the limit of detection is limited to  $10^4$  cells/mL. Using other quantification techniques can drastically improve this limit of detection. An overview of different purification methods and their respective recoveries can be found in the Supporting information, Table 5.3. These results show that the NP are capable of selectively capturing target bacteria from an aqueous solution, even though the Ab are coupled non-directionally and are not monospecific.

To further underline the capabilities of the functionalized NP, a separation experiment was performed on a mixed set of bacteria. This would give information about the specificity of the NP and the behavior of the negative control. In an experiment with only one bacterial species present, the negative control will always detect this bacterium, albeit aspecifically, since no other targets are present. By carefully selecting

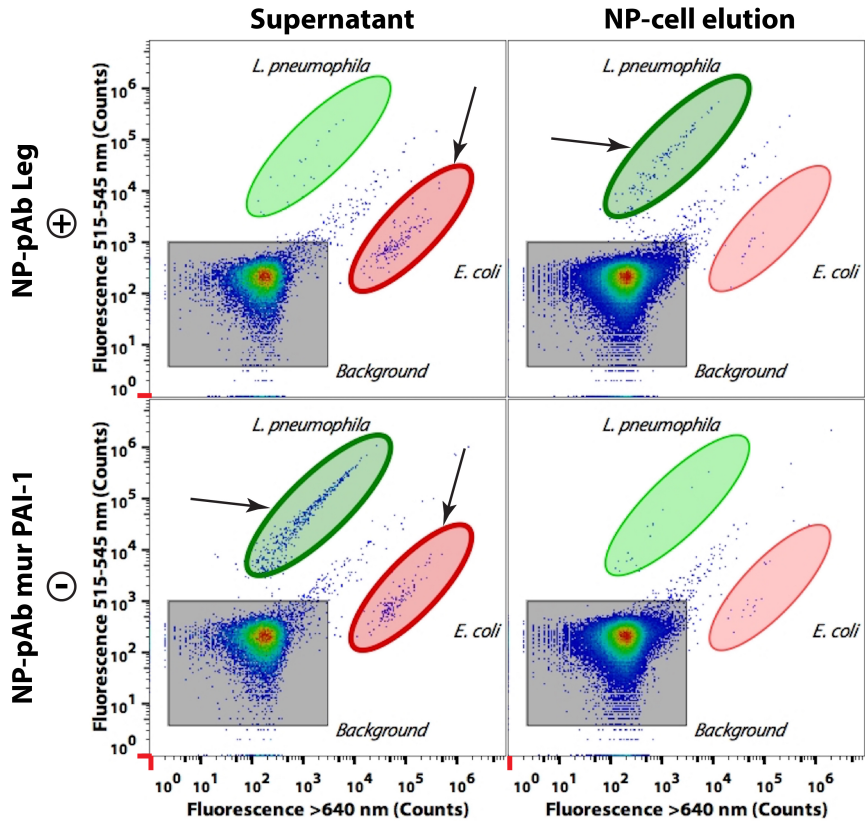


Figure 5.4: The separation capabilities of the nanoparticles are still active in a mixed bacteria environment. *L. pneumophila* bacteria (GFP-labeled) were mixed with *E. coli* bacteria (RFP-labeled) at a 65/35 ratio ( $1.4E5/7.4E4$  cells/mL). The flow cytometry measurements show that the RFP-labeled *E. coli* bacteria remain in the supernatant fraction of the pAb Leg coated NP (upper row), while the *L. pneumophila* bacteria are present in the NP-cell fraction. The negative control NP (pAb mur PAI-1, bottom row) show a different behavior: both species are visible in the supernatant fraction, with only minor presence in the NP-cell fraction.

Table 5.1: The type of antibody has a profound influence on the magnetic separation behavior. This dataset was measured by flow cytometry, based on 3 replicates. A large amount of the bacteria is present in the supernatant (SN) of the negative control (NP-pAb mur PAI-1), while the final fraction (NP-cell elution) in comparison only contains a few percent. The opposite can be seen for the bioconjugates that target *L. pneumophila* (NP-pAb Leg): a small number of cells can be found in the supernatant, while a large number is present in the final fraction. The ratio of the two types of conjugates is presented to clarify the difference. The full data set can be found in the supporting information (Table 5.2).

Collected cells/mL	Supernatant	Washing step	NP-cell elution
NP-pAb Leg	1.1E4 (2.3%)	5.0E3 (1.1%)	4.4E5 (96.6%)
NP-pAb mur PAI-1	1.9E6 (82.7%)	3.5E5 (15.5%)	4.0E4 (1.1%)
Ratio	0.0057	0.014	11

the two different bacteria (*L. pneumophila* GFP-labeled and *E. coli* RFP-labeled), we were able to discriminate them in the FCM plots and investigate the overall performance. Figure 5.4 summarizes the data of these experiments. The FCM plots of the supernatants are shown in the left column, while the NP-cell fractions are shown in the right column. The washing steps were omitted for clarity. In the nanoparticle samples coated with pAb Leg (upper row), only a minor presence of *L. pneumophila* in the supernatant is shown, while a high concentration is present in the NP-cell fraction. *E. coli* on the other hand stays in the supernatant and is hardly present in the NP-cell fraction. We noticed a small leak of green fluorescence into the red fluorescence detector, which accounts for a significant portion of the visible dots in the red ellipse. Keeping this background in mind, more than 90 percent of the bacteria were successfully separated. Nevertheless, this clearly underlines the target-specific magnetic separation that is occurring. In the negative control samples (bottom row), both bacterial species are mainly present in the supernatant, but only minimally in the NP-cell fraction. We can therefore conclude that the negative control nanoparticles only interact aspecifically with the bacteria, as expected.

The presented nanoparticle platform is capable of selectively attracting bacterial species from a complex mixture. Moreover the ligand design is straightforward and thanks to the usage of siloxanes, the ligand is covalently bound to the surface of the NP. Even though the coupling of Ab is non-directional, this did not hamper the properties of the NP. The selection of polyclonal Ab as targeting moieties broadened the range of epitopes to which the NP could attach. The magnetic separation strategy strongly reduces the presence of surfactants or metal ions that are present in complex environments, which are known inhibitors for sensitive quantification techniques like qPCR.<sup>218,219</sup> We believe that this proof of concept can be translated to a wide series of diagnostic applications as a fast and efficient pre-concentration step. Future experiments will optimize the antibody coupling and make use of monospecific Ab to further enhance the efficiency of the system.

## 5.4 Conclusions

Superparamagnetic iron oxide NP were functionalized with a heterobifunctional polyethylene glycol ligand and subsequently bioconjugated with Ab. The ligand has a siloxane moiety on one end and one carboxylic group, introduced by an anhydride ring opening, on the other end. We used thiol-ene click chemistry for the siloxane modification, since this type of reactions is fast and gives high yield without side reactions. After surface functionalization of the NP, Ab were coupled to the surface. These bioconjugates were added to *L. pneumophila* bacteria and after magnetic separation, the different fractions were investigated by flow cytometry and qPCR. An enrichment of bacteria was visible in the eluted fraction of the column, showing that the nanoparticle efficiently interact with the targeted species. The negative control showed a more than 10-fold lower enrichment, caused by aspecific adsorption. Moreover, the targeted species were also attracted from a mixture of bacteria, where a similar enrichment was obtained. These results indicate that the surface functionalized bioconjugates can be used for magnetic separation of bacteria from complex solutions, with great efficiency, even though the Ab are coupled non-directionally.

5.5 Supporting information

Table 5.2: Summary of all flow cytometry data, measured on the different sets of spiked samples. All values have as unit: cells/mL. The different Ab, coupled to the NP, are shown as: +, pAb Leg; -, pAb mur PAI-1. The flow cytometer underestimates the amount of cells in the NP-cell fraction, since small clusters of cells are formed, that are only counted as one event. The apparatus has a background signal of approximately 3E3 counts, but this value was not subtracted from the results since it is a systematic error.

	Reference	SN +	SN -	Wash +	Wash -	NP-cell +	NP-cell -
sample 1	5.8E+4	7.0E+3	6.8E+3	7.8E+3	6.4E+3	1.9E+4	9.0E+3
sample 2	5.0E+4	6.0E+3	9.8E+3	5.4E+3	8.8E+3	1.9E+4	7.6E+3
sample 3	4.3E+4	6.4E+3	1.1E+4	6.4E+3	8.8E+3	2.1E+4	1.1E+4
average	5.0E+4	6.5E+3	9.2E+3	6.5E+3	8.0E+3	2.0E+4	9.2E+3

	Reference	SN +	SN -	Wash +	Wash -	NP-cell +	NP-cell -
sample 1	5.1E+4	6.6E+3	2.1E+4	4.2E+3	1.1E+4	1.8E+4	1.1E+4
sample 2	5.6E+4	7.8E+3	3.0E+4	1.3E+4	8.4E+3	1.8E+4	1.0E+4
sample 3	4.6E+4	7.8E+3	3.0E+4	6.6E+3	1.1E+4	2.6E+4	8.2E+3
average	5.1E+4	7.4E+3	2.7E+4	8.1E+3	1.0E+4	2.1E+4	9.8E+3

	Reference	SN +	SN -	Wash +	Wash -	NP-cell +	NP-cell -
sample 1	3.9E+5	4.2E+3	2.0E+5	4.0E+3	3.6E+4	4.6E+4	7.0E+3
sample 2	4.5E+5	1.0E+4	2.0E+5	3.0E+3	3.4E+4	5.0E+4	8.8E+3
sample 3	4.2E+5	3.2E+3	1.8E+5	4.0E+3	2.9E+4	4.3E+4	1.2E+4
average	4.2E+5	5.8E+3	1.9E+5	3.7E+3	3.3E+4	4.6E+4	9.3E+3

	Reference	SN +	SN -	Wash +	Wash -	NP-cell +	NP-cell -
sample 1	4.5E+6	2.0E+4	1.8E+6	3.8E+3	3.0E+5	3.7E+5	3.1E+4
sample 2	4.4E+6	6.2E+3	1.9E+6	5.8E+3	3.2E+5	4.6E+5	5.4E+4
sample 3	4.3E+6	5.8E+3	1.9E+6	5.4E+3	4.4E+5	4.9E+5	3.5E+4
average	4.4E+6	1.1E+4	1.9E+6	5.0E+3	3.5E+5	4.4E+5	4.0E+4

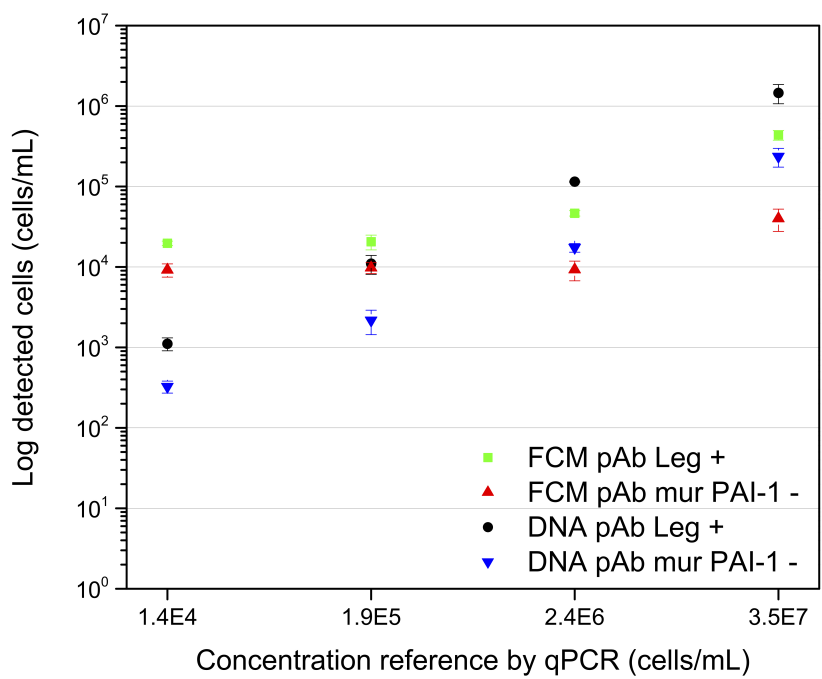


Figure 5.5: Comparison of flow cytometry and qPCR data of the NP-cell fractions. Since the FCM underestimates the amount of cells due to possible cluster formation, DNA data were collected as comparison. All values have as unit: cells/mL. The different antibodies, coupled to the nanoparticles, are shown as: +, pAb Leg; -, pAb mur PAI-1. The FCM data (green and red curve) clearly show the detection limit of the apparatus at lower cell concentrations and the underestimation at higher concentration. However, the ratio of magnetically separated cells by the different NP-Ab conjugates remains similar regardless the detection technique.

Table 5.3: Comparison of different pre-concentration methods for *L. pneumophila* and their respective quantification methods. An improvement of immunomagnetic separation over centrifugation and filtration is clearly visible. Individual cases are difficult to compare since many parameters influence the overall detection efficiency. The quantification method has a profound influence of the limit of detection, with qPCR being considerably better than FCM. For a complete review of bacterial separation methods, we direct to reader to a very complete review by Stevens et al.<sup>220</sup> Abbreviations: FCM, flow cytometry; EFM, epifluorescent microscopy; qPCR, quantitative polymerase chain reaction

Method	Recovery (percentage)	Reference	Quantification method	Sample
<b>Centrifugation</b>	13.8 (3.800 x g)	[221]	Cell cultures	Spiked tap water
	31.9 (8.150 x g)	[221]	Cell cultures	Spiked tap water
	10.7 (12.000 x g)	[222]	FCM	Metalworking cooling fluids
	13.5 (12.000 x g)	[222]	EFM	Metalworking cooling fluids
	43 (3.800 x g)	[223]	PCR	Spiked tap water
	49 (8.150 x g)	[223]	PCR	Spiked tap water
<b>Filtration</b>	52.6 (flat membrane)	[221]	Cell cultures	Spiked tap water
	13.1 (cast membrane)	[221]	Cell cultures	Spiked tap water
	55-81	[223]	PCR	Spiked tap water
<b>Immunoseparation</b>	12.7 (Dynabeads)	[222]	FCM	Metalworking cooling fluids
	29.7 (Dynabeads)	[222]	EFM	Metalworking cooling fluids
	46-71 (Dynabeads)	[210]	qPCR	Distilled water
	16-74 (Dynabeads)	[210]	qPCR	Potable water
	7-89 (Dynabeads)	[210]	qPCR	Cooling tower water
	57-96 (nanoparticles)	this work	FCM	Spiked distilled water



## Chapter 6

# Conclusions and outlook

### 6.1 Conclusions

Multifunctional iron oxide NP have already shown tremendous potential in a wide range of applications. From a biomedical point of view, their biocompatibility and low toxicity are important assets. Besides their usage in medical imaging techniques, such as MRI, drug delivery and hyperthermia are important fields of current research.

In this dissertation, the development of a *reliable, low cost and modular nanoparticle-based magnetic separation platform* was the main purpose. Three crucial material properties were identified beforehand and served as the basis for the design of the functional nanomaterial platform. (1) The synthesis of the core nanoparticle should be reproducible, scalable and low cost. A reduction of batch-to-batch differences was considered the main goal in this regard. (2) Functionalization of the surface of the nanoparticle should be performed by a covalently attached ligand to enhance to robustness of the final nanomaterial. (3) The colloidal stability of nanoparticles in complex environments is often an issue which might negatively influence the applicability. A heterobifunctional ligand that enhances the colloidal stability and has a group for subsequent coupling is required.

Chapter 2 focused on the synthesis and functionalization of iron oxide NP, with special attention to the characterization of the core material. A synthetic procedure for the large scale synthesis of the core nanoparticle was selected from the abundantly available protocols in literature. More specifically, the method reported by Park *et al.*, based on the thermal decomposition of iron(III+) oleate, is capable of producing high quality magnetite NP at an ultra large scale (up to 20-40 grams).<sup>12</sup> However, the nanoparticle's surface is coated by oleic acid after the synthesis, which is a very apolar molecule that is not easily replaced by another ligand. Due to the absence of reliable surface functionalization methods in scientific literature, a new procedure

was developed that is still one of the fastest available methods for covalent surface modification of oleic acid-coated NP by trialkoxy silanes. The use of an ultrasonication bath largely reduced the reaction time, by efficiently removing the initial ligand while keeping the particles separated spatially. A wide range of siloxanes was tested and the results showed that the proposed protocol is capable of introducing multiple different varieties onto the iron oxide particles. Moreover the colloidal stability of the functionalized NP was tested in complex environments, such as serum and plasma. The non-charged PEG and positively charged carboxylic acids showed an incredible stability during several days, which was very promising for further development.

After the successful development of the functionalization procedure, the research was focused onto the required heterobifunctional PEG ligand. Even though thousands of different siloxane molecules are commercially available, no ligand with all preferred properties (heterobifunctional based on PEG) is available. Chapter 3 describes the design and synthesis of the envisioned molecule that incorporates a siloxane at one end, a well-defined PEG chain and a single functional group at the other end. Since the modification of native PEG (with 2 hydroxyl groups) would be a less-favourable choice, an allyl-PEG-OH backbone was bought that allows a straightforward modification. The hydroxyl group at the end was used for a ring-opening reaction of succinic anhydride, that resulted in the formation of a carboxylic acid. The allyl group on the other side was attached to siloxane moiety by using thiol-ene click chemistry. This approach made it possible to produce the ligand at a large scale, with minimal reaction steps. As stated before, an elaborate synthetic protocol would largely reduce the applicability due to cost issues. To prove the added value of the developed ligand, Ab were covalently coupled to the carboxylic acid groups and their surface concentration and activity was investigated. The results indicated that the coupling of proteins resulted in the formation of an almost perfect monolayer, with minimal cross-linking. Furthermore, the Ab still retained their properties, which was investigated by SPR experiments, that showed an enhanced interaction with an Ag-coated fiber.

The complex interaction between ligands (with multiple functional groups) and metal oxides surfaces can result in a wrongful orientation or unwanted side reactions. To provide a general solution to this (commonly ignored) issue, a strategy was developed that is based on surface functionalization with protected functional siloxanes and subsequent deprotection on the nanoparticle. In Chapter 4 we show that this approach allows to functionalize the surface of iron oxide nanoparticles with different functional groups, such as amines, carboxylic acids, aldehydes, thiol or sugars. This elegant and easy method can be transposed onto virtually any (complex) ligand and might drastically enhance the quality of surface modifications of metal oxide surfaces in general, even though we showed the methodology on iron oxide NP.

Finally the applicability of the developed heterobifunctional ligand was tested thoroughly in a magnetic separation experiment with a high social relevance. Polyclonal Ab (full IgG fraction) were covalently coupled to the magnetic NP to make them target specific. More detailed, *Legionella pneumophila* bacteria were selectively magnetically purified from an aqueous environment. The results indicate that a very high efficiency can be achieved, even though the covalent coupling with the antibody is non-directional

and the Ab are not monospecific. A substantial aspecific signal (10%) was observed in the negative control experiment. To further investigate this potential issue, the target was separated from a mixture of two bacteria, *L. pneumophila* and *E. coli*. Flow cytometry measurements indicate that the target-specific NP are capable of selectively attracting a single type of bacteria. The negative control on the other hand showed no specificity, which is expected for aspecific interactions.

The results, presented in this dissertation, show that a nanoparticle-based platform was developed, that is capable of selectively targeting a bacterial species in complex environments. We believe that the cost-effective nature and simplicity of the design will enhance the broad applicability of the presented methodology.

## 6.2 Outlook

Even though we succeeded to develop a fully working magnetic separation methodology, several enhancements could improve the overall performance. The following section will focus on the fine-tuning of the presented approach, as well as other applications that could be developed from the core nanomaterial.

The most apparent modification that could improve the selectivity of the NP are the selected Ab and the method of covalent coupling. The latter is performed via a non-directional amide bond, that results in a potential loss of activity of the Ab since the antigen binding region can be blocked sterically. A few methods have been reported in scientific literature that are able to bind Ab directionally onto a surface. Well-known examples are the use of protein A or G as an intermediate layer. These proteins have a strong affinity for the Fc fragment of the antibody, which forces the Fab region to point outwards (see Section 1.6). Another option comprises the chemical modification of the antibody itself, either via a tag, or via the oxidation and modification of the inner carbohydrates. However Abraham *et al.* have shown that this could alter the affinity of the antibody, which could have a negative influence on the envisioned application.<sup>85</sup>

Besides the method of covalent coupling, the properties of the ligand itself could also have an influence on the separation efficiency. It has been reported by Stefanick *et al.* that the length of the linker molecule has a large effect on the rotational freedom of the coupled proteins.<sup>224,225</sup> They determined that the optimal length of a PEG linker was between 6 and 18 monomers. If the chain is too short, the functional group is buried in the stabilizing layer and hence cannot bind an antibody. If the chain becomes too long, the PEG chain can sterically hinder the association of the antibody to its antigen. A shorter linker will probably have a more linear conformation, which will allow some rotational freedom but will still present the antibody correctly to the surrounding environment. The optimal linker length will also be influenced by the size of the NP, since it alters the final surface area and consequently the size of the protein corona. Furthermore this surface area will influence the aspecific adsorption behavior

of proteins and contaminants in the surrounding medium. It is therefore recommended to perform a thorough evaluation of a range of linker lengths and coupling chemistries.

The selection of Ab could definitely improve the performance of the presented NP. If the polyclonal Ab would be purified to monospecific polyclonal Ab, a 20-fold increase in the selectivity could be obtained. The full IgG fraction is expected to contain only 1-5% of useful Ab. However, this upgrade would only make sense if the coupling procedure is improved first. The use of monoclonal Ab would ensure a high affinity, but they only target one epitope. In complex water samples this single type of epitope might not be accessible (due to pH, contaminants, ...), resulting in a potential loss of efficiency. Hence the usage of monospecific polyclonal Ab, targeting a broad range of epitopes, is regarded as the best option for future development.

When looking further into the production costs of the proposed product, it is clear that the development (and production) of Ab has the largest influence on the final price. The PEG-coated iron oxide NP have a raw material cost of less than 10 euro/gram. The Ab on the other hand are far more expensive. Taking the radius of the nanoparticle and its coating into account, it can be estimated that 10-15 Ab could be coupled on each nanoparticle (by an ideal directional coupling of the Fc fragment onto the surface).

For *polyclonal* Ab, the production is fast and the costs are rather low. It can be estimated that a batch of NP, coated with non-monospecific polyclonal Ab, would cost approximately 1,000 euro/gram. Keeping in mind that only a few milligrams are needed for each separation, this is an interesting option. However, the batch size of polyclonal Ab is limited (approximately 25 mg, since they are collected from the blood of an animal), so batch to batch differences can be expected. This limits the long-term applicability, but it can be sufficient for niche markets. If the polyclonal IgG fraction is purified further to a monospecific batch, we estimate that the price increases by at least a factor 10, but this depends largely on the concentration of monospecific Ab in the initial batch (usually 1-5%).

For *monoclonal* Ab, the initial development is slow and the costs are high (10,000 euro for creating the hybridoma cell lines). However the production can be scaled up (>100 mg), which significantly lowers the overall price per milligram of Ab. We estimate that the price of the product (NP-mAb) is 3,000-4,000 euro/gram. Even though this is more expensive than the polyclonal version, it is a better long-term option because all Ab are identical and their affinity is guaranteed. To extend the range of recognized and targeted epitopes, different monoclonal Ab can be mixed.

On the applications side, a wide range of opportunities is available. Thanks to the excellent colloidal stability of the NP in complex environments, such as waste water or blood, a logical next step would be their application in water quality monitoring or biomedical research. Since the properties of collected environmental water samples can be very diverse in terms of pH or ionic strength, the robustness and enhanced colloidal stability of the developed nanoparticles could be very advantageous. Detection of multiple different organisms (*Salmonella* spp., *E. coli* or *Vibrio cholerae*) is mandatory by law in different parts of the world and hence has a large market potential. The

proposed method of magnetic pre-concentration can be combined with almost any detection technique.

The selective purification of proteins (rather than bacteria) could also be of great interest. The targeting moiety in this regard could still be an antibody, but also a minor modification of the PEG ligand to introduce a different functional group could be an option. By using the strategy shown in Chapter 4, very complex ligands can be introduced onto the nanoparticle's surface.

In contrast to the diagnostic applicability, imaging is a very important future research domain. If the functional coating of the particles is enhanced by the addition of a dye, the resulting fluorescent signal will enable a straightforward localization in cells or tissue. Multiple approaches are possible in this regards: attaching the dye directly to a modified PEG ligand or developing a siloxane version of the required dye. Combined with the selective targeting by antibodies this could be a very valuable imaging approach.

Similarly, the iron oxide NP show a strong MRI response, which could be exploited further by the addition of dyes or Ab, to produce for instance a tumor-targeting bimodal contrast agent. It has been reported that doping the core nanoparticle with atoms such as cobalt or zinc can largely enhance the MRI contrast. In this context, the possible toxicity of the magnetite NP should be tested thoroughly. Even though they are FDA (US Food and Drug Administration) approved and their toxicity is expected to be low, every new surface coating or dopant atom could trigger negative effects in in-vivo situations.

In conclusion, the presented functionalized nanoparticles have a tremendous applicability in various biomedical areas, which will lead to many future research projects.



## Appendix A

# Selected experimental techniques

### A.1 Enzyme-linked immunosorbent assay (ELISA)

During an immune response, the concentration of Ab is of crucial importance (next to the specificity, isotype and affinity). Determination of the concentration of Ab or Ag can be done by an immunoassay. One of the most used formats is called ELISA. It was developed by the Swedish researchers Perlmann and Engvall, in 1971.<sup>226</sup> The technique exist in multiple variations, but is generally based on the concept of an antigen binding to its specific antibody in combination with an enzyme-mediated color change to detect the presence of proteins, peptides, hormones or Ab.<sup>227</sup> The following section will give an overview of the different possible approaches (see Figure A.1).

The key principle of ELISA is the direct or indirect detection of an antigen by coating it directly onto the surface of the well, or by coating an antibody with high affinity for the antigen to the well. For a *direct ELISA* (see Figure A.1) the well is coated with the sample, that has to be analyzed. Typically a blocking solution of noninteracting proteins is added as an intermediate step, to block uncoated areas. Finally a labeled antibody, with high affinity for the antigen, is added, that induces the colorimetric change. An *indirect ELISA* follows the same approach, but uses an unlabeled primary antibody first. By addition of a secondary label anti-antibody, the quantification is possible. The main disadvantage of this approach (direct and indirect) is that the immobilization of the antigen is not specific. Any other proteins in the sample might adhere to the well and interfere with the assay.<sup>226</sup>

To overcome this issue, the *sandwich ELISA* was developed. Now an antibody with affinity for the target is coated onto the wells. After addition of the sample and

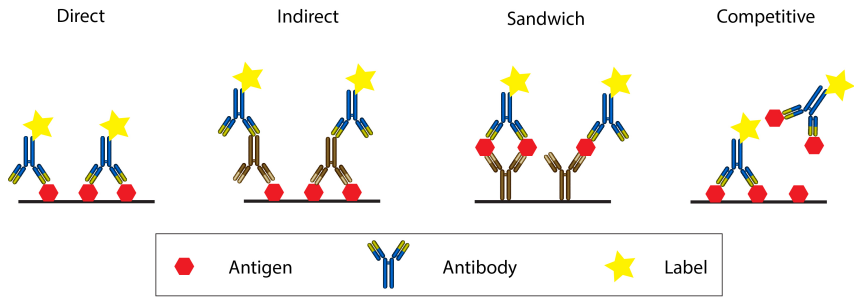


Figure A.1: Overview of the different types of ELISA.

sufficient washing, a labeled antibody can be used for the colorimetric quantification reaction. The antigen is sandwiched between the two Ab, hence the name of the technique. The purity of the sample is less important in this regard, which simplifies the assay.

A fourth ELISA approach is based on competition between the antigen in the sample and antigens coated onto the wells. First an antibody is added to the sample, which will capture the antigens. If this solution is added to the well, the excess Ab will bind to the well, but not the ones that already interacted with the target in the sample. Absence of color indicates the presence of the antigen for this approach. The main advantage is that the technique is very sensitive even in complex mixtures.<sup>227</sup>

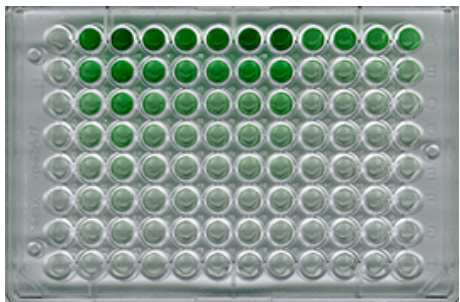


Figure A.2: Example of an ELISA well plate. Dilution series are made in the vertical direction to improve the concentration determination.

In this dissertation, the Ag to be quantified was an antibody. Its target was coated on the plate (e.g. PAI-1, see Chapter 3). The sample containing Ab towards PAI-1 was applied. A secondary labeled antibody targeting the Ab was added and a colorimetric reaction was started. Standard curves on the 96-well plate were used to deduct the

concentration from the absorbance measurement of the colored solutions (see Figure A.2).

## A.2 Flow cytometry (FCM)

Cytometry is defined as the measurement of physical and chemical characteristics of particles or cells. In FCM, these cells or particles pass through a narrow channel which separates them, so discrete signals can be measured. The obtained scattering and fluorescence data allow to study multiple different types of cells at the same time.

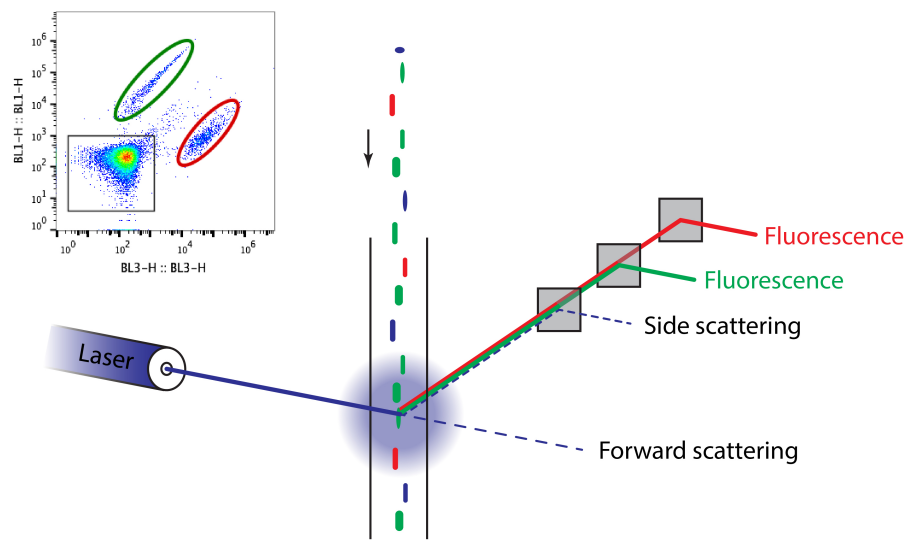


Figure A.3: The principle of FCM is based on the illumination of a focused stream of sample by a laser source. The forward and side scattering, as well as the different fluorescent signals are detected. The inset shows a typical graph with different cell populations.

Two types of signals are usually recorded during FCM measurements: scattering and fluorescence. The fluorescence signal can originate from labels or dyes and is often used to identify certain types of cells. By separating the signal into different wavelength regions (blue, green, red, ...), cell types or populations can be differentiated (see Figure A.3). The scattering signal is usually split into two parts, the forward and side scattering. The forward scattering is caused by the scattering of light by the surface of the cells and is roughly proportional to the cell size. Hence small cells will have low values, while large cells will have high values. The side scattering on the

other hand gives more information about the structural complexity inside the cell and the granularity.<sup>228</sup>

In this dissertation, FCM was used to quantify bacteria in the different fraction we obtained after magnetic isolation, see Chapter 5. Even though a substantial background signal limited the detection limit, the technique is able to discriminate between different populations of bacteria, which was a strong asset for the magnetic isolation experiments.

### A.3 Quantitative polymerase chain reaction (qPCR)

During a polymerase chain reaction which relies on thermal cycling, DNA is copied at an exponential rate. Figure A.4 shows the process of DNA amplification. The double stranded DNA is heated until the hydrogen bonds are disrupted and the two strands separate, which is called melting. Afterwards the temperature is lowered to enable the primers (short DNA fragments) to bind to the strands. Note that they bind at the 5' (phosphate group) end of the single strand and will extend at their 3' (hydroxyl group) end. The polymerase enzyme will now extend the strand to obtain the initial double stranded DNA. Since the amount of DNA is doubled in every step, one can obtain large amounts of DNA in a short amount of time. The selectivity of PCR is related to the use of specific primers that specifically bind to the targeted region in the DNA. Multiple inhibitors, such as metal ions, surfactants or polysaccharides can interfere with the reaction and their removal is crucial to obtain good PCR results.<sup>211</sup>

qPCR or realtime PCR (not to be mistaken with reverse transcriptase PCR (RT-PCR) which amplifies RNA) is based on the general PCR reaction but uses a fluorescent signal to quantify in situ the amount of present DNA. This can be achieved by using non-specific intercalating dyes or target-specific fluorescent-labeled probes. A very often used, inexpensive and easy to use non-specific dye is SYBR Green, that will bind to double stranded DNA molecules. However, it can also bind to primer-dimers and contaminations, hence overestimation of the DNA concentration can occur. Target-specific alternatives are TaqMan probes or molecular beacons. The first consist of a fluorescent marker and a quencher in the same probe. During DNA amplification, the probe is cut by the polymerase enzyme, releasing the fluorescent marker from the quencher and generating a signal. The molecular beacons are hairpin-like probes where the fluorophore and quencher are in close proximity. When the probe binds to the target DNA, the fluorophore is distantiated from the quencher which results in a fluorescent signal.<sup>211,229,230</sup>

The fluorescent signal of the DNA amplification is generally plotted (logarithmic) against the number of cycles. A threshold level is set above the background, but still in the linear part of the curve (amplification is exponential). The cycle number at which an amplification plot crosses this threshold fluorescence level is called the  $C_t$  or threshold cycle. This  $C_t$  value can be correlated to the initial concentration of DNA in the sample. A large amount of starting material will result in a rapid amplification

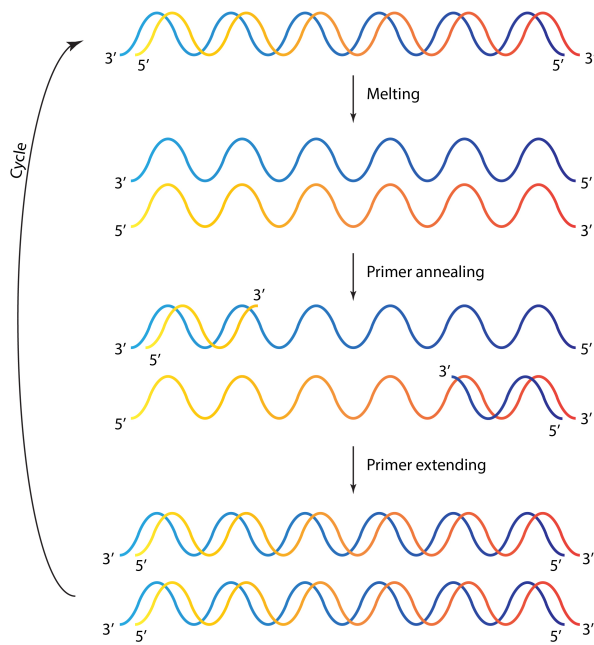


Figure A.4: During a PCR cycle, double stranded DNA is melted at elevated temperatures to obtain two single strands. After primer annealing, the extending process elongates the strand, until a double stranded DNA molecule is obtained. This process is repeated multiple times until concentration is sufficient for quantification.

and a small  $C_t$  value. A small amount on the other hand will take much longer to reach the threshold level and hence more cycles are required, increasing  $C_t$ . Standard curves are used to correlate the threshold cycle to the initial DNA concentration.<sup>231</sup>



# Bibliography

1. OECD/NNI. Assessing the Economic Impact of Nanotechnology. Tech. rep. 2013:81.
2. Mattoussi H, Palui G, and Na HB. Luminescent quantum dots as platforms for probing in vitro and in vivo biological processes. *Advanced drug delivery reviews* 2012;64:138–166.
3. Inasawa S, Sugiyama M, and Yamaguchi Y. Laser-induced shape transformation of gold nanoparticles below the melting point: the effect of surface melting. *The journal of physical chemistry. B* 2005;109:3104–3011.
4. Merali Z. This 1,600-Year-Old Goblet Shows that the Romans Were Nanotechnology Pioneers. 2013.
5. Whitesides GM. The 'right' size in nanobiotechnology. *Nature biotechnology* 2003;21:1161–1165.
6. Sapsford KE, Algar WR, Berti L, Gemmill KB, Casey BJ, Oh E, Stewart MH, and Medintz IL. Functionalizing nanoparticles with biological molecules: developing chemistries that facilitate nanotechnology. *Chemical reviews* 2013;113:1904–2074.
7. Montellano A, Da Ros T, Bianco A, and Prato M. Fullerene C60 as a multifunctional system for drug and gene delivery. *Nanoscale* 2011;3:4035–4041.
8. Warner MG and Hutchison JE. Linear assemblies of nanoparticles electrostatically organized on DNA scaffolds. *Nature materials* 2003;2:272–277.
9. Langereis E, Heil SBS, Knoops HCM, Keuning W, Sanden MCM van de, and Kessels WMM. In situ spectroscopic ellipsometry as a versatile tool for studying atomic layer deposition. *Journal of Physics D: Applied Physics* 2009;42:073001.
10. Pang C, Lee C, and Suh KY. Recent advances in flexible sensors for wearable and implantable devices. *Journal of Applied Polymer Science* 2013;130:1429–1441.

11. Finne R and Klein D. A Water-Amine-Complexing Agent System for Etching Silicon. *Journal of The Electrochemical Society* 1967;114:965–970.
12. Park J, An K, Hwang Y, Park JG, Noh HJ, Kim JY, Park JH, Hwang NM, and Hyeon T. Ultra-large-scale syntheses of monodisperse nanocrystals. *Nature materials* 2004;3:891–895.
13. Jun Yw, Lee JH, and Cheon J. Chemical design of nanoparticle probes for high-performance magnetic resonance imaging. *Angewandte Chemie (International ed. in English)* 2008;47:5122–5135.
14. Sun S, Zeng H, Robinson DB, Raoux S, Rice PM, Wang SX, and Li G. Monodisperse  $\text{MFe}_2\text{O}_4$  ( $\text{M} = \text{Fe}, \text{Co}, \text{Mn}$ ) nanoparticles. *Journal of the American Chemical Society* 2004;126:273–279.
15. Lu AH, Salabas EL, and Schüth F. Magnetic nanoparticles: synthesis, protection, functionalization, and application. *Angewandte Chemie (International ed. in English)* 2007;46:1222–1244.
16. Jokerst JV, Lobovkina T, Zare RN, and Gambhir SS. Nanoparticle PEGylation for imaging and therapy. *Nanomedicine (London, England)* 2011;6:715–728.
17. Mahmoudi M, Laurent S, Shokrgozar MA, and Hosseinkhani M. Toxicity evaluations of superparamagnetic iron oxide nanoparticles: cell "vision" versus physicochemical properties of nanoparticles. *ACS nano* 2011;5:7263–7276.
18. Schmid G and Klabunde K. *Nanoscale materials in chemistry*. Vol. 3. 2001.
19. Cornell RM and Schwertmann U. *The Iron Oxides*. Weinheim, FRG: Wiley-VCH Verlag GmbH & Co. KGaA, 2003. DOI: 10.1002/3527602097.
20. Chatterjee J, Haik Y, and Chen CJ. Size dependent magnetic properties of iron oxide nanoparticles. *Journal of Magnetism and Magnetic Materials* 2003;257:113–118.
21. Bean CP and Livingston JD. Superparamagnetism. *Journal of Applied Physics* 1959;30:120S–129S.
22. Knobel M, Nunes W, Socolovsky L, De Biasi E, Vargas J, and Denardin J. Superparamagnetism and Other Magnetic Features in Granular Materials: A Review on Ideal and Real Systems. *Journal of Nanoscience and Nanotechnology* 2008;8:2836–2857.
23. Laurent S, Forge D, Port M, Roch A, Robic C, Vander Elst L, and Muller RNR. Magnetic iron oxide nanoparticles: synthesis, stabilization, vectorization, physicochemical characterizations, and biological applications. *Chemical reviews* 2008;108:2064–2110.

24. Willard M, Kurihara L, Carpenter E, Calvin S, and Harris V. Chemically prepared magnetic nanoparticles. *International Materials Reviews* 2004;49:125–170.
25. Jolivet JP, Chanéac C, and Tronc E. Iron oxide chemistry. From molecular clusters to extended solid networks. *Chemical communications* 2004:481–487.
26. Brulot W, Reddy N, Wouters J, Valev V, Goderis B, Vermant J, and Verbiest T. Versatile ferrofluids based on polyethylene glycol coated iron oxide nanoparticles. *Journal of Magnetism and Magnetic Materials* 2012;324:1919–1925.
27. Kwon SG and Hyeon T. Formation Mechanisms of Uniform Nanocrystals via Hot-Injection and Heat-Up Methods. *Small* 2011:2685–2702.
28. Kwon SG, Piao Y, Park J, Angappane S, Jo Y, Hwang NM, Park JG, and Hyeon T. Kinetics of Monodisperse Iron Oxide Nanocrystal Formation by “Heating-Up” Process. *Journal of the American Chemical Society* 2007;129:12571–12584.
29. LaMer V and Dinegar R. Theory, Production and Mechanism of Formation of Monodispersed Hydrosols. *Journal of the American Chemical Society* 1950;72:4847–4854.
30. Xia Y, Xiong Y, Lim B, and Skrabalak SE. Shape-controlled synthesis of metal nanocrystals: simple chemistry meets complex physics? *Angewandte Chemie (International ed. in English)* 2009;48:60–103.
31. Jana N, Chen Y, and Peng X. Size-and shape-controlled magnetic (Cr, Mn, Fe, Co, Ni) oxide nanocrystals via a simple and general approach. *Chem. Mater* 2004;16:3931–3935.
32. Peng X, Wickham J, and Alivisatos A. Kinetics of II-VI and III-V colloidal semiconductor nanocrystal growth:focusing of size distributions. *Journal of the American Chemical Society* 1998;120:5343–5344.
33. Park J, Lee E, Hwang NM, Kang M, Kim SC, Hwang Y, Park JG, Noh HJ, Kim JY, Park JH, and Hyeon T. One-nanometer-scale size-controlled synthesis of monodisperse magnetic iron oxide nanoparticles. *Angewandte Chemie (International ed. in English)* 2005;44:2873–2877.
34. Pérez N, López-Calahorra F, Labarta A, and Batlle X. Reduction of iron by decarboxylation in the formation of magnetite nanoparticles. *Physical chemistry chemical physics : PCCP* 2011;13:19485–19489.
35. Thanh NTK, Maclean N, and Mahiddine S. Mechanisms of nucleation and growth of nanoparticles in solution. *Chemical reviews* 2014;114:7610–7630.

36. Wu W, He Q, and Jiang C. Magnetic iron oxide nanoparticles: synthesis and surface functionalization strategies. *Nanoscale research letters* 2008;3:397–415.
37. Turcheniuk K, Tarasevych AV, Kukhar VP, Boukherroub R, and Szunerits S. Recent advances in surface chemistry strategies for the fabrication of functional iron oxide based magnetic nanoparticles. *Nanoscale* 2013;5:10729–10752.
38. Muthiah M, Park IK, and Cho CS. Surface modification of iron oxide nanoparticles by biocompatible polymers for tissue imaging and targeting. *Biotechnology Advances* 2013;31:1224–1236.
39. Liu Z, Zhao B, Shi Y, Guo C, Yang H, and Li Z. Novel nonenzymatic hydrogen peroxide sensor based on iron oxide-silver hybrid submicrospheres. *Talanta* 2010;81:1650–1654.
40. Prucek R, Tuček J, Kilianová M, Panáček A, Kvítek L, Filip J, Kolář M, Tománková K, and Zbořil R. The targeted antibacterial and antifungal properties of magnetic nanocomposite of iron oxide and silver nanoparticles. *Biomaterials* 2011;32:4704–4713.
41. Ji X, Shao R, Elliott AM, Stafford RJ, Esparza-Coss E, Liang G, Luo ZP, Park K, Markert JT, and Li C. Bifunctional Gold Nanoshells with a Superparamagnetic Iron Oxide-Silica Core Suitable for Both MR Imaging and Photothermal Therapy. *The journal of physical chemistry. C, Nanomaterials and interfaces* 2007;111:6245–6251.
42. Stöber W, Fink A, and Bohn E. Controlled growth of monodisperse silica spheres in the micron size range. *Journal of colloid and interface science* 1968;26:62–69.
43. Butterworth M, Bell S, Armes S, and Simpson A. Synthesis and characterization of polypyrrole-magnetite-silica particles. *Journal of colloid and interface science* 1996;183:91–99.
44. Ding HL, Zhang YX, Wang S, Xu JM, Xu SC, and Li GH. Fe<sub>3</sub>O<sub>4</sub>-SiO<sub>2</sub> Core/Shell Nanoparticles: The Silica Coating Regulations with a Single Core for Different Core Sizes and Shell Thicknesses. *Chemistry of Materials* 2012;24:4572–4580.
45. Kim J, Kim HS, Lee N, Kim T, Kim H, Yu T, Song IC, Moon WK, and Hyeon T. Multifunctional uniform nanoparticles composed of a magnetite nanocrystal core and a mesoporous silica shell for magnetic resonance and fluorescence imaging and for drug delivery. *Angewandte Chemie (International ed. in English)* 2008;47:8438–8441.

46. Chiang IC and Chen DH. Structural characterization and self-assembly into superlattices of iron oxide-gold core-shell nanoparticles synthesized via a high-temperature organometallic route. *Nanotechnology* 2009;20:015602.
47. Iglesias-Silva E, Vilas-Vilela J, López-Quintela M, Rivas J, Rodríguez M, and León L. Synthesis of gold-coated iron oxide nanoparticles. *Journal of Non-Crystalline Solids* 2010;356:1233–1235.
48. Brulot W, Valev VK, and Verbiest T. Magnetic-plasmonic nanoparticles for the life sciences: calculated optical properties of hybrid structures. *Nanomedicine: Nanotechnology, Biology and Medicine* 2011;8:559–568.
49. Zhou L, Yuan J, and Wei Y. Core-shell structural iron oxide hybrid nanoparticles: from controlled synthesis to biomedical applications. *Journal of Materials Chemistry* 2011;21:2823–2840.
50. Liu J, Sun Z, Deng Y, Zou Y, Li C, Guo X, Xiong L, Gao Y, Li F, and Zhao D. Highly Water-Dispersible Biocompatible Magnetite Particles with Low Cytotoxicity Stabilized by Citrate Groups. *Angewandte Chemie* 2009;121:5989–5993.
51. Yee C, Kataby G, Ulman A, Prozorov T, White H, King A, Rafailovich M, Sokolov J, and Gedanken A. Self-Assembled Monolayers of Alkanesulfonic and -phosphonic Acids on Amorphous Iron Oxide Nanoparticles. *Langmuir* 1999;15:7111–7115.
52. Smolensky ED, Park HYE, Berquó TS, and Pierre VC. Surface functionalization of magnetic iron oxide nanoparticles for MRI applications - effect of anchoring group and ligand exchange protocol. *Contrast media & molecular imaging* 2011;6:189–199.
53. Xu C, Xu K, Gu H, Zheng R, Liu H, Zhang X, Guo Z, and Xu B. Dopamine as a robust anchor to immobilize functional molecules on the iron oxide shell of magnetic nanoparticles. *Journal of the American Chemical Society* 2004;126:9938–9939.
54. Zürcher S, Wäckerlin D, Bethuel Y, Malisova B, Textor M, Tosatti S, and Gademann K. Biomimetic surface modifications based on the cyanobacterial iron chelator anachelin. *Journal of the American Chemical Society* 2006;128:1064–1065.
55. Lee H, Dellatore SM, Miller WM, and Messersmith PB. Mussel-inspired surface chemistry for multifunctional coatings. *Science* 2007;318:426–430.
56. Holten-Andersen N, Harrington MJ, Birkedal H, Lee BP, Messersmith PB, Lee KYC, and Waite JH. pH-induced metal-ligand cross-links inspired by mussel yield self-healing polymer networks with near-covalent elastic moduli. *Proceedings of the National Academy of Sciences of the United States of America* 2011;108:2651–2655.

57. Taylor S, Luther G, and Waite J. Polarographic and Spectrophotometric Investigation of Iron(III) Complexation to 3,4-Dihydroxyphenylalanine-Containing Peptides and Proteins from *Mytilus edulis*. *Inorganic Chemistry* 1994;19:5819–5824.
58. Amstad E, Gehring AU, Fischer Hk, Nagaiyanallur VV, Hahner G, Textor M, and Reimhult E. Influence of Electronegative Substituents on the Binding Affinity of Catechol-Derived Anchors to Fe<sub>3</sub>O<sub>4</sub> Nanoparticles. *The Journal of Physical Chemistry C* 2011;115:683–691.
59. Shtykova E, Huang X, Remmes N, Baxter D, Stein B, Dragnea B, Svergun D, and Bronstein L. Structure and Properties of Iron Oxide Nanoparticles Encapsulated by Phospholipids with Poly(ethylene glycol) Tails. *Journal of Physical Chemistry C* 2007;111:18078–18086.
60. Alonso JM, Reichel A, Piehler J, and Campo A del. Photopatterned surfaces for site-specific and functional immobilization of proteins. *Langmuir* 2008;24:448–457.
61. Bantignies JL, Vellutini L, Maurin D, Hermet P, Dieudonné P, Wong Chi Man M, Bartlett JR, Bied C, Sauvajol JL, and Moreau JJE. Insights into the self-directed structuring of hybrid organic-inorganic silicas through infrared studies. *The Journal of Physical Chemistry B* 2006;110:15797–15802.
62. Fadeev A and McCarthy T. Self-Assembly Is Not the Only Reaction Possible between Alkyltrichlorosilanes and Surfaces: Monomolecular and Oligomeric Covalently Attached Layers of Dichloro- and Trichloroalkylsilanes on Silicon. *Langmuir* 2000;16:7268–7274.
63. Demirci S and Caykara T. Formation of dicarboxylic acid-terminated monolayers on silicon wafer surface. *Surface Science* 2010;604:649–653.
64. Sanchez C, Rozes L, Ribot F, Laberty-Robert C, Grosso D, Sassoye C, Boissiere C, and Nicole L. Chimie douce: A land of opportunities for the designed construction of functional inorganic and hybrid organic-inorganic nanomaterials. *Comptes Rendus Chimie* 2010;13:3–39.
65. Nagarale RK, Shin W, and Singh PK. Progress in ionic organic-inorganic composite membranes for fuel cell applications. *Polymer Chemistry* 2010;1:388–408.
66. Derjaguin B and Landau L. Theory of the stability of strongly charged lyophobic sols and of the adhesion of strongly charged particles in solutions of electrolytes. *Acta Phys. Chim. USSR* 1941;14:633–662.
67. Verwey E and Overbeek J. Theory of stability of lyophobic colloids. Elsevier, 1948.
68. Xu R. Particle Characterization: Light Scattering Methods. Kluwer Academic Publishers, 2001:403.

69. Cedervall T, Lynch I, Lindman S, Berggard T, Thulin E, Nilsson H, Dawson KA, and Linse S. Understanding the nanoparticle-protein corona using methods to quantify exchange rates and affinities of proteins for nanoparticles. *Proceedings of the National Academy of Sciences of the United States of America* 2007;104:2050–2055.
70. Nel AE, Madler L, Velegol D, Xia T, Hoek EMV, Somasundaran P, Klaessig F, Castranova V, and Thompson M. Understanding biophysicochemical interactions at the nano-bio interface. *Nature materials* 2009;8:543–557.
71. Lynch I, Cedervall T, Lundqvist M, Cabaleiro-Lago C, Linse S, and Dawson KA. The nanoparticle-protein complex as a biological entity; a complex fluids and surface science challenge for the 21st century. *Advances in colloid and interface science* 2007;134-135:167–174.
72. Walkey CD and Chan WCW. Understanding and controlling the interaction of nanomaterials with proteins in a physiological environment. *Chemical Society reviews* 2012;41:2780–2799.
73. Lynch I and Dawson K. Protein-nanoparticle interactions. *Nano Today* 2008;3:40–47.
74. De M, You CC, Srivastava S, and Rotello VM. Biomimetic interactions of proteins with functionalized nanoparticles: a thermodynamic study. *Journal of the American Chemical Society* 2007;129:10747–10753.
75. Janeway C, Travers P, Walport M, and Shlomchik M. *Immuno Biology: the immune system in health and disease*. Garland Science, 2005:823.
76. Köhler G and Milstein C. Continuous cultures of fused cells secreting antibody of predefined specificity. *Nature* 1975;256:495–497.
77. Leenaars M and Hendriksen C. Critical Steps in the Production of Polyclonal and Monoclonal Antibodies: Evaluation and Recommendations. *ILAR journal* 2005;46:269–279.
78. Kennett R. Hybridomas: a new dimension in biological analyses. *In Vitro* 1981;17:1036–1050.
79. Huse K, Böhme HJ, and Scholz GH. Purification of antibodies by affinity chromatography. *Journal of biochemical and biophysical methods* 2002;51:217–231.
80. Cooper HM and Paterson Y. Production of polyclonal antisera. *Current protocols in neuroscience* 2009;5:5.5.1–5.5.10.
81. Hjelm B, Forsström B, Igel U, Johannesson H, Stadler C, Lundberg E, Ponten F, Sjöberg A, Rockberg J, Schwenk JM, Nilsson P, Johansson C, and Uhlén M. Generation of monospecific antibodies based on affinity capture of polyclonal antibodies. *Protein science* 2011;20:1824–1835.

82. Low D, O'Leary R, and Pujar NS. Future of antibody purification. *Journal of chromatography B* 2007;848:48–63.
83. Hermanson G. *Bioconjugate techniques*. 2nd. Elsevier, 2008:1202.
84. Andersen B, Abele D, and Vannier W. Effects of mild periodate oxidation on antibodies. *The Journal of Immunology* 1966;97:913–924.
85. Abraham R, Moller D, and Gabel D. The influence of periodate oxidation on monoclonal antibody avidity and immunoreactivity. *Journal of immunological methods* 1991;144:77–86.
86. Nakajima N and Ikada Y. Mechanism of amide formation by carbodiimide for bioconjugation in aqueous media. *Bioconjugate chemistry* 1995;6:123–130.
87. Staros JV, Wright RW, and Swingle DM. Enhancement by N-hydroxysulfosuccinimide of water-soluble carbodiimide-mediated coupling reactions. *Analytical Biochemistry* 1986;156:220–222.
88. Montalbetti CA and Falque V. Amide bond formation and peptide coupling. *Tetrahedron* 2005;61:10827–10852.
89. Fields BS. The molecular ecology of legionellae. *Trends in microbiology* 1996;4:286–290.
90. Sheehan KB, Henson JM, and Ferris MJ. *Legionella* species diversity in an acidic biofilm community in Yellowstone National Park. *Applied and environmental microbiology* 2005;71:507–511.
91. World Health Organization (WHO). *Legionella and the prevention of legionellosis*. Tech. rep. 2007.
92. Ortiz-Roque C and Hazen T. Abundance and distribution of Legionellaceae in Puerto Rican waters. *Applied and environmental microbiology* 1987;53:2231–2236.
93. Steinert M, Hentschel U, and Hacker J. *Legionella pneumophila*: an aquatic microbe goes astray. *FEMS microbiology reviews* 2002;26:149–162.
94. Vlaamse Overheid. Besluit van de Vlaamse Regering betreffende de preventie van de veteranenziekte op publiek toegankelijke plaatsen. *Belgisch Staatsblad* 2007:23822–23830.
95. Calders R. *Legionella pneumophila* in vlaanderen presentatie. Tech. rep. 2008.
96. Vincent C and Vogel JP. The Dot/Icm Type IVB Secretion System of *Legionella*. *Legionella: Molecular Microbiology*. 2008.
97. Fraser DW, Tsai TR, Orenstein W, Parkin WE, Beecham HJ, Sharrar RG, Harris J, Mallison GF, Martin SM, McDade JE, Shepard CC, and Brachman PS. Legionnaires' disease: description of an epidemic of pneumonia. *The New England journal of medicine* 1977;297:1189–1197.

98. Pernin P, Pélandakis M, Rouby Y, and A. Comparative recoveries of *Naegleria fowleri* amoebae from seeded river water by filtration and centrifugation. *Applied and environmental microbiology* 1998;64:955–959.
99. Lazcka O, Del Campo FJ, and Muñoz FX. Pathogen detection: a perspective of traditional methods and biosensors. *Biosensors & bioelectronics* 2007;22:1205–1217.
100. Maiwald M, Helbig JH, and Lück PC. Laboratory methods for the diagnosis of *Legionella* infections. *Journal of Microbiological Methods* 1998;33:59–79.
101. Hoefel D, Grooby W, Monis P, Andrews S, and CP. Enumeration of water-borne bacteria using viability assays and flow cytometry: a comparison to culture-based techniques. *journal of microbiological methods* 2003;55:585–597.
102. Füsichlin HP, Köttsch S, Keserue HA, and Egli T. Rapid and quantitative detection of *Legionella pneumophila* applying immunomagnetic separation and flow cytometry. *Cytometry. Part A : the journal of the International Society for Analytical Cytology* 2010;77:264–274.
103. Grow AE, Wood LL, Claycomb JL, and Thompson PA. New biochip technology for label-free detection of pathogens and their toxins. *Journal of Microbiological Methods* 2003;53:221–233.
104. Janib SM, Moses AS, and MacKay JA. Imaging and drug delivery using theranostic nanoparticles. *Advanced drug delivery reviews* 2010;62:1052–1063.
105. Ma J, Fan Q, Wang L, Jia N, Gu Z, and Shen H. Synthesis of magnetic and fluorescent bifunctional nanocomposites and their applications in detection of lung cancer cells in humans. *Talanta* 2010;81:1162–1169.
106. Tran DT, Chen CL, and Chang JS. Immobilization of *Burkholderia* sp. lipase on a ferric silica nanocomposite for biodiesel production. *Journal of biotechnology* 2012;158:112–119.
107. Wang Z, Wang J, Yue T, Yuan Y, Cai R, and Niu C. Immunomagnetic separation combined with polymerase chain reaction for the detection of *Alicyclobacillus acidoterrestris* in apple juice. *PloS one* 2013;8:e82376.
108. Chalasani R and Vasudevan S. Cyclodextrin functionalized magnetic iron oxide nanocrystals: a host-carrier for magnetic separation of non-polar molecules and arsenic from aqueous media. *Journal of Materials Chemistry* 2012;22:14925–14931.
109. Speliotis D. Magnetic recording beyond the first 100 Years. *Journal of Magnetism and Magnetic Materials* 1999;193:29–35.

110. Sun J, Zhou S, Hou P, and Yang Y. Synthesis and characterization of biocompatible Fe<sub>3</sub>O<sub>4</sub> nanoparticles. *Journal of Biomedical Materials Research Part A* 2006;333–341.
111. Bronstein LM, Huang X, Retrum J, Schmucker A, Pink M, Stein BD, and Dragnea B. Influence of Iron Oleate Complex Structure on Iron Oxide Nanoparticle Formation. *Chemistry of Materials* 2007;19:3624–3632.
112. Zhang L, He R, and Gu H. Oleic acid coating on the monodisperse magnetite nanoparticles. *Applied Surface Science* 2006;253:2611–2617.
113. Fauconnier N, Pons J, Roger J, and Bee A. Thiolation of Maghemite Nanoparticles by Dimercaptosuccinic Acid. *Journal of colloid and interface science* 1997;194:427–433.
114. Wang Y, Wong JF, Teng X, Lin XZ, and Yang H. “Pulling” Nanoparticles into Water: Phase Transfer of Oleic Acid Stabilized Monodisperse Nanoparticles into Aqueous Solutions of  $\alpha$ -Cyclodextrin. *Nano Letters* 2003;3:1555–1559.
115. Park JW, Bae KH, Kim C, and Park TG. Clustered magnetite nanocrystals cross-linked with PEI for efficient siRNA delivery. *Biomacromolecules* 2011;12:457–465.
116. Soderholm KJ and Shang SW. Molecular Orientation of Silane at the Surface of Colloidal Silica. *Journal of Dental Research* 1993;72:1050–1054.
117. Zhang Y, Kohler N, and Zhang M. Surface modification of superparamagnetic magnetite nanoparticles and their intracellular uptake. *Biomaterials* 2002;23:1553–1561.
118. De Palma R, Peeters S, Van Bael M, Van den Rul H, Bonroy K, Laureyn W, Mullens J, Borghs G, and Maes G. Silane ligand exchange to make hydrophobic superparamagnetic nanoparticles water-dispersible. *Chem. Mater* 2007;19:1821–1831.
119. Larsen EKV, Nielsen T, Wittenborn T, Birkedal H, Vorup-Jensen T, Jakobsen MH, Ostergaard L, Horsman MR, Besenbacher F, Howard Ka, and Kjems Jr. Size-Dependent Accumulation of PEGylated Silane-Coated Magnetic Iron Oxide Nanoparticles in Murine Tumors. *ACS nano* 2009;3:1947–1951.
120. Kohler N, Fryxell GE, and Zhang M. A bifunctional poly(ethylene glycol) silane immobilized on metallic oxide-based nanoparticles for conjugation with cell targeting agents. *Journal of the American Chemical Society* 2004;126:7206–7211.
121. Mason T and Lorimer J. *Applied Sonochemistry: Uses of power ultrasound in chemistry and Processing*. WILEY-VCH Verlag Weinheim, 2002.

122. Morel AL, Nikitenko SI, Gionnet K, Wattiaux A, Lai-Kee-Him J, Labrugere C, Chevalier B, Deleris G, Petibois C, Brisson A, and Simonoff M. Sonochemical approach to the synthesis of Fe(3)O(4)@SiO(2) core-shell nanoparticles with tunable properties. *ACS nano* 2008;2:847–856.
123. Prasad NK, Rathinasamy K, Panda D, and Bahadur D. Mechanism of cell death induced by magnetic hyperthermia with nanoparticles of  $\gamma$ -MnxFe<sub>2-x</sub>O<sub>3</sub> synthesized by a single step process. *Journal of Materials Chemistry* 2007;17:5042–5051.
124. Chen ZP, Xu RZ, Zhang Y, and Gu N. Effects of Proteins from Culture Medium on Surface Property of Silanes- Functionalized Magnetic Nanoparticles. *Nanoscale research letters* 2008;4:204–209.
125. Chen ZP, Zhang Y, Xu K, Xu RZ, Liu JW, and Gu N. Stability of Hydrophilic Magnetic Nanoparticles Under Biologically Relevant Conditions. *Journal of Nanoscience and Nanotechnology* 2008;8:6260–6265.
126. Can K, Ozmen M, and Ersoz M. Immobilization of albumin on aminosilane modified superparamagnetic magnetite nanoparticles and its characterization. *Colloids and surfaces. B, Biointerfaces* 2009;71:154–159.
127. Ma M, Zhang Y, Yu W, Shen Hy, Zhang Hq, and Gu N. Preparation and characterization of magnetite nanoparticles coated by amino silane. *Colloids and Surfaces A: Physicochemical and Engineering Aspects* 2003;212:219–226.
128. Harder P, Grunze M, Dahint R, Whitesides G, and Laibinis P. Molecular Conformation in Oligo(ethylene glycol)-Terminated Self-Assembled Monolayers on Gold and Silver Surfaces Determines Their Ability To Resist Protein Adsorption. *The Journal of Physical Chemistry B* 1998;102:426–436.
129. Valiokas R, Svedhem S, and Svensson S. Self-assembled monolayers of oligo (ethylene glycol)-terminated and amide group containing alkanethiolates on gold. *Langmuir* 1999;15:3390–3394.
130. Schweiss R, Welzel P, Werner C, and Knoll W. Dissociation of surface functional groups and preferential adsorption of ions on self-assembled monolayers assessed by streaming potential and streaming current measurements. *Langmuir* 2001;17:4304–4311.
131. Kreuzer HJ, Wang RLC, and Grunze M. Hydroxide ion adsorption on self-assembled monolayers. *Journal of the American Chemical Society* 2003;125:8384–8389.
132. Barreto Ja, Matterna M, Graham B, Stephan H, and Spiccia L. Synthesis, colloidal stability and <sup>64</sup>Cu labeling of iron oxide nanoparticles bearing different macrocyclic ligands. *New Journal of Chemistry* 2011;35:2705–2712.

133. Bhattacharya D, Sahu SK, Banerjee I, Das M, Mishra D, Maiti TK, and Pramanik P. Synthesis, characterization, and in vitro biological evaluation of highly stable diversely functionalized superparamagnetic iron oxide nanoparticles. *Journal of Nanoparticle Research* 2011;13:4173–4188.
134. Tartaj P, Morales MDP, Veintemillas-Verdaguer S, Gonzalez-Carreno T, and Serna CJ. The preparation of magnetic nanoparticles for applications in biomedicine. *Journal of Physics D: Applied Physics* 2003;36:182–197.
135. Montenegro JM, Grazu V, Sukhanova A, Agarwal S, Fuente JM de la, Nabiev I, Greiner A, and Parak WJ. Controlled antibody/(bio-) conjugation of inorganic nanoparticles for targeted delivery. *Advanced drug delivery reviews* 2013;65:677–688.
136. Jeong U, Teng X, Wang Y, Yang H, and Xia Y. Superparamagnetic Colloids: Controlled Synthesis and Niche Applications. *Advanced Materials* 2007;19:33–60.
137. Lee N and Hyeon T. Designed synthesis of uniformly sized iron oxide nanoparticles for efficient magnetic resonance imaging contrast agents. *Chemical Society reviews* 2012;41:2575–2589.
138. Park J, Joo J, Kwon SG, Jang Y, and Hyeon T. Synthesis of monodisperse spherical nanocrystals. *Angewandte Chemie (International ed. in English)* 2007;46:4630–4660.
139. Wang X, Zhuang J, Peng Q, and Li Y. A general strategy for nanocrystal synthesis. *Nature* 2005;437:121–124.
140. Lin Fh, Chen W, Liao YH, Doong Ra, and Li Y. Effective approach for the synthesis of monodisperse magnetic nanocrystals and M-Fe<sub>3</sub>O<sub>4</sub> (M = Ag, Au, Pt, Pd) heterostructures. *Nano Research* 2011;4:1223–1232.
141. Park EJ, Kim H, Kim Y, Yi J, Choi K, and Park K. Inflammatory responses may be induced by a single intratracheal instillation of iron nanoparticles in mice. *Toxicology* 2010;275:65–71.
142. Mendoza A, Torres-Hernandez JA, Ault JG, Pedersen-Lane JH, Gao D, and Lawrence DA. Silica nanoparticles induce oxidative stress and inflammation of human peripheral blood mononuclear cells. *Cell stress & chaperones* 2014;19:777–790.
143. Trickler WJ, Lantz SM, Murdock RC, Schrand AM, Robinson BL, Newport GD, Schlager JJ, Oldenburg SJ, Paule MG, Slikker W, Hussain SM, and Ali SF. Silver nanoparticle induced blood-brain barrier inflammation and increased permeability in primary rat brain microvessel endothelial cells. *Toxicological sciences : an official journal of the Society of Toxicology* 2010;118:160–170.

144. Petri-Fink A, Steitz B, Finka A, Salaklang J, and Hofmann H. Effect of cell media on polymer coated superparamagnetic iron oxide nanoparticles (SPIONs): colloidal stability, cytotoxicity, and cellular uptake studies. *European journal of pharmaceutics and biopharmaceutics* 2008;68:129–137.
145. Gerion D, Pinaud F, Williams SC, Parak WJ, Zanchet D, Weiss S, and Alivisatos AP. Synthesis and Properties of Biocompatible Water-Soluble Silica-Coated CdSe/ZnS Semiconductor Quantum Dots. *The Journal of Physical Chemistry B* 2001;105:8861–8871.
146. Jiang W, Kim BYS, Rutka JT, and Chan WCW. Nanoparticle-mediated cellular response is size-dependent. *Nature nanotechnology* 2008;3:145–150.
147. Bloemen M, Brulot W, Denis C, Vanysacker L, and Verbiest T. Core-shell nanoparticles as enhanced probes for imaging applications. *Proceedings of the Society of Photo-Optical Instrumentation Engineers: Vol. 8427* 2012;8427. Ed. by Popp J, Drexler W, Tuchin VV, and Matthews DL.
148. Tucker-Schwartz AK, Farrell RA, and Garrell RL. Thiol-ene click reaction as a general route to functional trialkoxysilanes for surface coating applications. *Journal of the American Chemical Society* 2011;133:11026–11029.
149. Moses JE and Moorhouse AD. The growing applications of click chemistry. *Chemical Society reviews* 2007;36:1249–1262.
150. Kolb HC, Finn MG, and Sharpless KB. Click Chemistry: Diverse Chemical Function from a Few Good Reactions. *Angewandte Chemie (International ed. in English)* 2001;40:2004–2021.
151. Hoyle CE and Bowman CN. Thiol-ene click chemistry. *Angewandte Chemie (International ed. in English)* 2010;49:1540–1573.
152. Bijnens AP, Gils A, Knockaert I, Stassen JM, and Declerck PJ. Importance of the Hinge Region between alpha -Helix F and the Main Part of Serpins, Based upon Identification of the Epitope of Plasminogen Activator Inhibitor Type 1 Neutralizing Antibodies. *Journal of Biological Chemistry* 2000;275:6375–6380.
153. Declerck PJ and Gils A. Three decades of research on plasminogen activator inhibitor-1: a multifaceted serpin. *Seminars in thrombosis and hemostasis* 2013;39:356–364.
154. Spivey AC and Arseniyadis S. Nucleophilic catalysis by 4-(dialkylamino) pyridines revisited—the search for optimal reactivity and selectivity. *Angewandte Chemie (International ed. in English)* 2004;43:5436–5441.
155. Dixit CK, Vashist SK, MacCraith BD, and O’Kennedy R. Multisubstrate-compatible ELISA procedures for rapid and high-sensitivity immunoassays. *Nature protocols* 2011;6:439–445.

156. Gils A, Ceresa E, Macovei AM, Marx PF, Peeters M, Compennolle G, and Declercq PJ. Modulation of TAFI function through different pathways—implications for the development of TAFI inhibitors. *Journal of thrombosis and haemostasis : JTH* 2005;3:2745–2753.
157. Bradford MM. A rapid and sensitive method for the quantitation of microgram quantities of protein utilizing the principle of protein-dye binding. *Analytical Biochemistry* 1976;72:248–254.
158. Casals E, Pfaller T, Duschl A, Oostingh GJ, and Puntjes V. Time evolution of the nanoparticle protein corona. *ACS nano* 2010;4:3623–3632.
159. Lundqvist M, Stigler J, Elia G, Lynch I, Cedervall T, and Dawson KA. Nanoparticle size and surface properties determine the protein corona with possible implications for biological impacts. *Proceedings of the National Academy of Sciences of the United States of America* 2008;105:14265–14270.
160. Cui M, Liu R, Deng Z, Ge G, Liu Y, and Xie L. Quantitative study of protein coronas on gold nanoparticles with different surface modifications. *Nano Research* 2014;7:345–352.
161. Zhang S, Zou L, Zhang D, Pang X, Yang H, and Xu Y. GoldMag nanoparticles with core/shell structure: characterization and application in MR molecular imaging. *Journal of Nanoparticle Research* 2011;13:3867–3876.
162. Ranjbakhsh E, Bordbar a.K., Abbasi M, Khosropour a.R., and Shams E. Enhancement of stability and catalytic activity of immobilized lipase on silica-coated modified magnetite nanoparticles. *Chemical Engineering Journal* 2012;179:272–276.
163. Shi B, Wang Y, Ren J, Liu X, Zhang Y, Guo Y, Guo Y, and Lu G. Superparamagnetic aminopropyl-functionalized silica core-shell microspheres as magnetically separable carriers for immobilization of penicillin G acylase. *Journal of Molecular Catalysis B: Enzymatic* 2010;63:50–56.
164. Cui Y, Li Y, Yang Y, Liu X, Lei L, Zhou L, and Pan F. Facile synthesis of amino-silane modified superparamagnetic Fe<sub>3</sub>O<sub>4</sub> nanoparticles and application for lipase immobilization. *Journal of biotechnology* 2010;150:171–174.
165. Cao H, He J, Deng L, and Gao X. Fabrication of cyclodextrin-functionalized superparamagnetic Fe<sub>3</sub>O<sub>4</sub>/amino-silane core-shell nanoparticles via layer-by-layer method. *Applied Surface Science* 2009;255:7974–7980.
166. Pollet J, Delport F, Janssen KPF, Jans K, Maes G, Pfeiffer H, Wevers M, and Lammertyn J. Fiber optic SPR biosensing of DNA hybridization and DNA-protein interactions. *Biosensors & bioelectronics* 2009;25:864–869.

167. Ge Y, Zhang Y, Xia J, Ma M, He S, Nie F, and Gu N. Effect of surface charge and agglomerate degree of magnetic iron oxide nanoparticles on KB cellular uptake in vitro. *Colloids and surfaces. B, Biointerfaces* 2009;73:294–301.
168. Osaka T, Nakanishi T, Shanmugam S, Takahama S, and Zhang H. Effect of surface charge of magnetite nanoparticles on their internalization into breast cancer and umbilical vein endothelial cells. *Colloids and surfaces. B, Biointerfaces* 2009;71:325–330.
169. Hoyle CE, Lee TY, and Roper T. Thiol-enes: Chemistry of the past with promise for the future. *Journal of Polymer Science Part A: Polymer Chemistry* 2004;42:5301–5338.
170. Northrop BH and Coffey RN. Thiol-ene click chemistry: computational and kinetic analysis of the influence of alkene functionality. *Journal of the American Chemical Society* 2012;134:13804–13817.
171. Mahon E, Salvati A, Baldelli Bombelli F, Lynch I, and Dawson KA. Designing the nanoparticle-biomolecule interface for "targeting and therapeutic delivery". *Journal of controlled release : official journal of the Controlled Release Society* 2012;161:164–174.
172. Noh SH, Na W, Jang JT, Lee JH, Lee EJ, Moon SH, Lim Y, Shin JS, and Cheon J. Nanoscale magnetism control via surface and exchange anisotropy for optimized ferrimagnetic hysteresis. *Nano letters* 2012;12:3716–3721.
173. Babes L, Denizot B, Tanguy G, Le Jeune J, and Jallet P. Synthesis of Iron Oxide Nanoparticles Used as MRI Contrast Agents: A Parametric Study. *Journal of colloid and interface science* 1999;212:474–482.
174. Schladt TD, Schneider K, Schild H, and Tremel W. Synthesis and bio-functionalization of magnetic nanoparticles for medical diagnosis and treatment. *Dalton transactions* 2011;40:6315–6343.
175. Yu W, Falkner J, Yavuz C, and Colvin V. Synthesis of monodisperse iron oxide nanocrystals by thermal decomposition of iron carboxylate salts. *Chem. Commun* 2004;20:2306–2307.
176. Sun S and Zeng H. Size-controlled synthesis of magnetite nanoparticles. *Journal of the American Chemical Society* 2002;124:8204–8205.
177. Harisinghani MG, Barentsz J, Hahn PF, Deserno WN, Tabatabaei S, Hulsbergen van de Kaa C, Rosette J de la, and Weissleder R. Noninvasive detection of clinically occult lymph-node metastases in prostate cancer. *The New England Journal of Medicine* 2003;348:2491–2499.
178. Bloemen M, Debruyne D, Demeyer PJ, Clays K, Gils A, Geukens N, Bartic C, and Verbiest T. Catechols as ligands for CdSe–ZnS quantum dots. *RSC Advances* 2014;4:10208–10211.

179. Na HB, Palui G, Rosenberg JT, Ji X, Grant SC, and Mattoussi H. Multidentate catechol-based polyethylene glycol oligomers provide enhanced stability and biocompatibility to iron oxide nanoparticles. *ACS nano* 2012;6:389–399.
180. Daniels M and Francis L. Silane Adsorption Behavior, Microstructure, and Properties of Glycidoxypolytrimethoxysilane-Modified Colloidal Silica Coatings. *Journal of colloid and interface science* 1998;205:191–200.
181. Boerio FJ, Armogan L, and Cheng S. The structure of  $\gamma$ -aminopropyl triethoxysilane films on iron mirrors. *Journal of Colloid and Interface Science* 1980;73:416–424.
182. Vandenberg ET, Bertilsson L, Liedberg B, Udval K, Erlandsson R, Elwing H, and Lundström I. Structure of 3-Aminopropyl Triethoxy Silane on Silicon Oxide. *Journal of Colloid and Interface Science* 1991;147:103–118.
183. Gu RA, Chen H, Liu GK, and Ren B. Study on Films of Organofunctional Silanes on Transition Metal Surfaces- The Structure of Aminopropyltrimethoxysilane Films on Nickel Electrodes. *Acta Chimica Sinica* 2003;61:1550–1555.
184. Brulot W, Strobbe R, Bynens M, Bloemen M, Demeyer PJ, Vanderlinden W, De Feyter S, Valev VK, and Verbiest T. Layer-by-Layer synthesis and tunable optical properties of hybrid magnetic–plasmonic nanocomposites using short bifunctional molecular linkers. *Materials Letters* 2014;118:99–102.
185. Crouch DR, Burger JS, Zietek KA, Cadwallader AB, Bedison JE, and Smielewska MM. Removal of Acyl Protecting Groups Using Solid NaOH and a Phase Transfer Catalyst. *Synlett* 2003;7:991–992.
186. Keating CD, Musick MD, Keefe MH, and Natan MJ. Kinetics and Thermodynamics of Au Colloid Monolayer Self-Assembly: Undergraduate Experiments in Surface and Nanomaterials Chemistry. *Journal of Chemical Education* 1999;76:949–955.
187. Golub A, Zubenko A, and Zhmud B. APTES Modified Silica Gels : The Structure of the Surface Layer. *Journal of colloid and interface science* 1996;187:482–487.
188. Ung T, Liz-Marzán L, and Mulvaney P. Controlled method for silica coating of silver colloids. Influence of coating on the rate of chemical reactions. *Langmuir* 1998;14:3740–3748.

189. Maczynski A, Shaw DG, Goral M, Wisniewska-gocłowska B, Skrzecz A, Owczarek I, Blazej K, Haulait-Pirson MC, Hefter GT, Kapuka F, Maczynska Z, Szafranski A, and Young CL. IUPAC-NIST Solubility Data Series. 81. Hydrocarbons with Water and Seawater-Revised and Updated. Part 5. C7 Hydrocarbons with Water and Heavy Water. *Journal of Physical and Chemical Reference Data* 2005;34:1399–1487.
190. Wuts PGM and Greene TW. *Greene's Protective Groups in Organic Synthesis*. 4th. Hoboken, NJ, USA: John Wiley & Sons, Inc., 2006. DOI: 10.1002/0470053488.
191. Pittelkow M and Christensen JrB. Convergent synthesis of internally branched PAMAM dendrimers. *Organic letters* 2005;7:1295–1298.
192. Jung C and Jacobs P. Physical and chemical properties of superparamagnetic iron oxide MR contrast agents: ferumoxides, ferumoxtran, ferumoxsil. *Magnetic resonance imaging* 1995;13:661–674.
193. Lartigue L, Innocenti C, Kalaivani T, Awwad A, Sanchez Duque MDM, Guari Y, Larionova J, Guérin C, Montero JLG, Barragan-Montero V, Arosio P, Lascialfari A, Gatteschi D, and Sangregorio C. Water-dispersible sugar-coated iron oxide nanoparticles. An evaluation of their relaxometric and magnetic hyperthermia properties. *Journal of the American Chemical Society* 2011;133:10459–10472.
194. Larson TA, Bankson J, Aaron J, and Sokolov K. Hybrid plasmonic magnetic nanoparticles as molecular specific agents for MRI/optical imaging and photothermal therapy of cancer cells. *Nanotechnology* 2007;18:325101.
195. Bedanta S and Kleemann W. Supermagnetism. *Journal of Physics D: Applied Physics* 2009;42:013001.
196. Yang H, Qu L, Wimbrow AN, Jiang X, and Sun Y. Rapid detection of *Listeria monocytogenes* by nanoparticle-based immunomagnetic separation and real-time PCR. *International journal of food microbiology* 2007;118:132–138.
197. Shahbazi-Gahrouei D, Abdolahi M, Zarkesh-Esfahani SH, Laurent S, Sermeus C, and Gruettner C. Functionalized magnetic nanoparticles for the detection and quantitative analysis of cell surface antigen. *BioMed research international* 2013;2013:349408.
198. Xu H, Aguilar ZP, Yang L, Kuang M, Duan H, Xiong Y, Wei H, and Wang A. Antibody conjugated magnetic iron oxide nanoparticles for cancer cell separation in fresh whole blood. *Biomaterials* 2011;32:9758–9765.

199. Gillich T, Acikgöz C, Isa L, Schlüter aD, Spencer ND, and Textor M. PEG-stabilized core-shell nanoparticles: impact of linear versus dendritic polymer shell architecture on colloidal properties and the reversibility of temperature-induced aggregation. *ACS nano* 2013;7:316–329.
200. Bloemen M, Van Stappen T, Willot P, Lammertyn J, Koeckelberghs G, Geukens N, Gils A, and Verbiest T. Heterobifunctional PEG ligands for bioconjugation reactions on iron oxide nanoparticles. *PloS ONE* 2014;9:e109475.
201. Koh I, Wang X, Varughese B, Isaacs L, Ehrman SH, and English DS. Magnetic iron oxide nanoparticles for biorecognition: evaluation of surface coverage and activity. *The journal of physical chemistry. B* 2006;110:1553–1558.
202. Dupont D, Brulot W, Bloemen M, Verbiest T, and Binnemans K. Selective uptake of rare earths from aqueous solutions by EDTA-functionalized magnetic and nonmagnetic nanoparticles. *ACS applied materials & interfaces* 2014;6:4980–4988.
203. Dupont D, Luyten J, Bloemen M, Verbiest T, and Binnemans K. Acid-Stable Magnetic Core–Shell Nanoparticles for the Separation of Rare Earths. *Industrial & Engineering Chemistry Research* 2014;53:15222–15229.
204. Horák D, Babic M, Macková H, and Benes MJ. Preparation and properties of magnetic nano- and micro-sized particles for biological and environmental separations. *Journal of separation science* 2007;30:1751–1772.
205. Chalmers JJ, Xiong Y, Jin X, Shao M, Tong X, Farag S, and Zborowski M. Quantification of non-specific binding of magnetic micro- and nanoparticles using cell tracking velocimetry: Implication for magnetic cell separation and detection. *Biotechnology and bioengineering* 2010;105:1078–1093.
206. Atlas RM. *Legionella: from environmental habitats to disease pathology, detection and control.* *Environmental Microbiology* 1999;1:283–293.
207. Vogel JP and Isberg RR. Cell biology of *Legionella pneumophila*. *Current opinion in microbiology* 1999;2:30–34.
208. Behets J, Seghi F, Declerck P, Verelst L, Duvivier L, Van Damme A, and Ollevier F. Detection of *Naegleria* spp. and *Naegleria fowleri*: a comparison of flagellation tests, ELISA and PCR. *Water science and technology : a journal of the International Association on Water Pollution Research* 2003;47:117–122.

209. Behets J, Declerck P, Delaedt Y, Verelst L, and F. Quantitative Detection and Differentiation of Free-Living Amoeba Species Using SYBR Green-Based Real-Time PCR Melting Curve Analysis. *Current microbiology* 2006;53:506–509.
210. Yáñez MA, Carrasco-Serrano C, Barberá VM, and Catalán V. Quantitative detection of *Legionella pneumophila* in water samples by immunomagnetic purification and real-time PCR amplification of the *dotA* gene. *Applied and environmental microbiology* 2005;71:3433–3441.
211. Demeke T and Jenkins GR. Influence of DNA extraction methods, PCR inhibitors and quantification methods on real-time PCR assay of biotechnology-derived traits. *Analytical and bioanalytical chemistry* 2010;396:1977–1990.
212. Van De Craen B, Scroyen I, Vranckx C, Compennolle G, Lijnen HR, Declerck PJ, and Gils A. Maximal PAI-1 inhibition in vivo requires neutralizing antibodies that recognize and inhibit glycosylated PAI-1. *Thrombosis research* 2012;129:e126–133.
213. Van Stappen T, Brouwers E, Tops S, Geukens N, Vermeire S, Declerck PJ, and Gils A. Generation of a highly specific monoclonal anti-infliximab antibody for harmonization of TNF-coated infliximab assays. *Therapeutic drug monitoring* 2014.
214. Bloemen M, Brulot W, Luong TT, Geukens N, Gils A, and Verbiest T. Improved functionalization of oleic acid-coated iron oxide nanoparticles for biomedical applications. *Journal of Nanoparticle Research* 2012;14:1100–1109.
215. Köhler R, Bubert A, Goebel W, Steinert M, Hacker J, and Bubert B. Expression and use of the green fluorescent protein as a reporter system in *Legionella pneumophila*. *MGG - Molecular and General Genetics* 2000;262:1060–1069.
216. Behets J, Declerck P, Delaedt Y, Creemers B, and Ollevier F. Development and evaluation of a Taqman duplex real-time PCR quantification method for reliable enumeration of *Legionella pneumophila* in water samples. *Journal of microbiological methods* 2007;68:137–44.
217. Rao SV, Anderson KW, and Bachas LG. Oriented immobilization of proteins. *Mikrochimica Acta* 1998;128:127–143.
218. Fluit AC, Torensma R, Visser MJ, Aarsman CJ, Poppelier MJ, Keller BH, Klapwijk P, and Verhoef J. Detection of *Listeria monocytogenes* in cheese with the magnetic immuno-polymerase chain reaction assay. *Applied and environmental microbiology* 1993;59:1289–1293.

219. Coklin T, Farber JM, Parrington LJ, Bin Kingombe CI, Ross WH, and Dixon BR. Immunomagnetic separation significantly improves the sensitivity of polymerase chain reaction in detecting *Giardia duodenalis* and *Cryptosporidium* spp. in dairy cattle. *Journal of veterinary diagnostic investigation* 2011;23:260–267.
220. Stevens Ka and Jaykus LA. Bacterial separation and concentration from complex sample matrices: a review. *Critical reviews in microbiology* 2004;30:7–24.
221. Boulanger Ca and Edelstein PH. Precision and accuracy of recovery of *Legionella pneumophila* from seeded tap water by filtration and centrifugation. *Applied and environmental microbiology* 1995;61:1805–1809.
222. Chang SC, Anderson TI, Bahrman SE, Gruden CL, Khijniak AI, and Adriaens P. Comparing recovering efficiency of immunomagnetic separation and centrifugation of mycobacteria in metalworking fluids. *Journal of Industrial Microbiology and Biotechnology* 2005;32:629–638.
223. Villari P, Motti E, Farullo C, and Torre I. Comparison of conventional culture and PCR methods for the detection of *Legionella pneumophila* in water. *Letters in applied microbiology* 1998;27:106–110.
224. Stefanick JF, Ashley JD, Kiziltepe T, and Bilgicer B. A systematic analysis of peptide linker length and liposomal polyethylene glycol coating on cellular uptake of peptide-targeted liposomes. *ACS Nano* 2013;7:2935–2947.
225. Stefanick JF, Ashley JD, and Bilgicer B. Enhanced cellular uptake of peptide-targeted nanoparticles through increased peptide hydrophilicity and optimized ethylene glycol peptide-linker length. *ACS Nano* 2013;7:8115–8127.
226. Engvall E and Perlmann P. Enzyme-linked immunosorbent assay (ELISA) quantitative assay of immunoglobulin G. *Molecular Immunology* 1971;8:871–874.
227. Gan SD and Patel KR. Enzyme immunoassay and enzyme-linked immunosorbent assay. *The Journal of investigative dermatology* 2013;133:e12.
228. Applied Biosystems. Attune Acoustic Focusing Cytometer Training Guide. Tech. rep. 2010.
229. Huggett J, Dheda K, Bustin S, and Zumla A. Real-time RT-PCR normalisation; strategies and considerations. *Genes and immunity* 2005;6:279–284.
230. Wong ML and Medrano JF. Real-time PCR for mRNA quantitation. *BioTechniques* 2005;39:75–85.
231. Agilent Technologies, Introduction to Quantitative PCR. Tech. rep. 2010.

232. Liu G, Gao J, Ai H, and Chen X. Applications and potential toxicity of magnetic iron oxide nanoparticles. *Small* 2013;9:1533–1545.
233. Murray AR, Kisin E, Inman A, Young SH, Muhammed M, Burks T, Uheida A, Tkach A, Waltz M, Castranova V, Fadeel B, Kagan VE, Riviere JE, Monteiro-Riviere N, and Shvedova Aa. Oxidative Stress and Dermal Toxicity of Iron Oxide Nanoparticles In Vitro. *Cell Biochemistry and Biophysics* 2013;67:461–476.
234. Ling D and Hyeon T. Chemical design of biocompatible iron oxide nanoparticles for medical applications. *Small* 2013;9:1450–1466.
235. Gupta AK and Wells S. Surface-Modified Superparamagnetic Nanoparticles for Drug Delivery: Preparation, Characterization, and Cytotoxicity Studies. *IEEE Transactions on Nanobioscience* 2004;3:66–73.
236. Wan S, Huang J, Guo M, Zhang H, Cao Y, Yan H, and Liu K. Biocompatible superparamagnetic iron oxide nanoparticle dispersions stabilized with poly(ethylene glycol)-oligo(aspartic acid) hybrids. *Journal of Biomedical Materials Research - Part A* 2007;80:946–954.
237. Yu M, Huang S, Yu KJ, and Clyne AM. Dextran and polymer polyethylene glycol (PEG) coating reduce both 5 and 30 nm iron oxide nanoparticle cytotoxicity in 2D and 3D cell culture. *International Journal of Molecular Sciences* 2012;13:5554–5570.

# Health, safety and environment

During the experiments, conducted for this dissertation, all health and safety guidelines and regulations from the HSE department of the KU Leuven were implemented. Risk analyses and proper waste management were evaluated before every experiment and were submitted to the appropriate channels.

The following sections will summarize several specific cases where special precautions should be taken.

## Nanoparticle synthesis by thermal decomposition

As stated in Chapter 2, the synthesis of iron oxide NP by the thermal decomposition methods is conducted at elevated temperatures, above 300°C. Special personal protection equipment, such as heat resistant gloves, should be worn when manipulating the reaction at this stage. Furthermore the reaction is known to produce CO<sub>2</sub> gas, which can cause a pressure buildup in the system. It is advised to keep the setup well ventilated and allow the excess pressure to escape. Finally, it is necessary to allow the hot mixture to cool down to room temperature before the purification is started.

## Nanoparticle toxicity

The scientific community is still debating whether or not NP are toxic. Since a general consensus has not been achieved so far, every nanoparticle system is being evaluated separately. In the case of iron oxide, a clear difference has been observed between the toxicity of the core and the different coatings.

Bare iron oxide is known to generate reactive oxygen species by the Fenton reaction, during which hydrogen peroxide is turned into hydroxyl (HO●) and hydroperoxyl (HOO●) radicals. These radical species can easily induce damage to proteins or DNA which can result in a decline in physiological function and cell death.<sup>232–234</sup>

The coating of a nanoparticle has a profound influence on the toxicity towards cells and tissue. PEG-coated particles generally perform well during toxicity tests, showing only a minor decrease in cell viability.<sup>235,236</sup> Mahmoudi *et al.* reported that particles with carboxylic acids show lower toxicity than amine-coated NP, but the effect is largely dependent on the cell type. Yu *et al.* wrote that the size of the nanoparticle and even the type of study (2D versus 3D) can have an influence on the observed toxicity.<sup>237</sup> Therefore it is advised to perform a complete toxicology study before *in vivo* experiments are conducted. Based on the available literature the expected toxic effects are small, but the lack of general consensus and understanding of the phenomenon requires that every type of nanoparticle is tested separately.

During the presented experiments, the particles were always manipulated in solution, to reduce any risks of dust formation and inhalation. Secondly, appropriate personal protection equipment, such as gloves, were worn at every step.

### ***Legionella pneumophila***

The KB of August 04, 1996 states that *Legionella pneumophila* is a class 2 pathogen and should be handled accordingly in a class 2 lab. A full risk analysis should be made before the start of the experiments and exposure should be minimized at all times. Moreover, proper disinfection of equipment (for instance with ethanol) was performed.



# List of publications

## Articles in internationally reviewed academic journals

10. Carron S, **Bloemen M**, Vander Elst L, Laurent S, Verbiest T and Parac-Vogt T. Potential Theranostic and Multimodal Iron Oxide Nanoparticles Decorated with Rhenium-Bipyridine and -Phenanthroline Complex. *Journal of Materials Chemistry B* 2015; Accepted.
9. **Bloemen M**, Denis C, Peeters M, De Meester L, Gils A, Geukens N and Verbiest T. Antibody-modified iron oxide nanoparticles for efficient magnetic isolation and flow cytometric determination of *L. pneumophila*. *Microchimica Acta* 2015; Accepted.
8. **Bloemen M**, Van Stappen T, Willot P, Lammertyn J, Koeckelberghs G, Geukens N, Gils A and Verbiest T. Heterobifunctional PEG Ligands for Bioconjugation Reactions on Iron Oxide Nanoparticles. *PLoS ONE* 2014; 9: e109475.
7. **Bloemen M**, Sutens B, Brullot W, Gils A, Geukens N and Verbiest T. Two-Step Directional Surface Modification of Iron Oxide Nanoparticles with Protected Siloxanes. *Chempluschem* 2014; 80: 50-53.
6. Dupont D, Luyten J, **Bloemen M**, Verbiest T and Binnemans K. Acid-Stable Magnetic Core-Shell Nanoparticles for the Separation of Rare Earths. *Industrial & Engineering Chemistry Research* 2014; 53: 15222–15229.
5. Brullot W, Strobbe R, Bynens M, **Bloemen M**, Demeyer P-J, Vanderlinden W, De Feyter S, Valev V and Verbiest T. Layer-by-Layer synthesis and tunable optical properties of hybrid magnetic–plasmonic nanocomposites using short bifunctional molecular linkers. *Materials Letters* 2014; 118: 99–102.
4. **Bloemen M**, Vandendriessche S, Goovaerts V, Brullot W, Vanbel M, Carron S, Geukens N, Parac-Vogt T and Verbiest T. Synthesis and Characterization of

- Holmium-Doped Iron Oxide Nanoparticles. *Materials* 2014; 7: 1155–1164.
3. **Bloemen M**, Debruyne D, Demeyer P-J, Clays K, Gils A, Geukens N, Bartic C and Verbiest T. Catechols as ligands for CdSe-ZnS quantum dots. *RSC Advances* 2014; 4: 10208–10211.
  2. Dupont D, Brulot W, **Bloemen M**, Verbiest T and Binnemans K. Selective uptake of rare earths from aqueous solutions by EDTA-functionalized magnetic and nonmagnetic nanoparticles. *ACS Applied Materials & Interfaces* 2014; 6: 4980–4988.
  1. **Bloemen M**, Brulot W, Luong TT, Geukens N, Gils A and Verbiest T. Improved functionalization of oleic acid-coated iron oxide nanoparticles for biomedical applications. *Journal of Nanoparticle Research* 2012; 14: 1100–1109.

### **Papers at international scientific conferences and symposia, published in full in proceedings**

5. **Bloemen M**, Denis C, Van Stappen T, De Meester L, Geukens N, Gils A and Verbiest T. Multifunctional iron oxide nanoparticles for biomedical applications. *Proceedings SPIE* 2015; Vol. 9338: 933816.
4. Van Stappen T, Lub J, **Bloemen M**, Geukens N, Spasic D, Delport F, Lammertyn J, Verbiest T and Ann Gils. Transferability of antibody pairs from ELISA to fiber optic-surface plasmon resonance for infliximab detection. *Proceedings SPIE* 2015; Vol. 9317: 931705.
3. **Bloemen M**, Brulot W, Denis C, Vanyssacker L and Verbiest T. Core-shell nanoparticles as enhanced probes for imaging applications. *Proceedings SPIE* 2012; Vol. 8427: 84272Q.
2. Demeyer P-J, **Bloemen M**, Verbiest T and Clays K. Tuning the properties of colloidal magneto-photonic crystals by controlled infiltration with superparamagnetic magnetite nanoparticles. *Proceedings SPIE* 2012; Vol. 8425: 84251R.
1. Demeyer P-J, **Bloemen M**, Verbiest T and Clays K. Engineering of colloidal magneto-photonic crystals by infiltration with superparamagnetic magnetite nanoparticles. *Proceedings symposium IEEE Photonics Society Benelux* 2011; Ghent, Belgium; pp. 13–16.

## Meeting abstracts, presented at international scientific conferences and symposia, published or not published in proceedings or journals

6. **Bloemen M**, Van Stappen T, Knez K, Lammertyn J, Geukens N, Gils A, Verbiest T. Multifunctional nanoparticles for biomedical applications. ISN2A. Lisbon, Portugal, 20-22 January 2014.
5. **Bloemen M**, Van Stappen T, Lammertyn J, Geukens N, Gils A, Verbiest T. Multifunctional iron oxide nanoparticles for biomedical applications. ISACS15 Challenges in nanoscience. San Diego, USA, 17-20 August 2014.
4. **Bloemen M**, Van Stappen T, Geukens N, Gils A, Verbiest T. Multifunctional iron oxide nanoparticles for biomedical applications. Nanomedicine UK. Edinburgh, UK, 26-27 March 2014.
3. Dupont D, Luyten J, Brullot W, **Bloemen M**, Verbiest T and Binnemans K. Extraction and separation of rare earths with functionalized magnetic nanoparticles. 1st European Rare Earth Resources Conference (ERES 2014). Milos (Greece), 4-7 September 2014.
2. **Bloemen M**, Vandendriessche S, Brullot W, Verbiest T. Synthesis and properties of holmium doped iron oxide nanoparticles. Collaborative Conference on Materials Research (CCMR). Jeju Island, South Korea, 24-28 June 2013.
1. Brullot W, Strobbe R, Bynens M, **Bloemen M**, Demeyer P-J, Valev V and Verbiest T. Hybrid Nanoparticle Networks (HyNANs): A modular approach to multifunctional nanomaterials. Collaborative Conference on Materials Research (CCMR) 2013. Jeju Island, South Korea, 24-28 June 2013, Abstract No. 521.